Master of Sciences in Astrophysics
Master Recherche en Astrophysique

Thesis

**Planet-Metallicity Correlation
for Kepler's Giant Planets**

Mémoire de fin d'études

**Correlation Planètes-Métallicité
pour les Planèts Géantes du Kepler**

Presented by
Présenté par

Mireille Nehmé

Member of the Jury:
Membres de Juries:

Dr. Cyrine Nehmé (Advisor) ———————————

Dr. Bassem Sabra (Referee) ———————————

Dr. Marie Abboud (Referee) ———————————

Dr. Roger Hajjar (Referee) ———————————

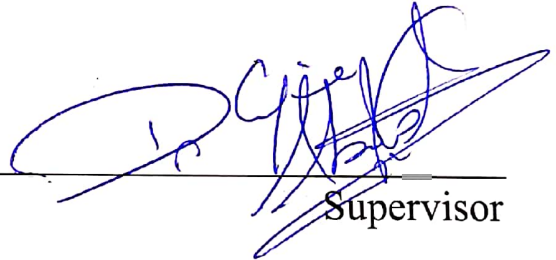**Date and Place / Date et Lieu:**
NDU (Louaise) - The 22nd of July 2014.
Reference:————— Code:—————

Faculty of Natural and Applied Sciences

Department of Physics and Astronomy

We hereby approve this thesis of

Mireille Hanna Nehme

Candidate for the degree of Masters in Science

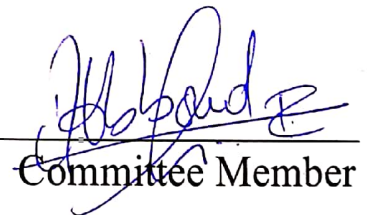|	
Dr. Cyrine Nehme	Supervisor
Dr. Bassem Sabra	Committee Member, Chair
Dr. Marie Abboud	Committee Member
Dr. Roger Hajjar	Committee Member

Planet-Metallicity Correlation for Kepler's Giant Planets

Mireille Nehmé [1]

July 2014

---

[1]mir.nehme@gmail.com

I dedicate this thesis to my Mom and Dad

"Somewhere, Something Incredible is Waiting to be known."
CARL SAGAN

Acknowledgements

Contents

List of Figures

List of Tables

List of Acronyms

CHEOPS CHaracterising ExOPlanets Satellite

CHZ Continuously Habitable Zone

CoRoT COnvection ROtation and planetary Transits

CZ Convective Zone

DR12 Dodson-Robinson 2012 [91]

ETHO Earth-Trailing Heliocentric Orbit

FOV Field of View

HZ Habitable Zone

IAU International Astronomical Union

JWST James Webb Space Telescope

KBO Kuiper Belt Objects

KIC Kepler Input Catalog

KOI Kepler Object of Interest

K2 Kepler's Second Exoplanet Mission

LC Light Curve

LOS Line of sight

PMC Planet-Metallicity Correlation

TCE Threshold Crossing Event

TESS Transiting Exoplanet Survey Satellite

TPS Transit Planet Search

WGESP Working Group on Extrasolar Planet

Abstract

This study is part of a newly growing science in exoplanet characteristics. We present an initial attempt to investigate the relationship between the eclipse depth of giant exoplanets and the metallicity of their host stars to show the best eclipse depth-metallicity trend. This will help us to better understand the conditions that lead to giant planets formation, which helps to postulate about the formation of our Solar System and more generally the planet formation theories.

Previous studies have shown that stars with giant planets tend to have higher metallicities than stars without giant planets. This was explained by the core accretion theory. According to this theory, one must expect to see an increase in median eclipse depth with metallicity. Furthermore, since metal-rich stars have smaller radii than metal-poor stars of the same mass and age, a uniform population of planets should show a rise in median eclipse depth with [M/H].
Investigation of the relation between exoplanets and their host stars has greatly evolved due to the Kepler Mission. Since this mission is providing a large sample of candidate planets, Sarah E. Dodson Robinson 2012 studied the relation between the eclipse depth of 213 Kepler gas giant candidates (from Q0 till Q5) and the metallicity of their parent stars. The author found a negative eclipse depth-metallicity trend with -2.3σ significance level. This could be explained by the disk instability model: the higher the metallicity, the higher the disk opacity which leads to less cooling therefore, the smaller the probability to form giant planets.

Is there really a negative correlation between the eclipse depths of Kepler gas giant planets and the metallicity of their parent stars? In an attempt to answer this question and to figure out a more accurate trend we start by removing the biased planets (false positive and planets that are out of range of the sample selection criteria) from the sample of Sarah E. Dodson Robinson 2012. Based on the Kendall's τ correlation coefficient we found that the significance level decreased to -0.7σ. This suggests that this negative trend may not be so significant. We then identified a larger sample of candidate and confirmed planets (From Q0 till Q12), provided by the Kepler mission as on June 2013. We quantify a positive eclipse depth-metallicity trend with 0.4σ statistical significance. With the publication of an extended data on March 2014 (From Q0 till Q16) we found, again, a positive eclipse depth-metallicity trend with a bigger significance level of 0.9σ.

From this work, we can conclude that the negative eclipse depth-metallicity trend is not that obvious and it tends to be more likely a positive trend. Nevertheless, we propose a scenario that supports the formation of planets by the core accretion process at high metallicity and by the disk instability at small metallicity.

Keywords: Planets and satellites: formation - planets and satellites: fundamental parameters - stars: planetary systems - method: statistical

Résumé

Cette étude s'inscrit dans le cadre de la caractérisation des exoplanètes. Ce domaine de l'astrophysique qui est en plein effervescence ces dernières années. On propose dans ce présent travail une démarche pour examiner la relation entre la profondeur du transit des planètes géantes et la métallicité de leurs étoiles-mères. Ce qui est primordial pour comprendre la formation planétaires.

Les études précédentes ont montrées que les étoiles autour desquelles gravitent des planètes géantes sont généralement plus riches en métaux que les étoiles sans planètes géantes. Cela est expliqué par la théorie d'accrétion. Selon cette théorie, on attend à avoir une augmentation de la profondeur du transit avec la métallicité. En outre, comme les étoiles riches en métaux possèdent des rayons plus petits que celles pauvres en métaux ayant les mêmes masses et âges, une population uniforme de planètes autour de ces étoiles va affirmer une augmentation dans la profondeur du transit avec la métallicité [M/H].
L'avènement de la mission Kepler a donné un coup de pouce sans précèdent. Dotée d'un échantillon de 213 planètes gazeuses géantes candidates, Sarah E. Dodson Robinson 2012, entreprend l'étude statistique de la relation entre la profondeur du transit et la métallicité de leurs étoiles-mères. Dès lors un niveau de confiance de -2.3σ est obtenu. Une tendance négative qui peut être expliquée par le modèle de formation planétaire par instabilité dans le disque. La métallicité augmente, l'opacité du disque augmente ce qui diminue le refroidissement et la formation des planètes géantes.

Avec ce résultat qui privilégie un modèle alternatif au modèle "traditionnel" de formation planétaire, il était plus que stimulant d'approfondir et d'étendre l'exploration de la validité de cette corrélation ou pas. Pour se faire, on a procédé par étapes. En premier lieu on a enlevé des données utilisées par DR12 toutes celles qui présentent des biais et qui ne correspondent pas aux critères de sélection. Basé sur le coefficient de corrélation de Kendall, on trouve un niveau de confiance qui passe à -0.7σ. Par la suite, on augmente notre échantillon de données en nombre et en qualité à deux reprises: jusqu'en Juin 2013 (Q0 à Q12) et Mars 2014 (Q0 à Q16). Et pour les deux séries de données on reproduit la même étude statistique et on trouve pour les deux une tendance positive entre la profondeur du transit et la métallicité de leurs étoiles-mères avec des niveaux de confiance respectifs : 0.4σ et 0.9σ

Tout au long de ce travail présent dans ce manuscrit, une certitude d'une tendance négative entre la profondeur du transit des planètes géantes et la métallicité de leurs étoiles-mères n'est pas aussi évidente. Cependant, une faible tendance positive jaillit de cette analyse. Pour cela, un scenario a été proposé recelant les deux théories de formation planétaires: l'accrétion à haute métallicité et l'instabilité du disque à faible métallicité.

Mots Clés: Étoiles: systèmes planétaires - méthode: statistique - planètes et satellites: formation - planètes et satellites : paramètres fondamentales

Chapter 1

Introduction

Before jumping into the exciting part of this thesis, this chapter will provide a historical overview on exoplanet as well as the aim for doing this work.

1.1 Historical Overview

We have more than 100 billion galaxies in the observable Universe; each one contains $\sim$ 100 billion of stars. These 10^{22} stars may all potentially host planets, a planet that is orbiting a star or stellar remnants outside our Solar System, called exoplanet or extrasolar planet.

This staggering number of stars raises some intriguing questions. What is an exoplanet or extrasolar planet, and how can we define it? How many of these are there? How did they form? Did they form like our Solar System formed? If we want to detect one of these exoplanets, do we have to observe all these 10^{22} stars? Where do we have to search? Can we find any correlation between the planets and their host star, to narrow this huge number of targets? There were also the question of the habitability of such planets; are we alone in the Universe? This is a question mankind has pondered for centuries, but only now we have the technology to begin to answer that age old question. And if there were Earth-like planets, around which type of stars can we find them?

Since the 5th century B.C., Leucippus, the Greek philosopher, together with Democritus, originate the theory of atomism[1] which was popularized and used to argue for the existence of extraterrestrial life. Although no original writings of Leucippus or Democritus survive, fragments of their teachings have been transmitted by later scholars such as Diogenes Laertius of the 3rd century AD who, in his *Lives of Famous Philosophers*, notes:

"Leucippus holds that the whole is infinite... part of it is full and part void... Hence arise innumerable worlds, and are resolved again into these elements."

---

[1] The belief that all matter consists of atoms.

In the 4th century B.C., 341-270 B.C, the Greek philosopher Epicurus developed further the doctrine of atomism, he reflected the idea that life exists elsewhere in the universe, he wrote:

"There are infinite worlds both like and unlike this world of ours... We must believe that in all worlds there are living creatures and plants and other things we see in this world."

His student, the Greek philosopher Metrodorus of Chios, 350 B.C., summed up the altitude of his mentor toward extraterrestrial life:

"To consider the Earth as the only populated world in infinite space is as absurd as to assert that in an entire field of millet, only one grain will grow."

In the 13th-century A.D. the Chinese philosopher Teng Mou from the Souing dynasty wrote:

"Empty space is like a kingdom, and earth and sky are no more than a single individual person in that kingdom. Upon one tree are many fruits, and in one kingdom there are many people. How unreasonable it would be to suppose that, besides the earth and the sky which we can see, there are no other skies and no other earths."

In the 16th century, 1548-1600, Giordano Bruno, an Italian Dominican friar, philosopher, mathematician, and astronomer known also as a pioneer thinker in the Copernicus model; believed that Earth rotates around the Sun and that the Sun is like other stars in the sky hence they are many other worlds orbiting other stars/suns. He said in his book *"De L'infinito Universo E Mondi"*:

"There are countless suns and countless Earths all rotating around their suns in exactly the same way as the seven planets of our system. We see only the suns because they are the largest bodies and are luminous, but their planets remain invisible to us because they are smaller and non-luminous. The countless worlds in the universe are no worse and no less inhabited than our Earth"

It was until 1992, that Aleksander Wolszcan and Dale Frail discovered the first confirmed exoplanets (Wolszcan & Frail 1992)[108]. A pair of bodies with masses of at least $2.8M_{\oplus}$ and $3.4M_{\oplus}$, respectively. However, rather than orbiting a normal star, they were found around a Pulsar (PSR 1257+12) - the supermassive remnant of a massive star that has exploded as a supernova.

The first detection of a planet orbiting a Solar-Like star[2] was made by Michel Mayor and Didier Queloz of the University of Geneva, in October 1995 (Mayor & Queloz 1995)[77]. This planet, 51 Pegasi b, is a giant planet orbiting the main sequence star 51 Peg about 50.9 Ly from Earth in the constellation Pegasus. It has a

---

[2]See section 2.1 for definition

period of $4.2 \pm 5e - 05$ days and a semi-major axis of $\sim 0.05 \pm 0.0030$ AU (about eight times closer than Mercury orbits the Sun), the exoplanet's surface temperature reaches $1,200\,°C$ hot enough to melt most rocks, thus it was dubbed as "hot-Jupiter"- planets with mass greater or close to that of Jupiter, their characteristic (mass, radius...) are close to Jupiter but they have higher temperature since they orbit very close to their host stars.

This was not an expected discovery by far, since the planet formation theory had not predicted the existence of such close-in planets, this has shown that by studying only our Solar System we cannot draw limited conclusion about the planetary system formation theory, our Solar System is just one sample and to understand the formation of our Solar System we need to do more discoveries, a bigger number of planetary systems to analysis them.

Since the discovery of the first exoplanet, significant development in exoplanets research techniques (Wright & Gaudi 2012)[63] and new discoveries of exoplanets with different sizes were made day after day. But the question asked was: What actually constitutes a planet? What is a planet?

In February 2003, the Working Group on Extrasolar Planet (WGESP) of the International Astronomical Union (IAU) produced a reasonable working definition of a "planet", agreeing to revise the definition as and when necessary. The WGESP has agreed the following statements:

1. Objects with true masses below the limiting mass for thermonuclear fusion of deuterium (currently calculated to be 13 Jupiter masses for objects of solar metallicity) (Burrows et al. 2001)[26] that orbit stars or stellar remnants are "planets" (no matter how they formed). The minimum mass/size required for an extrasolar object to be considered a planet should be the same as that used in our Solar System.

2. Substellar objects with true masses above the limiting mass for thermonuclear fusion of deuterium are **"brown dwarfs"**[3], no matter how they formed nor where they are located.

3. Free-floating objects in young star clusters with masses below the limiting mass for thermonuclear fusion of deuterium are not "planets", but are **"sub-brown dwarfs"** (or whatever name is most appropriate).

But, of course, there has been a lot of debate considering the definition of "planet" and the minimum mass/size required for an extrasolar object to be considered a planet especially after the discovery of Pluto's moon Charon in 1978 (Christy & Harrington 1978)[34], which permits us to accurately calculate Pluto's mass - roughly one twenty-fifth of Mercury's, making Pluto by far the smallest planet in our Solar System.

In the 1990, astronomers began finding objects in the Kuiper Belt, now called Kuiper Belt Objects (KBO) with the same composition as Pluto and in 2003, Mike Brown discovered a planetary-sized object farther than the orbit of Pluto (Brown et al. 2003)[24],

---

[3]At about 80 Jupiter masses, nuclear fusion of Hydrogen can begin and the object could potentially become a regular star and cannot be considered as brown dwarf.

named 2003 UB313 and later designated as Eris. It is larger than Pluto and has approximately 25% more mass. Hence the fact that we have nine planets in our Solar System begin to fall apart and Astronomers asked the question: What is Iris, a planet or a Kuiper Belt Object? They had to decide either Eris is a planet too or Pluto is not a planet.

The final decision, till now, about the definition of a planet was at the XXVIth General Assembly of the IAU, which was held from August 14 to August 25, 2006 in Prague, Czech Republic (Dymock R. 2006)[40] , the outcome of this meeting was that our Solar Sytem is made up of 8 planets (Mercury, Venus, Earth, Mars, Jupiter, Saturn, Uranus, Neptune), dwarf planets (Pluto and Eris was classified as dwarf planets, and hence Pluto is not considered as planet anymore) and small Solar System bodies, where the following new specifications completes the old ones and specify more what is a planet, a dwarf planet and a small solar system body:

1. A **"planet"** is a celestial body that (a) is in orbit around the Sun, (b) has sufficient mass for its self-gravity to overcome rigid body forces so that it assumes a hydrostatic equilibrium (nearly round) shape, and (c) has cleared the neighborhood around its orbit.

2. A **"dwarf planet"** is a celestial body that (a) is in orbit around the Sun, (b) has sufficient mass for its self-gravity to overcome rigid body forces so that it assumes a hydrostatic equilibrium (nearly round) shape, (c) has not cleared the neighborhood around its orbit, and (d) is not a satellite

3. All other objects, except satellites, orbiting the Sun shall be referred to collectively as **"Small Solar System Bodies"**.

As on July 2014, astronomers have discovered 1810 exoplanets around 1125 different stars (466 multiple planet systems)[4]. Many of these discovered planets are so different than planets in our Solar System and show extreme characteristics; some of the most important discoveries are:

- Kepler-10b, the first confirmed rocky exoplanet (Batalha et al. 2010)[10].

- kepler-7b, "the Styrofoam planet", it is a hot Jupiter with a really small density of only $0.166 g/cm^3$, about the same as polystyrene, a substance used to manufacture lightweight, disposable commercial plastic products (Latham et al. 2010)[69]

- 55 Cancri e, "the diamond planet", it rotates around a Sun-like star. It has a radius double the size of Earths, and weighs eight times more. The surface of this planet is likely covered in graphite and diamond rather than water and granite like Earth (Demory et al. 2011) [37]

- Kepler-16ABb, the first circumbinary planet - a planet that orbits two stars instead of one (Doyle et al. 2011)[38]

- kepler-22b, a $2.38 R_{\oplus}$ in the Habitable Zone (HZ) [5] (Borucki et al. 2012)[18]

---

[4]See *Extrasolar Planets Encyclopedia* at `http://exoplanet.eu/` for an updated list
[5]Zone around a star where it is neither too hot nor too cold for water to exist in liquid form

- Kepler-20 e & f, firsts Earth size planets (Fressin et al. 2012)[44]

- HD 10180, the largest known exoplanetary system in terms of total confirmed planets. It is a Sun-like star with at least seven planets and possibly as many as nine (Tuomi 2012)[101]

- Gliese 581 e, used to hold the title of smallest alien planet (Bonfils et al. 2007)[13], until the discovery of kepler-10b in January 2010. But today as on July 2013, kepler-37b is the smallest exoplanet and the first to be smaller than Mercury and it is barely bigger than our Moon (Barclay et al. 2013)[6]

- Kepler-62, a five-planet system with 2 planets falling in the Habitable Zone; Kepler-62 e and Kepler-62 f have 1.6 and 1.4 Earth radii respectively (Borucki et al. 2013)[19]

- PH1b (Kepler-64b), a transiting circumbinary planet in a quadruple star system (Schwamb et al. 2013)[92]

- Kepler-186f, the first Earth-size planet orbiting a star in the HZ (Quintana et al. 2014)[82]

Astronomers have detected different types of exoplanets, with different characteristics: mass, density, composition, temperature, period, metallicity, with or without atmosphere... ranging in size from that of terrestrial planets similar to Earth to that of gas giants larger than Jupiter. All these discoveries show that planetary formation theories are not accurate or at least something is missing. Hence, Astronomers started to study those discovered planetary systems, and to simplify their study and analysis, they tried to put exoplanets into groups, by comparing them to planets they know, the Solar System planets. Hence we have five main groups divided based on the exoplanet radius (R_p) relative to the Earth radius ($R_\oplus$):

1. Earth-like planets ($R_p < 1.25R_\oplus$)

2. Super-Earth planets ($1.25R_\oplus < R_p < 2R_\oplus$)

3. Small-Neptunian planets ($2R_\oplus < R_p < 4R_\oplus$)

4. Large-Neptunian planets ($4R_\oplus < R_p < 6R_\oplus$)

5. Giant planets ($R_p > 6R_\oplus$), where Jupiter-size planets range between $6R_\oplus < R_p < 15R_\oplus$ and larger exoplanets (super-Jupiter-size planets) have radius bigger than $15R_\oplus$.

Exoplanets can be completely defined by their mass too, and the term does not imply temperatures, compositions, orbital properties, adaptability, or environments similar to that of Earth, Neptune or Jupiter.
While Earth-like planets have mass similar to that of Earth, Super-Earth planets are planets with mass smaller than 10 Earth masses ($\sim 69\%$ of Uranus' mass, the least massive gas giant planet in our Solar System); considering the lower mass of a Super-Earth it varies from 1 (Valencia et al. 2007)[104], 1.9 (Charbonneau et al. 2009)[33]

to 5 (Fortney et al. 2007)[43] Earth's mass $R_\oplus$.

Other said that they are planets without a significant atmosphere, or planets that have not just atmospheres but also solid surfaces or oceans with a sharp boundary between liquid and atmosphere, which the four giant planets in our Solar System do not have (Seager et al. 2077)[93]. Hence, planets above 10 Earth masses are termed giant planets. Giant planets may be subdivided into "super-Jupiters" (more than 2-3 Jupiter masses up to brown dwarf mass), "Jupiters" (like Jupiter and Saturn, greater than 30 Earth masses), and "Neptunes" (of a mass similar to Uranus and Neptune, of 10-30 Earth masses).

1.2   Why studing the Planet-Metallicity Correlation?

We have more than 10^{22} stars in the observable universe, as mentioned above, hence it is something primordial to know where to look, where to search and around which star we can find a precise type of planets. Even if direct detection of exoplanet is now within reach, the bright host stars are accessible to even modest-sized telescopes equipped with high-resolution spectrometers. This is why we started to study the properties of parent stars (Gonzalez 1997)[50] since the detection of the first exoplanet, 51 Peg on October 1995.

And as many other exoplanets candidates were announced, many astronomers studied the intrinsic properties of their parent stars (Francois et al. 1996; Henry et al.1996; Perryman et al. 1996; Baliunas et al. 1997)[49][60][80][5] trying to find any correlation between the properties of exoplanets and the properties of their host stars; First, to narrow the number of stars selected for future planet search and second, to better understand the conditions that lead to planet formation.

With the help of the Kepler space mission a big sample of planets is available now to search for a relationship between the properties of exoplanets and that of their hosting parent stars. While the eclipse depth-metallicity correlation is not yet on firm statistical footing and was done before by studying a sample of 213 gas giant candidate planets (Dodson-Robinson 2012 [91] (DR12)), we will study in this thesis, using an extended sample, the correlation between the eclipse depths of Kepler's giant candidate/confirmed planets and the metallicity of their parent stars - Solar Like stars (FGK).

The aim of this work is to present statistical support for the correlation between the eclipse depths of giant planets and star metallicity. By using a larger sample of candidate and confirmed Kepler giant planets we aim to figure out a more accurate eclipse depth-metallicity trend and speculate about the implications for planet formation theory.

This thesis is organized as follows: Ch.2 will give a general review on some astronomical context necessary for the comprehensibility of this work. Ch.3 will provide an overview on all previous studies related to the plannet-metallicity relation. Ch.4

will outline the Kepler's data used in this thesis, and the statistical studies applied to interpret the eclipse depth-metallicity relation. The discussion and the implication of the results on planetary system formation theory will be presented in ch.5. Finally, the appendix contains tables presenting the sample of giant candidate/confirmed planets used to do this study as well as the Python scripts used to draw our graphs and to analyze the data.

Chapter 2

Astronomical Context

All giant planets used in our data are planets orbiting Solar-Like stars. The purpose of this chapter is to draw a small astronomical context in terms of definition of Solar-like stars, metallicity and its role and planet formation process.

2.1 Solar-Like Stars and their Importance

We are trying to find a carbon-based life, the only biological life we know of, and until now Earth is the only planet that harbors life. Since the Earth is rotating around the Sun it is obvious that we should search for other planets similar to ours, or "Earth-like planet" around stars similar to our Sun, or "Sun-like stars". But the question is why not to look around other type of stars?

Every star has a region around it that could support Earth-like life on an Earth-like planet, in this region the temperature is not too hot nor too cold for water to exist in liquid form, and it is called the Habitable Zone (HZ). As the age of the star increases, its luminosity increases and the HZ moves outward from the center of the system. For a planet to continuously support life, it should remain in the HZ as the star's age increases. We can say that the planet is in a Continuously Habitable Zone (Continuously Habitable Zone (CHZ)), in which a particular planetary orbit may remain while the star is on the main sequence (Kasting et al. 1993)[67].

Stars more massive than the Sun (O, B and A stars) have a larger Habitable Zone, but remain on the main sequence for a shorter time interval. Small red dwarf stars (late K and M stars) have the opposite problem, with a smaller HZ that is subject to higher levels of magnetic activity and the effects of tidal locking from close orbits. For example, hot O-type stars, which may remain on the main sequence for fewer than 10 million years, would have rapidly changing Habitable Zones not conducive to the development of life; planets may only have a brief window inside the HZ and a correspondingly smaller chance of developing life. Planets orbiting red dwarf stars, however, would have enough time for life to develop and evolve, due to the fact that their host stars can live for hundreds of billions of years on the main sequence. But the nuclear reactions of red dwarf stars proceed so slowly and they emit very little light,

any planet orbiting around one of them must be so close to attain Earth-like temperature. As a result this planet is a subject to higher levels of magnetic activity and it is mostly tidally locked in close orbits - this means that one face always points at the star (creating continuous day) and one face always points away (creating continuous night). Potential life could be limited to a ring-like region, known as the terminator, where the parent star would always appear on the horizon.

Hence, stars in the intermediate mass range such as the Sun have a greater likelihood for Earth-like life to develop (Selis 2006)[94]. Late F, G, K stars are only ones with right HZ stable for more than 4 billion years. And this is why it is so important to search around Solar-Like stars when we want to search for life in exoplanets.

Solar-Like stars or Sun-like stars, also called Habitable Stars are stars similar to the Sun in mass and evolutionary state. This means that physically they have broadly similar structure. They have spectral type of about F8V to K2V (from late F, G to mid-K), this corresponds to effective temperatures of a little more than 7,000 K down to a little more than 4,000 K. They seem to have the right balance: They are of high enough mass that they are more likely to host habitable planets, but they are of low enough mass that they live long enough for intelligent life to develop, and are not extremely rare.

2.2 The Metallicity and its Importance

2.2.1 Overview

13.7 billion years ago space and time began their fast expansion from a point of infinite density in the Big Bang. After a few minutes of matter-antimatter annihilation, the remaining matter particles settled into a ratio of 90% Hydrogen and 10% Helium, with trace amounts of Lithium and Beryllium. Clouds formed from those primordial particles collapsed through gravity to form stars and galaxies and then due to nuclear fusion inside stars, heavier elements were synthesized; those elements heavier than Hydrogen and Helium (the lightest 2 elements) are called "metals".

We represent the abundance of chemical composition by X, Y and Z where:

- $X \equiv \dfrac{m_H}{M}$ is the Hydrogen mass fraction, with m_H the mass of Hydrogen and M the total mass of the object.

- $Y \equiv \dfrac{m_{He}}{M}$ is the Helium mass fraction, with m_{He} the mass of Helium

- $Z = 1 - X - Y$ is the the metllicity or the mass fraction of all elements heavier than Helium.

For the Sun, $X_{sun} = 0.73$, $Y_{sun} = 0.25$ and the metallicity is $Z_{sun} = 0.02$

But in fact most Astronomers denoted the metallicity as "[Fe/H]" which represents the logarithm of the ratio of a star's Iron[1] abundance compared to that of the Sun. Spectroscopy is the technique used to find the amount of Iron and the amount of Hydrogen in an object by analyzing the absorption lines of Iron and Hydrogen respectively in a stellar spectrum. The ratio of the amount of Iron to the amount of Hydrogen in that object divided by the ratio of the amount of Iron to the amount of Hydrogen in our Sun gives us the metallicity of an object relative to the Sun. The formula for the logarithm is the following:

$$[Fe/H] = \log_{10}\left(\frac{N_{Fe}}{N_H}\right)_{star} - \log_{10}\left(\frac{N_{Fe}}{N_H}\right)_{Sun} \tag{2.1}$$

Where N_{Fe} and N_H are the number of Iron and Hydrogen atoms per unit volume respectively. The unit used for metallicity is "dex". And as we are using a logarithmic scale, stars with positive values would have higher metallicities than our Sun. Stars with negative values would have lower metallicities than our Sun while for the Sun [Fe/H] =0.0dex. So if we have a star with [Fe/H] = + 1, it means that this star have 10 times (10^1) the metallicity of the Sun since the logarithm is based on powers of 10. While if we have a star with [Fe/H] = - 1, it means that this star have on tenth (10^{-1}) the metallicity of the Sun.

Also the metallicty can be denoted as "[M/H]", which represents the star's total metal abundance not only the Iron abundance. It is a more general expression for the metallicity, it is the measurement of the amount of metal with respect to the amount of Hydrogen, in an object of study, compared to the solar metallicity (amount of metal per respect to the amount of Hydrogen in our Sun) plotted on a logarithmic scale as following:

$$[M/H] = \log_{10}\left(\frac{Z/X}{Z_{sun}/X_{sun}}\right) \tag{2.2}$$

$$[M/H] = \log_{10}\left(\frac{N_M}{N_H}\right)_{star} - \log_{10}\left(\frac{N_M}{N_H}\right)_{Sun} \tag{2.3}$$

Where N_M is the number of metal atoms per unit volume.

Those two ways to represent the metallicty are in fact related through the following equation:

$$[M/H] = c \times [Fe/H] \tag{2.4}$$

where c is a constant between 0.9 and 1.

Therefore, using equation 2.2 and 2.4 we can find the relation between Z and [Fe/H]:

$$c \times [Fe/H] = \log_{10}\left(\frac{Z/X}{Z_{sun}/X_{sun}}\right) \tag{2.5}$$

---

[1]Iron is not the most abundant element, but it is among the easiest to measure using Spectroscopy in the visible.

2.2.2 Metallicity Role

Mass and chemical composition are key quantities in the formation, evolution and fate of stars. A star of a given age is, to first order, characterized by these two physical parameters, and the influences of mass and metallicity extend to the formation and evolution of planets (Johnson et al. 2009)[64].

The metallicity is directly related to the age of the Universe. Stars formed from the primordial clouds directly after the Big-Bang are "metal-free" stars, called "Population III" stars[2]. Since those clouds contains only Hydrogen, Helium and a trace amount of Lithium and Beryllium, it is believed that those stars synthesized all the heavier elements (up to Iron) in their core via nucleosynthesis (Heger A. & Woosley S. E. 2002)[59]. It is also believed that Population III stars are very massive stars with masses hundreds of times larger than the Sun. Therefore they exhaust their fuel and die young in extremely energetic supernovae, ejecting some or all the elements they produced in their life time back into the interstellar medium. By doing so they make it a place more rich in metals and cause the formation of a newer star generation with a relatively good amount of metals, called "Population II" or "metal-poor" stars. In their turn, the massive Population II stars exhaust their fuel and eject all their metals in the interstellar medium clouds, leading to the formation of "metal-rich" stars or "Population I" stars. Therefore, each generation of stars is enriched by metals produced in the previous generations and older stars have lower metallicities than younger stars such as our Sun.

As the metallicity is related to the age and the formation of stars, it is also related to the formation of planets. Planets require the presence of heavy elements to form and to assemble their core, and since those heavy elements have been produce by fusion reactions in the early generations of stars and were not produce in the early Universe (directly after the Big Bang), many generation of stars must have passed to produce the material from which the planets formed (Johnson J. L. & Li H., 2012) [66]. This is why it is so important to study the metallicity of stars and check if any correlation exists between the metallicity of host stars and the size of planets around them to better understand the planetary system formation and hence the formation of our Solar System which, until now still have some missing points.

2.3 Planetary System Formation Theory

Planetary system formation theories were developed based on one unique sample, our Solar System and were not based on the observation of other planetary systems which have different characteristics than ours. Here, we will talk only about the theories of our Solar System formation.

As we know, we have eight planets in our Solar System, divided into two groups:

---

[2]Those stars are hypothetical and we did not detect any one since they formed at the early universe

- **Terrestrial planets:** Mercury, Venus, Earth and Mars also called Earth-like planets. They are rocky and dense planets, mainly composed of an Iron core surrounded by a Silicate mantle and an atmosphere.

- **Jovian planets:** Jupiter, Saturn, Uranus and Neptune also called Jupiter-like planets. Those planets lack solid surfaces. They are composed of a rocky core, surrounded with a liquid envelope and an atmosphere. And since they are so massive, the central temperature is so high therefore the rocky core is not solid, it is composed of heavy elements in liquid form. While the atmosphere is mainly composed of Hydrogen and Helium as well as water, Methane and Ammonia.

Core Accretion   Since 1897, T. C. Chamberlin baptist the concept of "planetismals" - accumulated solid objects to form planets. Suggesting with F. R. Moulton that planets were formed by accretion of cold solid particles (T. C. Chamberlin, 1916)[31]. Until now, the core accretion theory is the most accepted theory for planets formation, this is why we are going to develop it in details.

4.6 billion years ago, the Solar System formed from a "molecular cloud" called Nebula - It is a cool diffuse interstellar cloud of gas and dust, constituting mostly from molecular Hydrogen and Helium (98% of the total mass: 73% Hydrogen, 25% Helium), with traces of Oxygen, Carbon, Nitrogen, Neon, Silicon, Magnesium, Sulfur, Iron... Where the most abundant metals are Oxygen, Carbon and Nitrogen, together with Hydrogen they form the ice present in our Solar System: Water (H_2O), solid Methane (CH_4), Ammonia (NH_3), Carbon Monoxide (CO) and Carbon Dioxide (CO_2)...All this elements are called volatile elements because they condense at a temperature of $\sim 150k$, while less abundant metals like Iron, Silicon, Magnesium condense at a higher temperature of $\sim 1600K$.

A shock wave from a nearby supernova may have induced the formation of our Solar System, by creating regions of over-density within the nebular cloud causing these regions to collapse (Hoyle 1960; Cameron 1962; Cassen & Moosman 1981; Terebey et al. 1984)[61][28][30][99]. One of these regions has formed our Solar System. To conserve its angular momentum, the nebular cloud rotates faster as it collapsed. Due to this fast rotation, the nebular cloud collapsed with gas radiation into a fattened gaseous protoplanetary disk, as a result of centrifugal force from initial oriented rotation. And due to gravitational forces the material in the disk spiral inward toward the center. Therefore, the temperature and pressure increases, in the center, to start the fusion of Hydrogen and the formation of what we call "Proto-Sun" (Montmerle et al. 2006)[100]

The protoplanetary disk contain a mixture of gas and condensed matter consisting of surviving interstellar grains and solar nebula condensates (Lissauer 1993)[74]. From observations, we know that the gaseous part of the disk lasts only on the order of 1-10 Myr (Walter et al. 1988; Haisch et al. 2001)[106][55]. Planets form in the circumstellar disk that accompanies the star formation process therefore gas giants must form within this relatively short time.

Planets grow within circumstellar disks via collisions and accretion of small bodies which are known as planetesimals (Lissauer 1993)[74]. First, those planetesimals which may be a centimeter or meter in size, formed from further condensation where one atom or molecule attached itself to the main body. Then accretion takes over, and the two bodies collide to each other and stick together to form a bigger body which in turn collide to form larger bodies. This continues through further collision and once bodies on the order of 1-100 kilometers in diameter form, gravitational interactions between pairs of these planetesimals dominate and continue until the formation of large planetesimals called "protoplanets".

Protoplanets continue to grow and their gravitational well increases hence they can retain more amounts of gases from their surrounding disk. Certainly, massive protoplanets can capture larger amount of gas, producing Jovian-planets (Mizuno 1980; Hayashi et al. 1985; Bodenheimer & Pollack 1986; Pollack et al. 1996)[79][57][12][81]. And since the inner part of the Solar System is closer to the Proto-Sun, it is warmer than the outer part of the Solar System. Hence, volatile elements cannot condense at such a hot temperature and the planetesimals formed in the inner part of the Solar System could only form from metals with high melting point as Iron, Nickel, Silicates, etc... which form the rocky planets - terrestrial planets. And since those elements (Iron, Nickel, Silicates...) are so rare in the nebular cloud, terrestrial planets do not grow to be large as giant planets. While, on the other side, the most abundant elements after Hydrogen and Helium, form with Hydrogen the volatile elements which form in the outer region of the Solar System where the temperature is smaller and cool enough for volatile icy objects to remain solid. This allow the formation of larger planets in the outer part of our Solar System with a mass big enough (10-15 times the Earth mass) to allow the capture of Hydrogen and Helium (lightest and most abundant elements) to form the Jovian planets.
Some planetesimals did not grow up to form protoplanets, they stay in the circumstellar disk as asteroids, comets and debris (Lissauer 1993)[74].

However the time scale is a significant problem for this model; the giant planets must form its gas envelope during the lifetime of the gas disk ($\sim$1-10 Myr) while to form a core massive enough to accrete Hydrogen and Helium they take of order a million years. Also, this model cannot be simulated from the beginning since we have in the disk on the order of 10^{12} planetesimals, which is beyond today's computational reach. All simulations start with planetary embryos already as large as an Earth-mass.

Disc Instability Another planetary formation theory is possible for giant planet formation mechanism known as the "gravitational instability". In this model, density instabilities in the protostellar gas disk fragment into gravitationally-bound regions that contract in a similar way to the star formation (Cameron 1962, 1978; Boss 1998)[28][29][20]. However, this theory suffers from some problems (e.g. Rafikov 2005)[83] and there is a debate in the literature whether density instabilities survive to become protoplanets (Vorobyov & Basu 2006; Durisen et al. 2007)[105][39].

Planets Migration According to the core accretion theory, Uranus, Neptune, the Kuiper Belt and the Oort Cloud are in the wrong place, they could not be formed in a region where the smaller density of the Solar nebulae and the longer orbital times reduce their formation, they should be formed at smaller orbit where more material was available and then migrated away. Also, the existence of Hot Jupiter at such a close radii to their host star (51 Pegasi orbit it star about 8 times closer than Mercury is per respect to our Sun) is not explained by the core accretion theory, there was simply not enough matter in the disk so close to the star to form a giant planet there, and the temperature is too high to allow the formation of rocky or icy planetesimals. Planetary migration is the only way to explain the existence of such planets; it is the process by which a forming planet undergoes a drift of its semi-major axis caused by the tidal interaction with its parent protoplanetary disc. (Lin et al. 1996; Laughlin G. & Adams F. C. 1997)[72][70].

Many studies have been done to study the planetary systems formation theories to find which one is the most relevant. By discovering gaseous and dust disks around proto-star and T-Tauri stars (Deborah et al 1999[35]), the formation of terrestrial planets by the core accretion theory can be considered as an almost solved problem. However the time scale taken for giant planets formation is still a major problem for this theory. Therefore, in this work, we are trying to find the relation between the radius of giant planets and the metallicity of their host stars, in the aim of better understanding the formation process of those planets.

Chapter 3

Planet-Metallicity Relation

In this chapter all previous studies showing a planet-metallicty relation are discussed, as well as the work done by Dodson-Robinson 2012 [91] (DR12) which suggested a negative planet-metallicity correlation.

3.1 Planet-Metallicity Correlation

Spectroscopic studies of host stars of exatrasolar planets have revealed that stars with giant exoplanets tend to have higher metallicities than stars without giant exoplanets.

Scientists have two explanations for this Planet-Metallicity Correlation (PMC). The first explanation is that higher metallicity improves the formation of giant exoplanets, since it increases the availability of small condensed particles, the building blocks of planetesimals, which leads the formation of bigger cores with mass high enough to accrete Hydrogen and Helium and form giant planets. On the other hand, the second explanation is that the high metallicity in host star may be the result of late stage accretion of gas-depleted material, or what is called the "pollution of the Convective Zone (CZ)" of the star; metal-rich planetesimals or planets could have been consumed in the outer layer of their host stars during the formation process of planets, following migration through the protoplanetary disk (Lin et al. 1996; Laughlin G. & Adams F. C. 1997)[72][70] or gravitational interaction with other planets (Rasio F. A. & Ford E. B. 1996)[84]. And since the CZ is sufficiently thin for F-G stars, the depletion of one or a few Jupiter-like planets is enough to explain the observed metallicity enhancements above the field star average (Gonzalez 1997; Ford et al. 1999)[50][42]. The two explanations have different marks in the host star, in the first case, the star is formed from a nebular cloud rich in metal, therefore the star is metal-rich throughout. While in the second case, the CZ has only a high metallicity and the interior of the star has a lower metallicty.

In what follows, we will present the most important studies showing the PMC, which lasted for more than a decade.

Gonzalez 1997: Gonzalez (1997)[50] studies the metallicities of host stars of the first four detected exoplanets. Using Spectroscopy he found that ν And or HR 458 (F2V) and τ Boo or HR 5185 (F7V) are metal-rich stars relative to the Sun, which followed the trend set by the first two planetary systems studied before, 51Peg (G5V) and ρ^1 55 Cnc (G8V) which are super metal-rich stars with a metallicity [Fe/H] > 0.2 dex much higher than the average content of nearby dwarfs 0.17 ± 0.06 dex (Gonzalez G. & Lambert D. L. 1996; Taylor 1996)[52][98]. Those four systems share the same characteristics: approximately Jupiter-size planet in a very small and nearly circular orbit around a metal-rich Solar-Like host star. Hence Gonzalez concluded that the likelihood of a star harboring a planet was closely tied to stellar Iron content, or metallicity [Fe/H] and he proposed that the best explanation is the scenario of Lin et al. (1996)[72] where a gas giant spirals inward and caused the disc material to be accreted by the parent star during the planet formation epoch.

Santos et al. 2001: With the goal of settling the question about the PMC Fuhrmann et al. (1997; 1998)[45][46], Gonzalez (1998; 2001)[51][52] and Santos et al. (2000a)[87] studied the abundance of planets around metal-rich stars and found the same result. Nevertheless, the first uniform and unbiased comparison between stars with and without planetary-mass companions in a limited sample was done by Santos et al. (2001)[88]. The sample constitutes of 43 stars without giant planets, included in the CORALIE (Udry et al. 2000)[102] planet search program and a list of stars with giant planets were also observed and analyzed. Some of them have spectroscopic measurements made by CORALIE[1] and FEROS[2] spectra and others have spectroscopic measurements made by other authors, all having precise spectroscopic Iron abundance determined using the same technique and with nearly the same systematic error.

They studied the metallicity distribution of both samples (Fig. 3.1); it is the relative frequency of stars with and without giant planets (the number of star with or without giant planets for each metallicity bin over the total number of stars) in function of the metallicity of the star. We can see clearly from figure 3.1 that stars with giant planets companion (shaded histogram) are more metal-rich than stars without giant planets companion (empty histogram). The sample of stars with giant planets has a mean metallicity of $+0.15 \pm 0.23$ dex, while the sample of stars without giant planets has a mean metallicity of -0.1 ± 0.18 dex. The mean difference in [Fe/H] is ~ 0.25 dex. We will show the results in the table below (Table 3.1) in order to clarify the comparison.

---

[1]High resolution Spectrograph at the Swiss 1.2m Euler Swiss Telescope(La Silla Chile)
[2]High resolution Spectrogaph at the ESO 1.52m Telescope (La Silla)
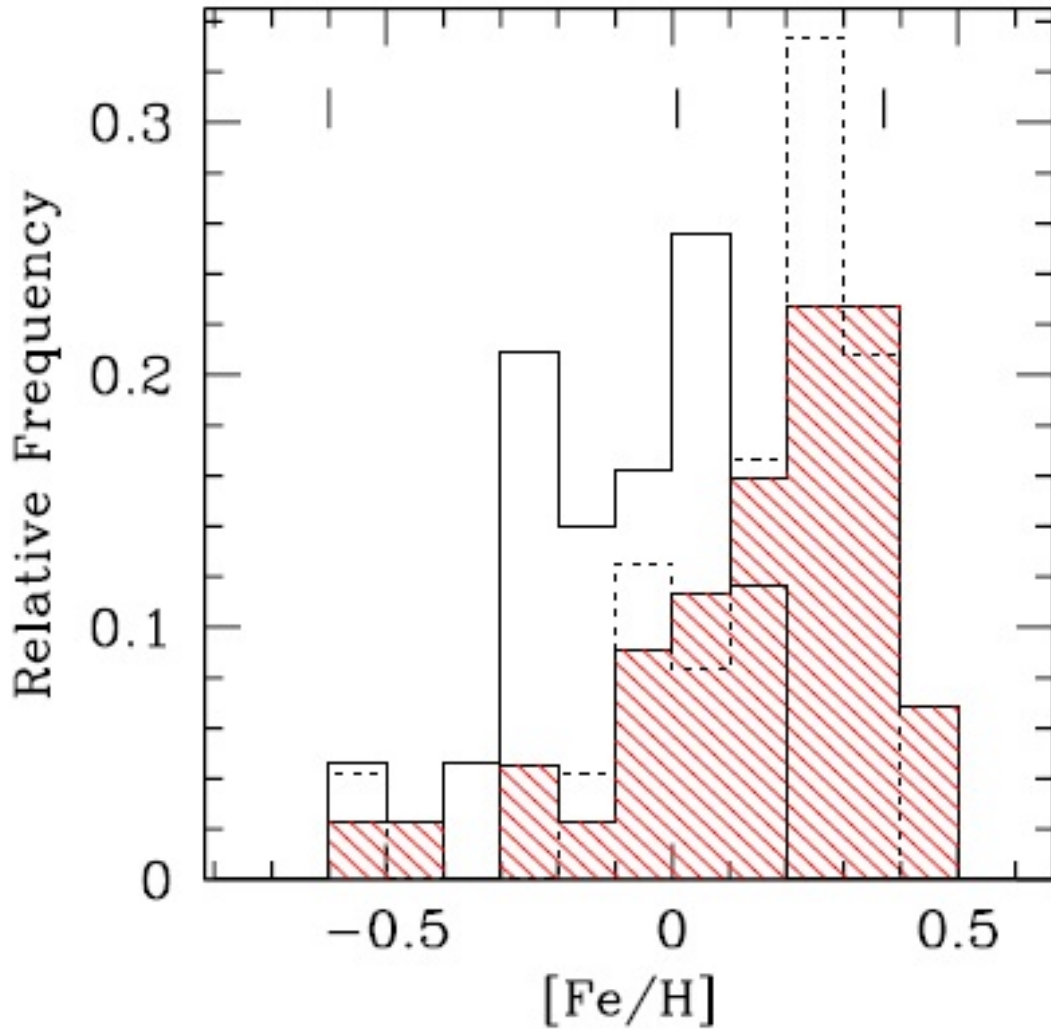
Figure 3.1: *A plot showing the metallicity [Fe/H] distribution of stars with giant planets (shaded histogram) and that of stars without giant planets (empty histogram). The dashed histogram represents the metallicity distribution if we consider only the stars taken from CORALIE survey. We can see clearly, that stars with giant planet companion (shaded histogram) are more metal-rich than stars without giant planet companion (empty histogram). The relative frequency of stars with and without giant planets, is the number of stars with or without giant planets for each metallicity bin over the total number of stars in that bin (Figure from Santos et al. 2001)[88].*

Table 3.1: The difference in metallicity between both samples of stars with and without giant planets

	Mean Metallicity (dex)
Stars with giant planets	$+0.15 \pm 0.23$
Stars without giant planets	-0.1 ± 0.18
Mean difference between both samples	0.25

And if we look at the shape of the distribution of stars with giant planets alone (Fig. 3.2), we can see clearly that it is rising with [Fe/H] (up to [Fe/H]~ 0.35), also this distribution is rising with the mass fraction of heavy elements Z (up to a value of 0.04) falling then abruptly. The only explanation for this cut-off was that we may be looking at a limit on the metallicity of stars in the solar neighborhood and it was difficult to explain it as pollution of the CZ.

The rising with [Fe/H] of the distribution of stars with giant planets has important inferences on the planetary systems formation theories. We can conclude that we have here a first support of core accretion that goes with no pollution of the CZ. This result is primordial, it is the simple fact that the higher metallicity in the original nebular cloud, the higher the metallicity in the star, the higher the availability of building block of planetismals hence the formation of bigger cores and the higher the probability of the formation of giant planets.

Santos et al. 2004b Spectroscopic studies of stars hosting giant planets continue (e.g Reid 2002; Santos et al. 2003a; Laws et al. 2003)[85][89][71], all of them found the same previous result: Stars hosting giant exoplanets are more metal-rich with respect to the average field dwarfs and they suggest that the high content of metal in stars was common to the nebular cloud that gave origin to the planetary system.

Santos et al. (2004b)[90], measured the metallicities using detailed spectroscopic analysis of a sample of: 93 extra-solar planet host stars and 41 stars not known to host any planet to confirm that giant planets are more common around metal rich stars. The Iron abundance of this sample (Fig. 3.3) show that stars with giant planets (shaded histogram) have higher metallicty than stars without giant planets (empty histogram) and the difference in Iron content is also ~ 0.25 dex (see table 3.1) which confirm all the most recent results on this subject (Santos et al. 2000a; Santos et al. 2003a)[87][89]...).

When they studied the metallicity distribution of giant planet hosts from CORALIE survey alone (Fig. 3.4), they found about 25-30% of stars above 0.3dex and 3% of stars with solar metallicity have giant planets, while there is a flat distribution for stars with [Fe/H]<0.0dex (Z<0.02).

Then they plotted the percentage of known giant planets (from the CORALIE planet search sample only) as a function of the mass fraction of heavy elements, Z (See figure 3.5). The plot suggested that the percentage of giant planets hosts is relatively
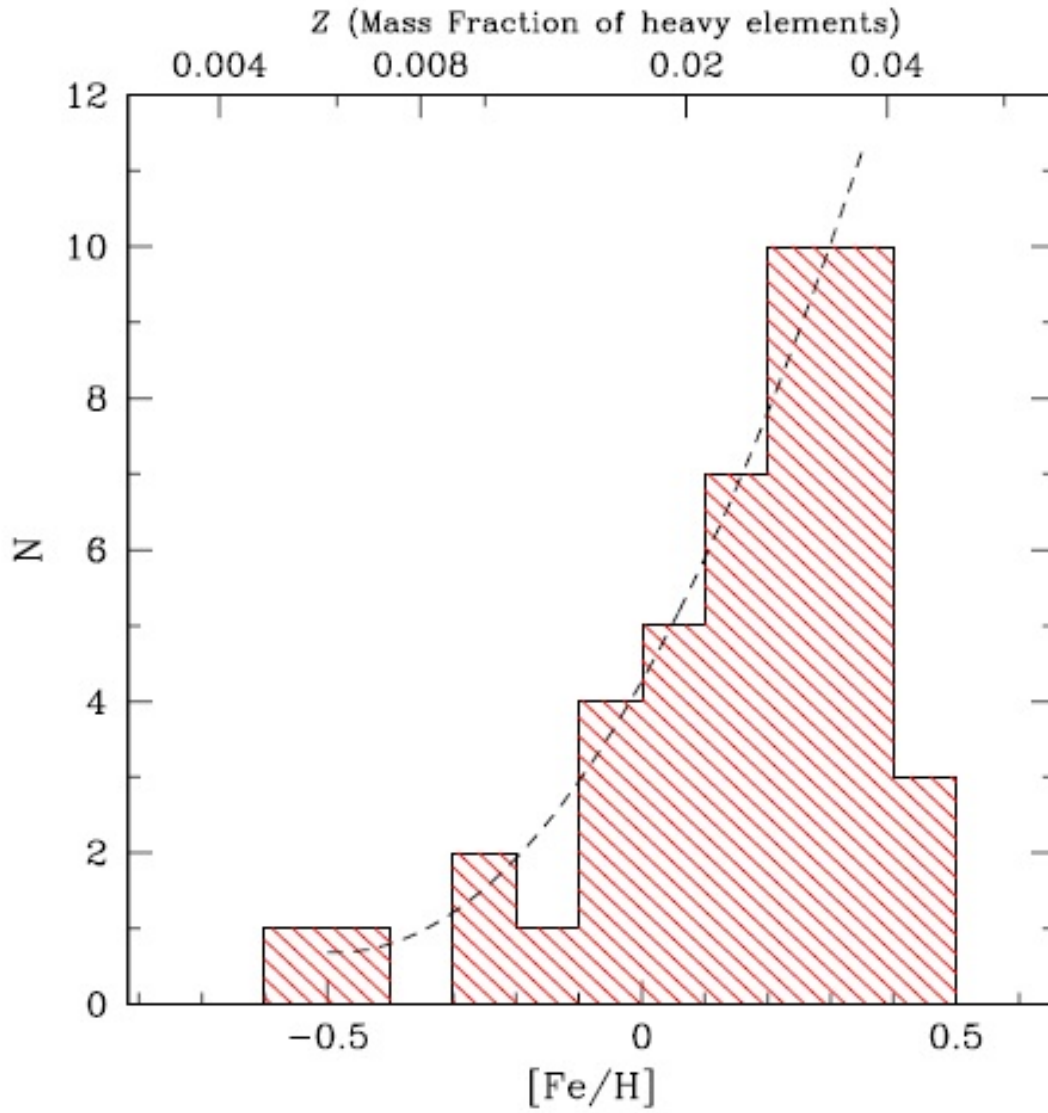
Figure 3.2: *Plot showing the number of stars with giant planets (N) in function of the star metallicity [Fe/H]. We can see that the shape of the distribution of stars with giant planets increases with [Fe/H] and with the mass fraction of heavy elements Z (Figure from Santos et al. 2001)[88].*
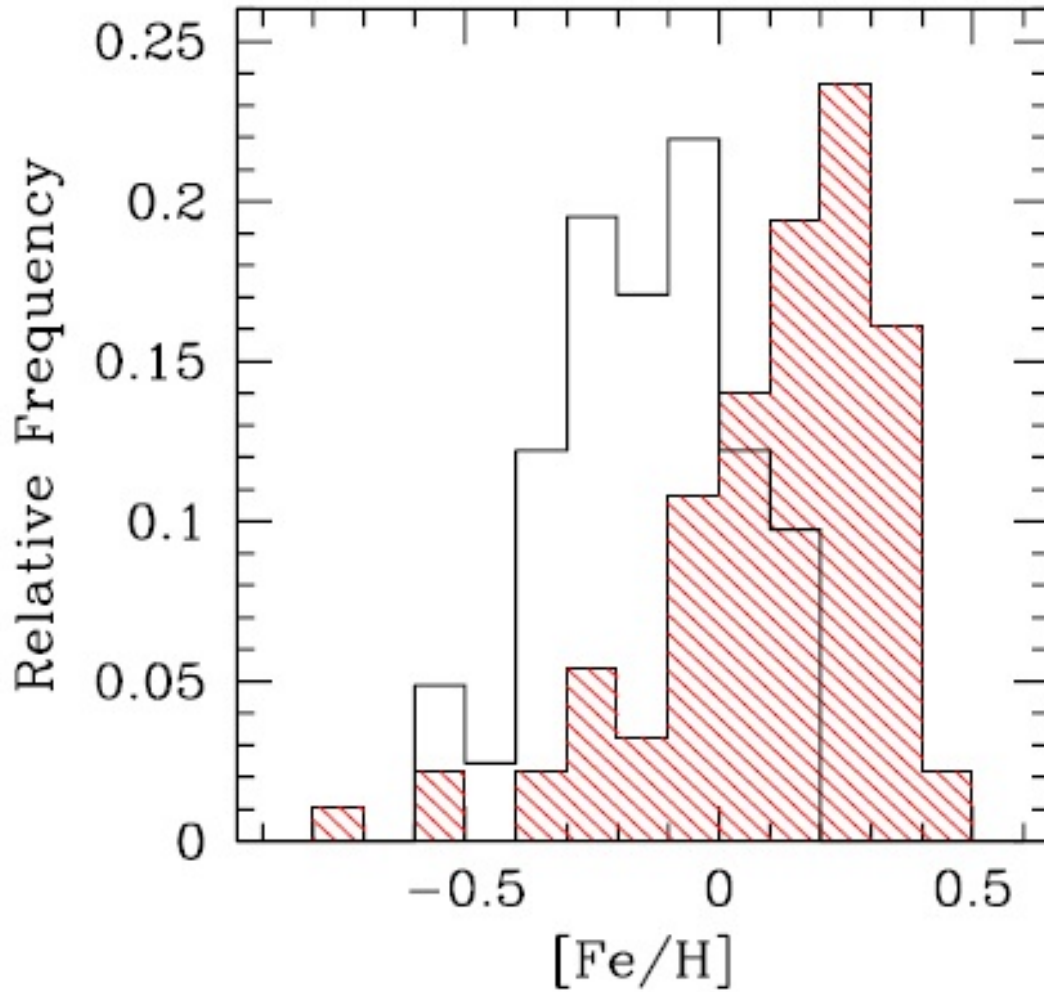
Figure 3.3: *A plot showing the metallicity [Fe/H] distribution of stars with giant planets (shaded histogram) and that of stars without giant planets (empty histogram). We can see clearly that giant planets are more common around metal rich stars (shaded histogram). The relative frequency of stars with and without giant planets is the number of star with or without giant planets for each metallicity bin over the total number of stars in that bin. (Figure from Santos et al. 2004b)[90].*

constant for Z < 0.02, reflecting therefore the flatness of metallicity distribution below the solar metallicity. The plot increases then linearly for higher Z values with an increase of 16% for each $\triangle$Z= 0.01 for $Z > 0.02$.

One possibility to explain this trend was the presence of two different populations of exoplanets, formed by two different processes. The first, the disk instability, does not depend on the metallicity and produces a constant minimum number of exoplanets as a function of [Fe/H] which explains the flat tail. While the second process, the core-accretion, is strongly metallicity-dependent, when the metallicity increases in the nebular primordial cloud, it increases in the star and in the planestesimals which increases the formation of giant planets and explains the runaway process for Z > 0.02.
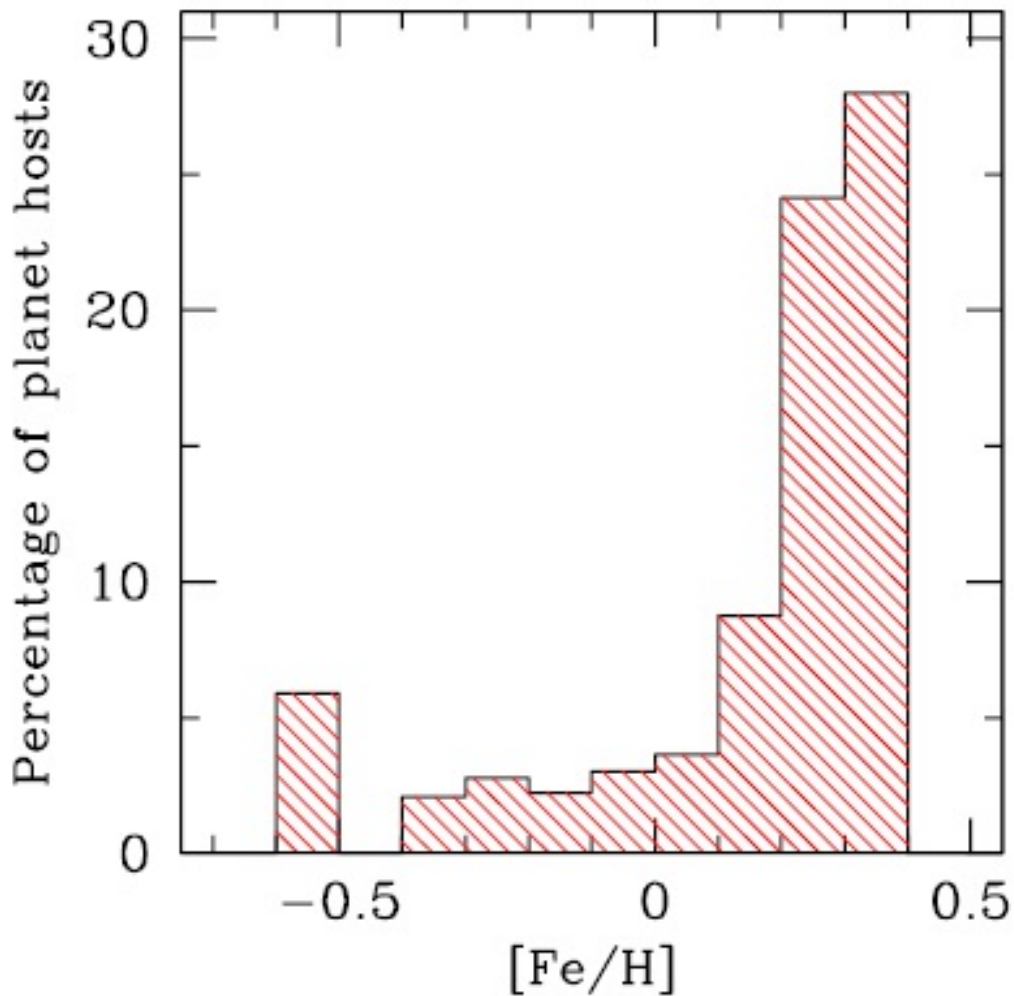
Figure 3.4: *Percentage of giant planets hosts from the CORALIE survey as a function of the stellar metallicity. From this plot, they found that $25 - 30\%$ of stars above 0.3dex and 3% of stars with solar metallicity have giant planets, while there is a flat distribution for stars with $[Fe/H] < 0.0$ dex $(Z < 0.02)$. (Figure from Santos et al. 2004b)[90].*
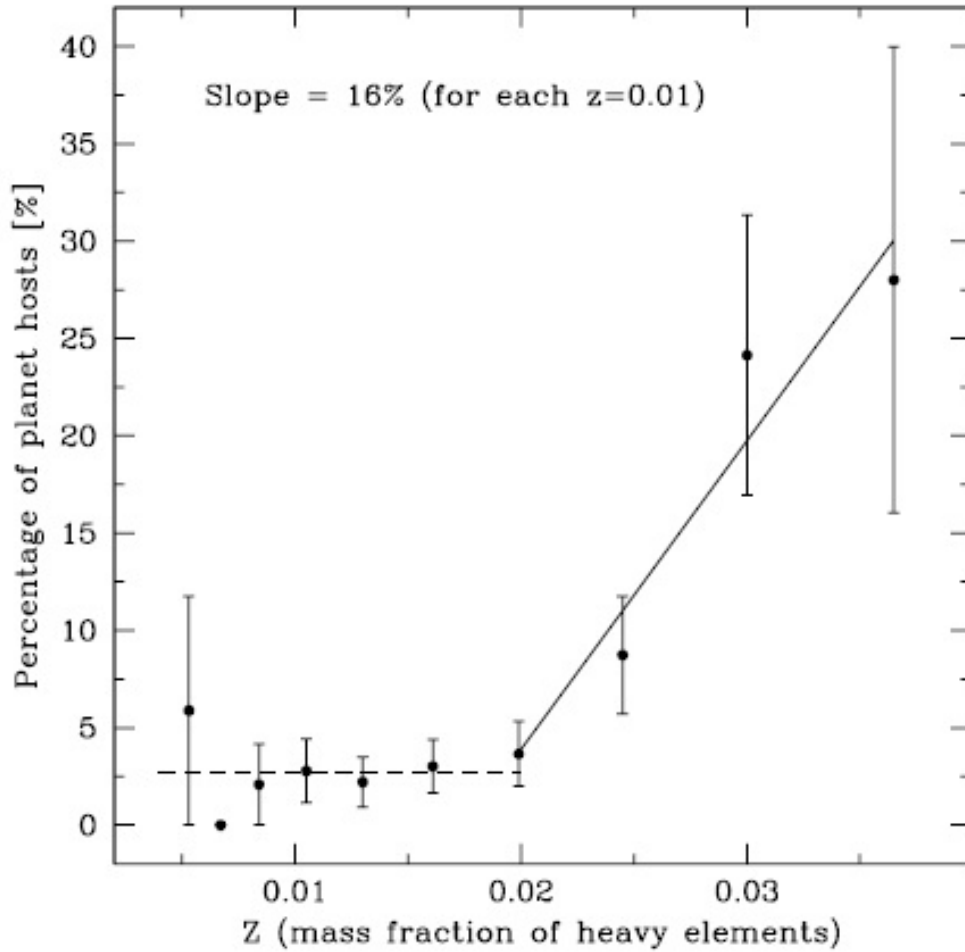
Figure 3.5: *Percentage of giant planets host (studied in fig. 3.4) as a function of the mass fraction of heavy elements Z. The plot reflects a linearly increase in the distribution of giant planets for Z > 0.0.2 and a flat distribution below the solar metallicity (Z < 0.02)(Figure from Santos et al. 2004b)[90].*

Fischer et al. 2005 [41] Debra A. Fischer and Jeff Valenti (2005), derived the metallicity [Fe/H] of 1040 FGK-type stars by carrying out a high precision spectroscopic analysis on the Keck, Lick, and Anglo-Australian Telescope planet search programs. It was the first time that a single and uniform spectroscopic analysis has been made for every star on a large Doppler planet search survey. From those stars they selected 850 stars, having at least 10 Doppler measurements over 4 years, allowing a uniform detection for all planets with radial velocity semi-amplitudes $K > 30ms^{-1}$ and orbital period shorter than 4 years.

Stars are then divided into bins of 0.25 dex, see figure 3.6, and in each bin they calculated the ratio of stars hosting giant planets to all stars in that bin and using Poisson Statistics they calculated the error in each bin. From this plot they found the same result as in previous papers: Stars with higher metallicities have bigger probability to host giant planets; we can see that no giant planets have been discovered around

stars with [Fe/H]< −0.1 dex and that the number of discovered giant planets increases when the metallicity increases (specially for [Fe/H]> 0.0dex).

And to examine the PMC in more detail they divided the star's metallicity into smaller bins of 0.1dex (see figure 3.7). This plot shows also an increase in the fraction of stars with giant planets as a function of increasing the metallicity above 0.0dex.

From figure 3.7 we can see that fewer than 3% of stars with $-0.5\text{dex} < [Fe/H] < +0.0\text{dex}$ have detected giant planets, while above the solar metallicity there is a smooth and rapid increase in the number of stars hosting giant planets, and above 0.3dex, 25% of observed stars have detected gas giant planets (Same result as Santos et al. 2004)[90]. The relationship shown in figure 3.7 quantifies the probability, of formation of a gas giant planet with orbital period < 4 yr and $K > 30ms^{-1}$ as a function of the metallicity by fitting an exponential to the histogram in [Fe/H]:

$$P(planet) = \alpha \times 10^{\beta[Fe/H]} \tag{3.1}$$

They find a best-fit of $\beta = 2.0$:

$$P(planet) = 0.03 \times 10^{2.0[Fe/H]} \tag{3.2}$$

Using equation 2.1, the correlation of planet-metallicity can be expresses as a power law:

$$P(planet) = 0.03 \left[\frac{N_{Fe}/N_H}{(N_{Fe}/N_H)_\odot} \right]^2 \tag{3.3}$$

Hence, according to Fischer et al. 2005[41], the probability of formation of giant planets is nearly proportional to the square of the number of iron atoms and what is interesting is that collision rates of particles are also proportional to the square of the number of particles which led to the conclusion saying that we have a link between dust particles collision rates in the primordial disk and the formation rate of giant planets. Therefore, we can say that giant planets formed by core accretion rather than gravitational instabilities within the disk.

Also, Fischer et al. 2005[41] used their sample to rule out the effect of the CZ pollution, arising from the capture of metal-rich material. To test the enrichment hypothesis, they used the fact that when a star leaves the main sequence its CZ deepens considerably leading to strong dilution if the high metallicity is the result of surface pollution. They compare the metallicity distributions of main-sequence and subgiant planet-bearing stars. As a subgiant evolve, the outer convective envelope is diluted by material in the stellar interior hence, if the PMC is limited to the convective envelope of main sequence stars, then subgiant with planets should show smaller metallicity. Nevertheless, the metallicity distribution of subgiants with planets was consistent with that of main-sequence stars with planets, and both subgiants and main-sequence stars with planets are more metal-rich than their counterparts without detected planets. This result supported the primordial theory of core accretion.
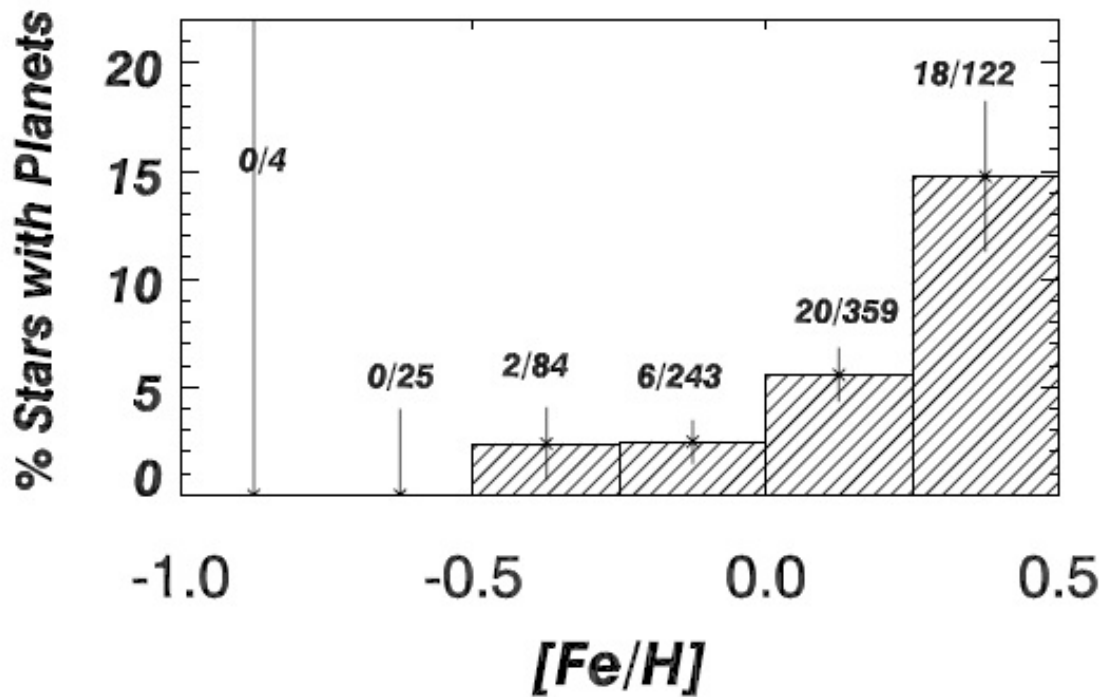
Figure 3.6: *The percentage of stars hosting giant planets increases with the metallicity. The number above each bar of the histogram, indicates the ratio of stars with giant planets to the number of all the stars within the bin of 0.25 dex (Figure from D. Fischer & J. Valenti 2005)[41].*
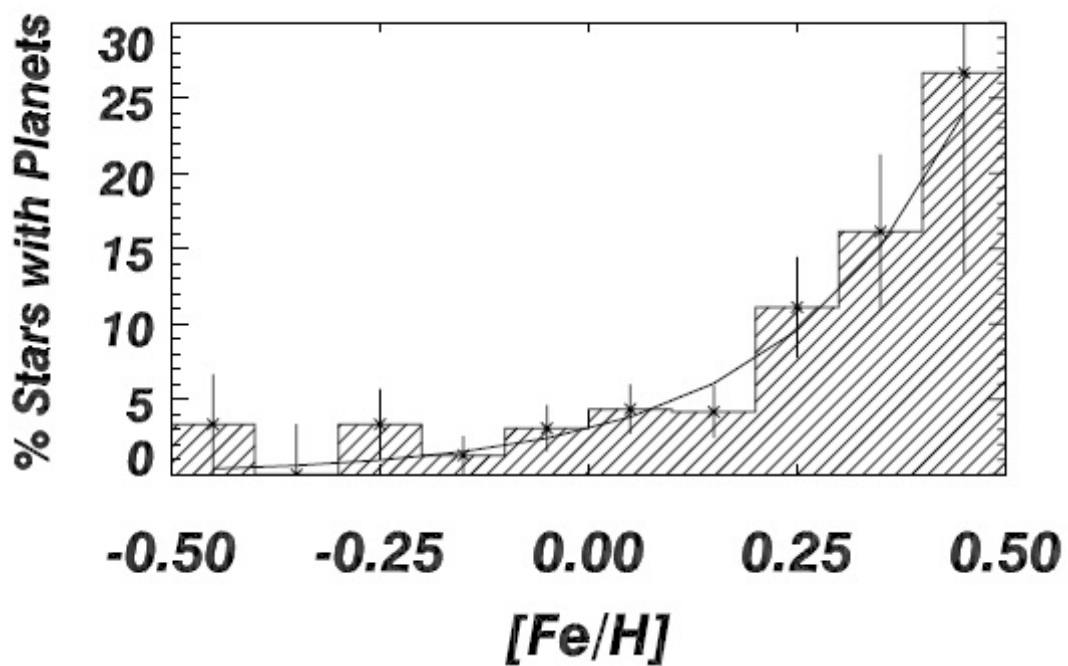
Figure 3.7: *The percentage of stars hosting giant planets increases with the metallicity. Same result as in fig.3.6, but with smaller metallicity bins of 0.01dex (Figure from D. Fischer & J. Valenti 2005)[41].*

Johnson et al. 2010 [65] To study the correlation between the occurrence rate of giant planets and the stellar properties, the metallicty and the mass of their host stars, Johnson et al. 2010 [65] analyze a sample of 1194 stars from the California Planet Survey. The stellar sample ranges from M dwarfs with mass as low as $0.2M_\odot$ to intermediate-mass subgiants with mass as high as $1.9M_\odot$.
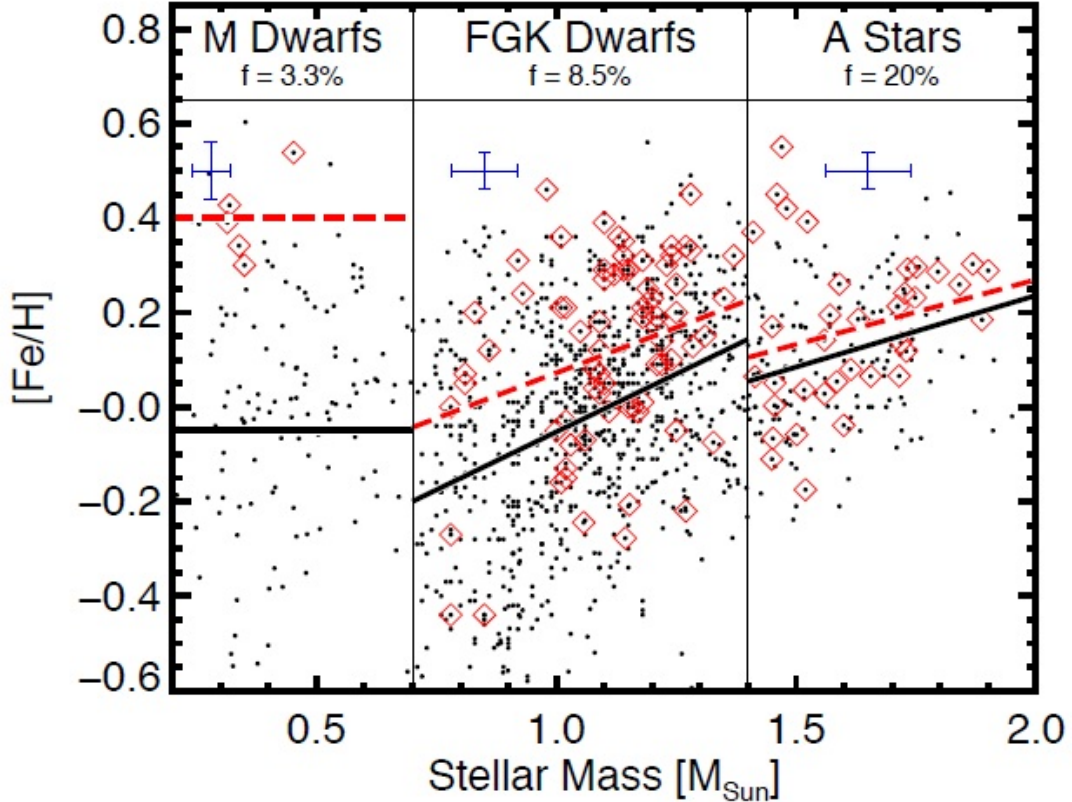
Figure 3.8: *Plot of stellar mass and metallicity for the 1194 stars (black dots) studied in Johnson et al. 2010. 115 of which harbor at least one giant planet (red diamonds). The plot is divided into three main groups above each one of them the fraction of stars with planet is plotted. This plot shows also the best-fitting linear relationships between mass and metallicity for all stars (black line), and for stars with giant planets (red dashed line). The blue 2-dimensional error bars represent the typical measurement uncertainties. (Figure from Johnson et al. 2010) [65]*
.

A plot of the stellar mass and metallicity is shown in figure 3.8 for all the 1194 stars (black dots), studies by Johnson et al., 115 of wich harbor giant planets (red diamonds). This plot is divided into three main groups: M dwarf stars, solar like stars, FGK stars and intermediate subgiant stars, A stars. From this plot we can see that stars with planets are more metal rich than stars without planets in the M dwarfs sample, the FGK dwarfs sample and the A subgiant sample.

As mentioned before in Fischer et al. 2005 [41], a lack of metallicity correlation in the subgiant sample is an evidence for the CZ pollution scenario. In this scenario as the star evolves of the main sequence, its CZ deepens and the metallicity is diluted by material in the stellar interior, so one might expect to see giant planets orbiting intermediate subgiant stars with small metallicties. From figure 3.8, we can clearly see that intermediate subgiant A stars with giant planets are more metal rich than their counterparts without detected giant planets. We can conclude that it is more likely to explain the PMC by the core accretion scenario than by the CZ pollution scenario.

Further studies have been done to prove the PMC, which continues and lasts for more than one decade (Guillot et al. 2006[54]; Grether D. & C. H. Lineweaver 2007[53]; M. Haywood 2009[58]; Johnson et al. 2010[65]).

All those studies show that the frequency of stars with giant planets increases with higher metallicity. This has important implications on the planetary system formation theories. As we said at the beginning of this chapter, we can explain this PMC by two theories: The core accretion theory and the pollution of the CZ which indicates that the formation of giant planets follows the disk instability theory. From the above studies, we can conclude that it is more likely to explain this PMC by the core accretion theory than by the pollution of the CZ; when the metallicity increases in the primordial nebular cloud, it increases also in the host star. High metallicity, means higher availability of small condensed particles, building blocks of planetismals increase and bigger cores with higher mass form, therefore they accrete more gas and form bigger giant planets with bigger eclipse depth. Hence, one should expect to see a rise in eclipse depth with increased metallicity.

Corresponding the flat distribution of giant planets at low metallicity (Fig3.2, fig3.4, fig3.7) we can say that we need a minimum metallicty in order to help gas radiation and cloud to collapse and to form bigger cores, therefore giant planets. Or, as found in Santos et al. 2004b [90], we may have another population of exoplanets formed by disk instability which is independent on the metallicty and produce a minimum number of exoplanet as a function of metallicity.

3.2 Eclipse depth Correlation: Negative Correlation between Star Metallicity and Gas Giant Radii

In both models of planet formation theories, the core accretion and the disk instability, a portion of a massive disk forms the bulk of the final mass of a giant or Jupiter-like planet. However, it is a race against time; as we said[3] the time scale is a major problem for the core accretion model, since the protoplanetary disc dissipates before the time needed to form a massive core allowing giant planets to form. Other-

---

[3]See section 2.3

wise, the disk instability model does not have this problem since planets can form from disk collapse in order of thousands of years compared to of order of millions of years required to form planets in the core accretion model. And what is important for our work, is that the disk instability model does not predict any correlation between the planet formation and the physical properties of their host stars, also it predicts that there is no correlation between the planet formation process and the disk metallicity (Boss 2002)[21]. Actually, Cai et al. (2006)[27] and Meru & Bate (2010)[78] show that the probability to form a giant planet in the disk instability model, *decreases* with increasing metallicity. But this prediction of the disk instability model was contradicted by all the previous studies[4] which show a strong correlation between the planets occurrence and the metallicity of their host stars and the disk instability was not considered as the primary mechanism for planets formation. Hence, proving that we have a correlation or a negative correlation between the planets occurrence and the metallicity of their host stars is something primordial to understand the Planetary System formation theories.

In what follows, we will present the work done by Dodson-Robinson (2012) to support the planet eclipse depth correlation.

Dodson-Robinson (2012) [91] proposed a negative correlation between the eclipse depth and stellar metallicity in the Kepler gas giant candidates(designated as planet eclipse depth correlation in this thesis). She showed that metal-poor stars host a higher proportion of gas giants with large radii than metal-rich stars, since metal-poor planets are less dense and have large radii than metal-rich planets of the same mass; Jupiter and Saturn should be larger, with bigger radii and smaller density if they were made up from pure Hydrogen and Helium (Demarcus 1958)[36]. Aslo she said that since metal-rich stars have smaller radii than metal-poor stars having the same mass and age, an identical population of planets would show a rise in median eclipse depth with the metallicity, but the fact that she find an opposite trend indicates that a change in the structure of gas giant must accompany the metallicity increasing to counteract the fact that eclipse depth must tend to rise with star metallicty for a uniform population of planets.

To show this trend, DR12 compares the radii of 213 gas giant planet candidates, from the Kepler survey, to the metallicity of their host stars.
The sample constitutes of giant planets with radius $5R_\oplus \leq R_p \leq 20R_\oplus$, whose host stars also have metallicities measurements from the Kepler Input Catalog (KIC), [M/H]. All planet candidates used in that study are listed in Table 1 in DR12. DR12 mentioned that the sample used is contaminated by as much as 40% eclipsing binaries, background eclipsing binaries, and hierarchical triples.

---

[4]Section 3.1

DR12 asked: "Is-are Kepler candidate giant planets orbiting low-metallicity stars larger in comparison to their host stars than candidate planets orbiting high-metallicity stars?"

To first answer this question, DR12 plotted the eclipse depth, ratio of the planet radius over its host star radius R_p/R_*, for all the candidate giant planets hosts in the selected sample as a function of the host star metallicity [M/H] and in terms of the insolation.

DR12 found that planets of all radii can appear around stars of all metallicities. Nevertheless there is a hint that eclipses may be deepest, on average, for low-metallicity stars since one might predict that planets orbiting low-metallicity hosts should have the lowest solid/gas ratio, making them the least dense, hence the biggest of planets. To quantify this expected trend in decreasing eclipse depth with metallicity, DR12 presented a statistical support by computing a running median with a 21-point window (solid black line) and a local polynomial regression of span 0.75 and degree 1 (dashed dot line). Both of them show decreasing trend in eclipse depth with [M/H] specially in the range $-0.1\text{dex}\leq [M/H] \leq 0.3\text{dex}$. This appears in figure one in DR12 (See fig. 3.9)

According to DR12, one possibility to explain this trend was that irradiation from the center star depends on metallicity, it affords the energy needed to inflate hot Jupiters and slows the planetary contraction. And since for a given mass a star of low metallicity is slightly bluer and hotter than a star with higher metallicity, it irradiates more than its counterpart at high metallicity and tend to host larger-radius planets. This is why points on the plot (Fig. 3.9) are color-coded by level of stellar irradiation, or "insolation" at the planet orbit. Nevertheless, in DR12 we found that there is no indication that planets orbiting low-metallicity hosts are more irradiated than other planets and therefore we can rule out difference in irradiation levels as the reason for this trend.

To confirm the trend that she may found from the polynomial regression, DR12 plotted a histogram (see figure 3.10), where she divided the metallicity into four broad bins and plotted the fraction of planets candidates for which $R_p/R_* > 0.13$[5] (Counting up the number of planets candidates in each histogram bin that have $R_p/R_* > 0.13$ and dividing it by the total number of candidates planets in that bin) and using Poisson Statistics she calculated the error in each bin.
From this histogram (Fig. 3.10), we can see that stars in the lowest-metallicity bin host higher fraction of planets that are large in comparison to their host stars than the stars in the higher metallicity bins. Nevertheless, we should notice that the error bar on the fraction of high eclipse depth are so big, and that the error bar in the lowest metallicity bin overlap with the error bars on two of the other three bins. Hence, we cannot be sure about this trend of decreasing eclipse depth with metallicity. More data are needed to have a more accurate plot and result.

---

[5]Sarah E. Dodson Robinson choose 0.13 since it is a typical eclipse depth of well studied giants planets.
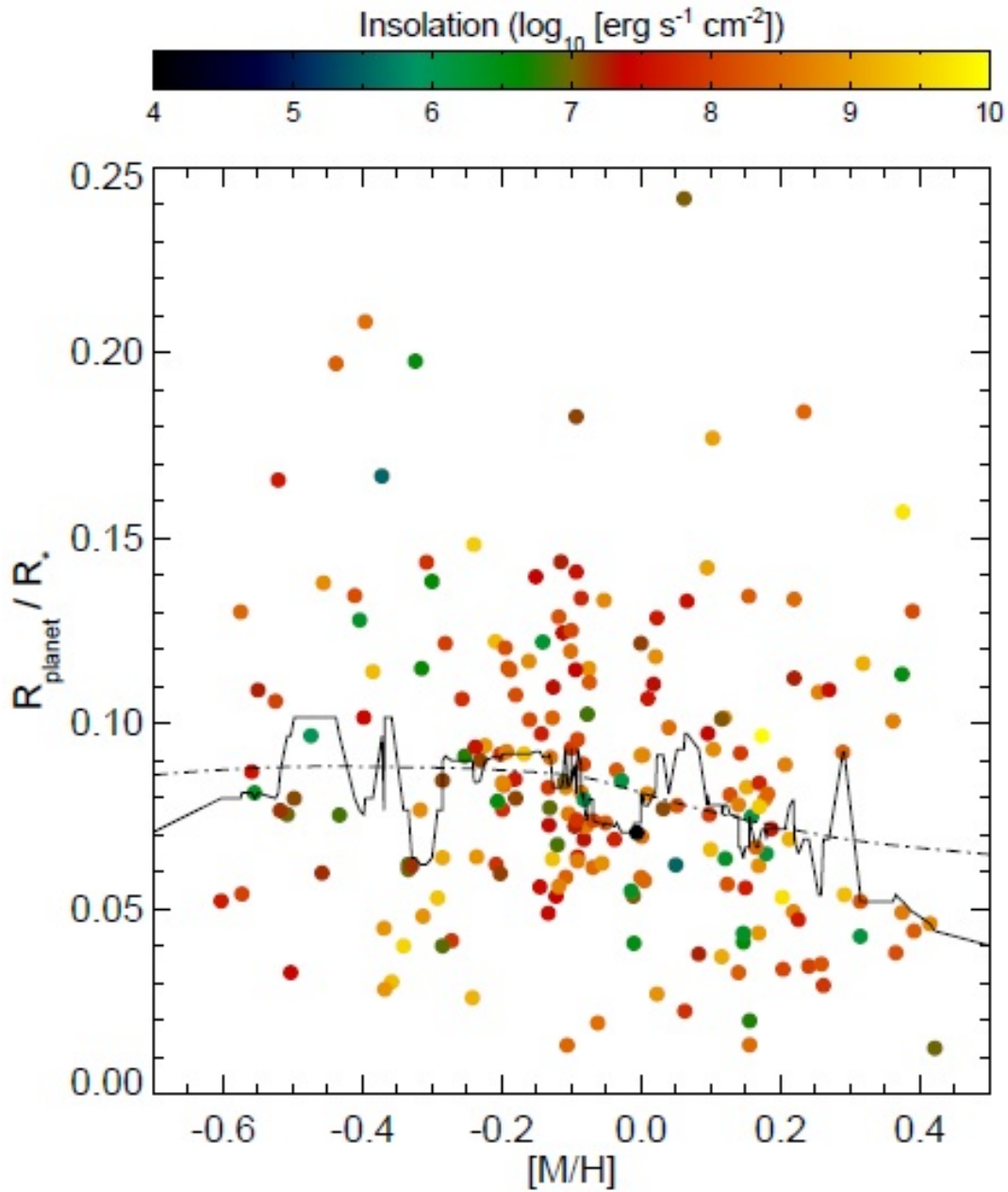
Figure 3.9: *Plot of the eclipse depth of Kepler's giant candidates R_p/R_* as a function of the host star metallicity [M/H]. Points on the plot are color-coded by level of stellar irradiation, "insolation" at the planet orbit. A running median with a 21-point window (solid black line) and a local polynomial regression of span 0.75 and degree 1 (dashed dot line) are computed and shown in the figure (Figure from DR12)*
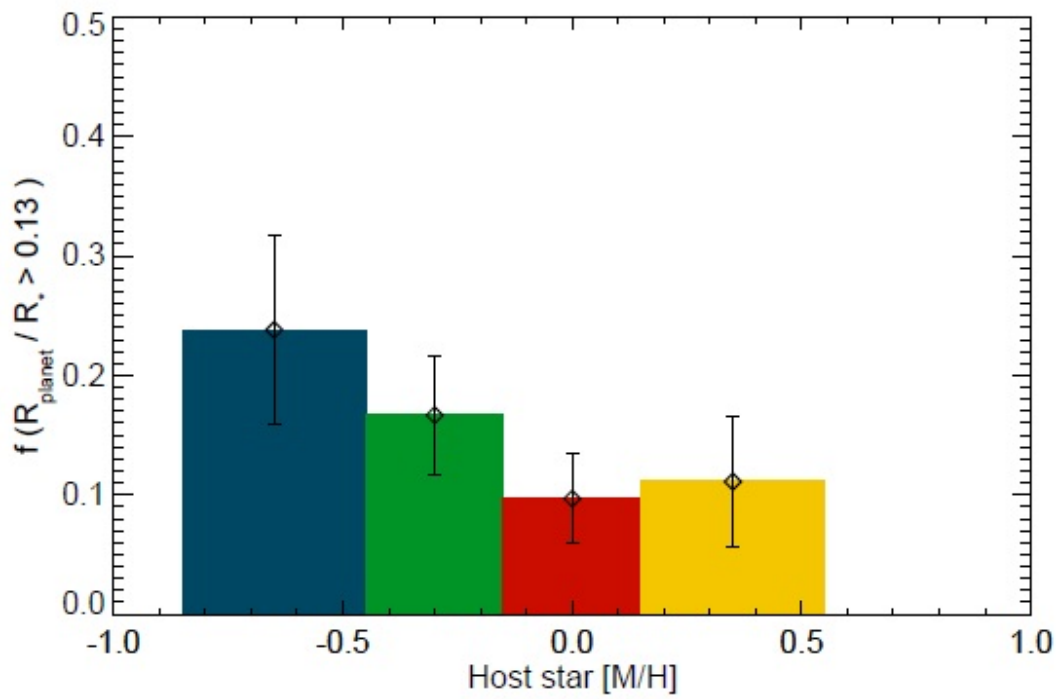
Figure 3.10: *Fraction of giant planet candidates having R_p/R_* > 0.13 in function of the metallicity. Planets orbiting lowest-metallicity host appear to have higher eclipse depth than planets orbiting higher-metallicity hosts (Figure from DR12)*

Sarah E. Dodson Robinson, proposed that this trend is due to the presence of two different population of planets formed by two different theories; Giant planets orbiting low-metallicity stars predominantly formed by gravitational instability while giant planets orbiting high-metallicity stars predominantly formed by core accretion. This explanation is consistent with that of previous studies of Santos et al. (2004)[90] and Udry & Santos (2007)[103] who found that the frequency of giant planets as a function of the metallicity is flat below the Solar metallicity.

Chapter 4

Application: Correlation between the Eclipse Depth and Metallicities of Stars Toward an Extended Sample

With a bigger sample of gas giant candidates/confirmed in hand than that studied in DR12, we now present in this chapter an extended statistical study of the correlation presented before. We will expose as well the Kepler's data used for this purpose.

4.1   The Kepler Mission

Mission's Goal

The *Kepler mission* is a NASA mission launched on 2009, March 6 in the aim of detecting Earth-like planets in the Habitable-Zone, around Solar-Like stars (F to K dwarfs) (Borucki et al. 2008; Borucki et al. 2010)[14][15].
Although, it main purpose is to detect Earth-like planets in the Habitable Zone, kepler has made a large number of observation with important value in Stellar Astrophysics, like in Astroseismology (Stello et al. 2009;Chaplin et al. 2010)[97][32], Astrometery and the study of Solar-Like stars (Basri et al. 2010; Chaplin et al. 2010)[7][32], the study of eclispsing binaries (Giménez 2006)[47]...

Method used

The method used to achieve this goal is the transit method (Fig. 4.1), which gives the orbital period and the planet's size relative to its host star; combined with radial velocity measurements we can obtain the mass, radius and density of the planet (Wright & Gaudi 2012)[63]. Those two techniques are by far the most important methods to detect exoplanets, we can see that clearly from figure 4.2-a. Both techniques infer the planetary existence from changes in their host stars, the first based on photometry and the second based on Spectroscopy.
The radial velocity technique measures the motion of the star along the Line of sight

(LOS) through the Doppler Shifts, by measuring the radial reflex motion of a star in response to an orbiting planet. It gives us the period, distance and shape of the orbit, also it provides information about the orbiting planet's mass. The problem in this technique is that we cannot know whether we are viewing the system edge-on or if we are viewing it at an angle to the line of sight between the plane of the orbit and the Earth - called inclination angle (i). Hence, the mass given by this technique is considered as a lower limit and the true mass of the detected exoplanet is higher by a factor of $1/\sin i$ (Wright & Gaudi 2012)[63].

A planetary transit occurs when the planet passes in front of its host star from our perspective (along our LOS). In this case, we will detect a brief, periodic dim in the Light Curve (LC) of the star, which indicates the passage of the planet (Wright & Gaudi 2012)[63], see fig. 4.1.

The best detection of a transit is when we are observing nearly perpendicular to the celestial sphere or edge-on. If we have a group of stars with planets orbiting in circular orbit around them with random inclination angles, the geometric probability to detect a transit will be:

$$P_{tr} = \frac{R_*}{a} \tag{4.1}$$

With R_* the stellar radius and a the semi-major axis.

If we take the case where Jupiter is transiting the Sun, the probability to observe such an event will be $P_{tr} = \frac{1}{1000}$, so if we consider that all stars host planets we have to observe 1000 stars in order to detect one transit. And this is why Kepler team selected a Field of View (FOV) rich in stars in order to increase the probability of detecting transits.

We can also notice that this probability increases if the planet orbits closer to its host star (lower semi-major axis a), or if the stellar radius R_* is larger, and this what lead the photometry method to be biased towards detecting short-period planets close to their stars, often of relatively large mass as we can see in figure 4.2-b. The lack in observing planets that have a long period and low mass is expected to be a selection effect, as these are very hard to detect with the current methods but since Kepler is observing the same FOV for a longer time, the probability to detect these kind of planets increases with time. Each successive catalog contains smaller planet candidates with longer orbital period. See figure 4.3 (Batalha et al. 2012).[11].

Photometric Precision

Although, we can see from Fig 4.1 that during a transit the planet blocks some of the starlight because planets are cooler than stars. The percentage of flux loss during transit is referred to as the transit depth and it depends on the size of planets relative to its host star:

$$\partial F = \left(\frac{R_p}{R_*}\right)^2 \tag{4.2}$$

Where R_p is the planet radius and R_* is the host star radius. Hence, a deeper transit depth can be due to a bigger planet or smaller star. The difference in brightness is important because it determines the photometric precision needed to detect such a
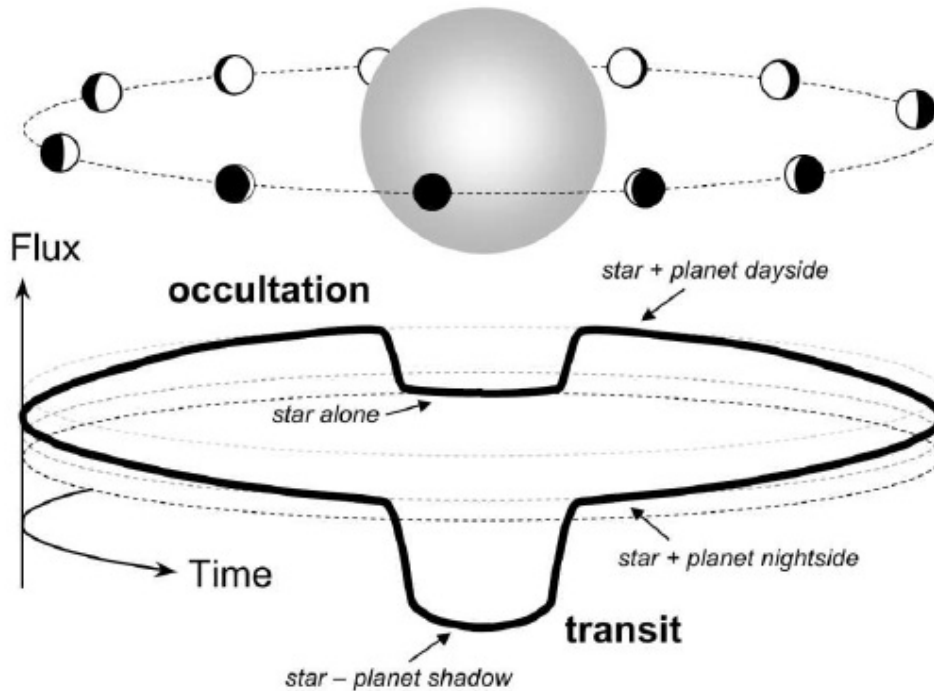
Figure 4.1: *Illustration of transits and occultations, considering the combined flux from the star and the planet versus time. During the transiting, the planet blocks a portion of the starlight causing a dim in the light curve. Then the planets dayside comes into view and the flux decreases again when the planet is behind the star, during the occulation (Winn, 2010)[107].*

transit. Taking again the case of Jupiter around the Sun, the difference in brightness is $\partial F \approx 0.01 mag$ or $\approx 1\%$. While for an Earth-size planet around the Sun, the transit LC has difference in brightness of 84 parts per million (ppm) or 0.0084% with a central transit time of 13h. For kepler, to detect an Earth-Sun analog with an 84ppm signal, the expected differential photometric precision is 20ppm at V=12 for a 6.5-hour transit (half of a central transit duration for an Earth-Sun analog) (Koch et al. 2010)[68].

Photometric and Spacecraft Design

The spacecraft is built around a Schmidt camera, with a 0.95m aperture and a 1.4m primary mirror. The instrument's FOV encompasses over a 105 square degrees (approximately the area covered by the spread hand held at arm's length) and its detector is a mosaic of $421,024 \times 2,048$ pixel CCDs (charged coupled devices). The CCDs are read out every 6 seconds to avoid saturation (See figure 2 in Koch et al. 2010[68]).
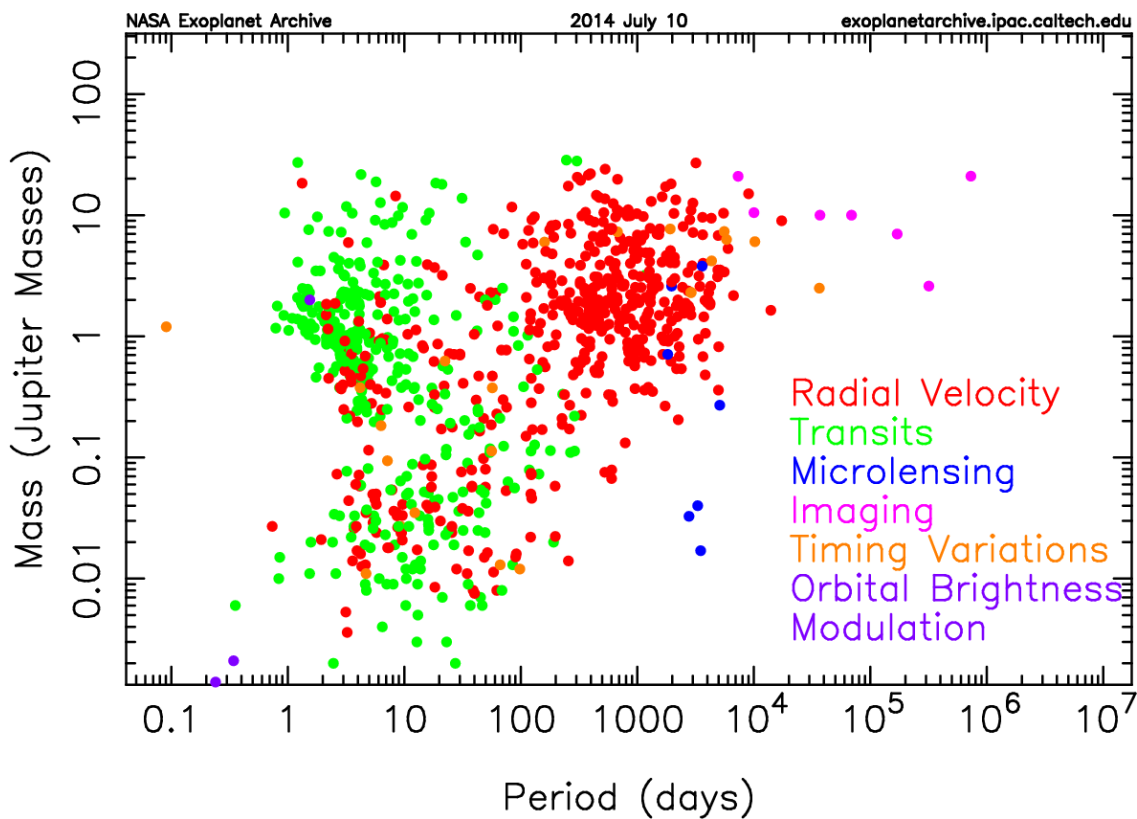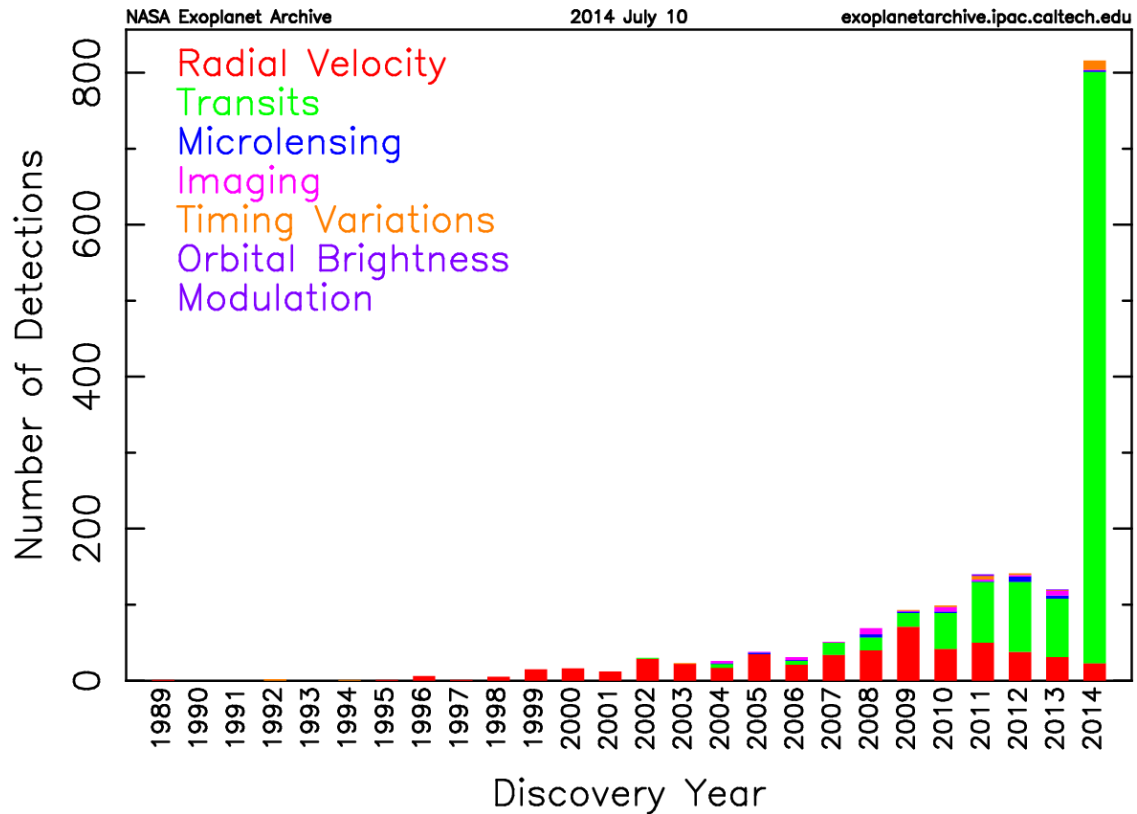
Figure 4.2: *The current status, as on July 2014, of the confirmed exoplanets, colorcoded for the different detection techniques. The top figure sorts the number of confirmed exoplanets by their discovery year, the bottom figure gives an overview of period and mass of the planets. Figures taken from the NASA Exoplanet Archive* `http://exoplanetarchive.ipac.caltech.edu/`

The Orbit

Kepler was launched in an Earth-Trailing Heliocentric Orbit (ETHO) with a period of 372.5 days. This has several advantages over a low-Earth orbit (such as e.g. COnvection ROtation and planetary Transits (CoRoT)). It is more stable for precision photometry, the spacecraft is not passing in and out of Earths shadow and heating from the Sun, there is no continuously varying earthshine getting into the telescope (Koch et al. 2010)[68]

Field of View

Kepler Science operation began on May 13, 2009 observing the same FOV which has the advantages of selecting the richest available star field; optimizing the spacecraft design; simplifying operations, data processing, and data accounting; maximizing the duty cycle and hence increasing the photometric stability; also allowing continuous Asteroseismic measurements over long periods of time. The 105 square degree FOV is centered on the Cygnus-Lyra region (RA:$19^h22^m40^s$, DEC $40°30'00''$) which is above the Orion arm of the galaxy just above the galactic plane (Borucki et al. 2008)[14]. This FOV was chosen because its the richest portion of the sky in stars, which always stay out of the ecliptic plane so it cannot be blocked by the Sun or the Moon (Koch et al. 2010)[68].

Mission Duration

It is so important that Kepler points at the exact same FOV throughout the whole mission in order to achieve the goal of this mission, we need enough time to detect and confirm transits of Earth-size planets in or near the Habitable Zone; and to have confidence that the signatures detected are of planet, we require at least a sequence of three transits all with a coherent period, brightness change, and duration. And for earth-like planets in the Habitable Zone (HZ) of a Sun-like star, those transits would only occur every year or so hence we need at least 3 years to detect Earth-size planets around Sun-like stars (Koch et al. 2010)[68]. That is why the mission duration was proposed to be 4 years, which permits the detection of four-transits of orbits up to 1 year in length and the detection of three-transits of orbits up to 1.33 years period. Also the Kepler team proposed a two years extension, which permits the detection of planets smaller than the Earth and the detection of Earth-size planets with period of 2 years (in orbit corresponding to that of Mars). But, on May 2013, the spacecraft experienced a serious technical error, two of the spacecraft's four reaction wheels which are used to steady the spacecraft were not functioning properly, the first one was damaged in 2012, the spacecraft is no longer able to perform necessary and to continue hunting for potentials planets.

The Kepler project has thus suggested the Kepler's Second Exoplanet Mission (K2) mission to NASA via the 2014 Senior Review process. The name K2 is chosen to distinguish between this new mission and the Kepler primary mission(Howell et al. 2014)[62]. K2 is named as being a 2-wheel Kepler, the second Kepler mission, or as comparison with the enigmatic and challenging mountain of the same name. In this

mission, engineers at Ball Aerospace, planned to use the pressure from the Suns light particles to push on the spacecraft on the right way, essentially acting as that mission third reaction wheel. K2 will examine the sky along the ecliptic plane for the next 2-3 years, it is capable of illuminating many aspects in stellar astrophysics across the H-R diagram and providing detailed observations of variable galaxies and early time observations of supernovae.

Target's Characteristics

Ground-based observing campaign choose $\sim 150,000$ stars from the half billion stars in Kepler's FOV that are brighter than 16th magnitude. The targets are dominated by G-type stars on or near the main sequence and stars fainter than 14th magnitude (Batalha et al. 2009; Batalha et al. 2010)[8][9].

Data Analysis

The data are divided into quarters. The first two data sets are Q0 (9.7 days taken during commissioning) and Q1 (33.5 days of data). All others quarter data contain 93 days of observations, after which the spacecraft must execute a $90°$ roll to keep the solar arrays pointed toward the Sun, in the aim of maximizing electric power production and thermal control, while keeping the instrument aimed toward the target FOV. This causes a data gap of 42 hours. Another gap of 26 hours, is caused once a month while the data is downloaded to the Earth via NASA's Deep Space Network (Batalha et al. 2012; Hass et al. 2012)[11][56]. For this work, data from Q0 until Q12 have been used[1].

After down-link and pixel archiving, the data arrive at the Kepler pipeline software module[2] which stitches together all quarterly data to form one continuous LC. Then systematic-error corrected light curves are passed to the Transit Planet Search (TPS) to identify possible transit event (Batalha et al. 2012)[11]; it identifies all LC where period and epoch exceed the detection Threshold Crossing Event (TCE) of 7.1σ - the threshold at which we expect less than one statistical false positive over the mission lifetime (Batalha et al. 2009)[8]. Therefore a TCE is each transit-event with a signal to noise ratio greater than 7.1.

Now all TCEs are applied to further studies and transit model (e.g. Mandel & Agol 2002)[75] to identify obvious false alarms and other astrophysical signals that are clearly not consistent with a planet transit (e.g. eclipsing binaries). The remaining TCEs are now called Kepler Object of Interest (KOI).

Twenty science team members evaluate the KOIs by statistical tests, e.g.: odd/even statistic, occulation test or secondary statistic - it is a test to see if we have a secondary eclipse which identifies diluted or grazing eclipsing star systems, quality of model fit, photo-center motion - it is measuring the position of the photocenter/center of the source of light; if we have a planetary transit then the center of the source of light should remain at the position of the primary star (target star) while if the primary star is blended with a nearby object, the photocenter can shift towards the neighbor

---

[1]See chapter 3, section 4.4 for detailed information

[2]The description of this module is described in the *Kepler Data Processing Handbook* at MAST

object as the light coming from the primary star is blocked out during the transit.

After those tests, the science team classifies the KOIs in three groups:

1. Viable planet candidates

2. Eclipsing binaries

3. False Positive

A false positive could be a background or foreground eclipsing binary system aligned with the target star or an eclipsing binary system physically associated with the target, called Hierarchical triple.

Follow-up Observations

Follow-up observations and further analysis are needed to confirm or validate[3] a candidate planet. High resolution spectroscopic measurements and radial velocity follow-up (Bouchy et al. 2009)[23] with many ground based telescope have been initiated to detect transits, e.g.: The Optical Gravitational Lensing Experiment (OGLE) at Las Campanas Observatory `http://ogle.astrouw.edu.pl/`; the Trans-atlantic Exoplanet Survey (TrES) with 10cm telescope at Lowell Observatory, Palomar Observatory, and the Canary Islands (Alonso et al. 2000)[2]; the XO Project `http://www.stsci.edu/~pmcc/xo/`; the Hungarian Automated Telescope Network (HAT) (Bakos et al. 2004)[4] and the Wide Angle Search for Planets (SuperWASP) which consists of two observatories, SuperWASP-North at Roque de los Muchachos Observatory on the island of La Palma in the Canaries and WASP-South at the South African Astronomical Observatory, South Africa `http://www.superwasp.org/`
Imaging is another method to confirm or validate a planet by observing high quality pictures of the field surrounding Kelper stars, using 1m telescope at Lick Observatory `http://mthamilton.ucolick.org/`, 2m telescope at Las Cumbres Observatory `http://lcogt.net/science`, Keck telescope at Hawaii `http://keckobservatory.org/`...
Also we can use space telescope as Spitzer Space Telescope `http://www.spitzer.caltech.edu/` to observe transit light curves in infra red (IR), and since a planetary transit depth is achromatic while a blend is not, we can compare the two LC observed in visible by Kepler and in IR by Spitzer to see if the transit is due to a planet or to an eclipsing binary.

Status of Kepler

Now as on July 2014, Kepler has contributed to the confirmation of 980 exoplanets, and the discovery of 4234 planets candidates with 661 in the HZand 2177 Eclipsing

---

[3]Kepler team reserves the use of the term "confirmed" only for planets with measured mass, from radial velocity follow-up observation or transit-timing variation.

Binary system all of them are archived[4]. With each new catalog released, we have a progression towards smaller planets with progressively longer orbital periods, suggesting that Earth-Like planets in the Habitable-Zone are forthcoming and showing that Kepler is a successful mission and it is achieving its goal. We can see in figure 4.3, the planet radius versus orbital period for the candidates in three successive catalogs. The B10 catalog released in June 2010 (blue) identified from the analysis of 43 days of Kepler data, the B11 catalog released in February 2011 (red) identified in the first 13 months of data (Quarter 1 through 5), and the newest catalog released in 2012 from the analysis of 16 months of data (Quarter 1 through 6). Over 73% of the candidates presented in the B11 catalog are smaller than Neptune. This continues to increase in the last catalog of new candidates, where over 91% are smaller than Neptune (Batalha et al. 2012)[11]. And as on February 2013, Francois Fressin improved the Kepler detection efficiency in the 221st American Astronmomical Society Meeting in Long Beach California, he announced preliminary results for the new candidate catalog showing that the number of candidates discovered has increased by 21% for Super-Earth size planets and by 43% for Earth-size planets. See figure 4.4

Data Archive

The LC, pixel data files, cotrending basis vectors and other engineering data are available at the Mikulski Archive for Space Telescopes or MAST `http://archive.stsci.edu/kepler/`. While the TCE list, the KOI lists (which contain both planet candidates and false positives), and the data validation reports are available in the Exoplanet Archive `http://exoplanetarchive.ipac.caltech.edu/`. In the Exoplanet Archive we can find all data related to a KOI presented in a table where we can find stellar parameters (effective temperature, gravity, etc.) and transit parameters (periods, depths, durations, etc.) and derived planet properties (radius, etc.). Also, they added parameters from the KIC to designate KOIs that have been confirmed as planets.
In this work, all the data used is taken from the Exoplanet Archive[5].

---

[4]Go to `http://exoplanetarchive.ipac.caltech.edu/docs/counts_detail.html` for updated numbers

[5]See chapter 3, section 4.4
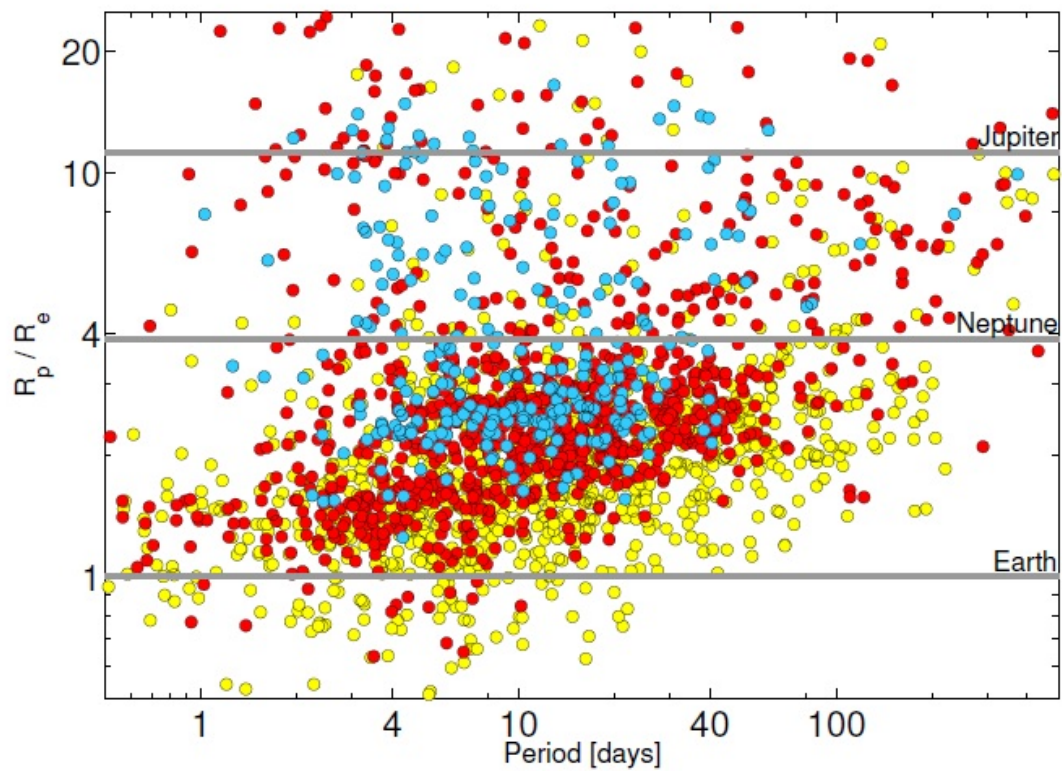
Figure 4.3: *Radius versus orbital period for each of the planet candidates in the B10 (Borucki et al. 2011a)[16] catalog released in June 2010 (blue points), the B11 (Borucki et al. 2011b)[17] catalog released in February 2011 (red points), and the final catalog released in 2012 (yellow points)(Batalha et al. 2012)[11]. The horizontal lines mark the radius of Jupiter, Neptune, and Earth. Figure is taken from (Batalha et al. 2012)[11]*
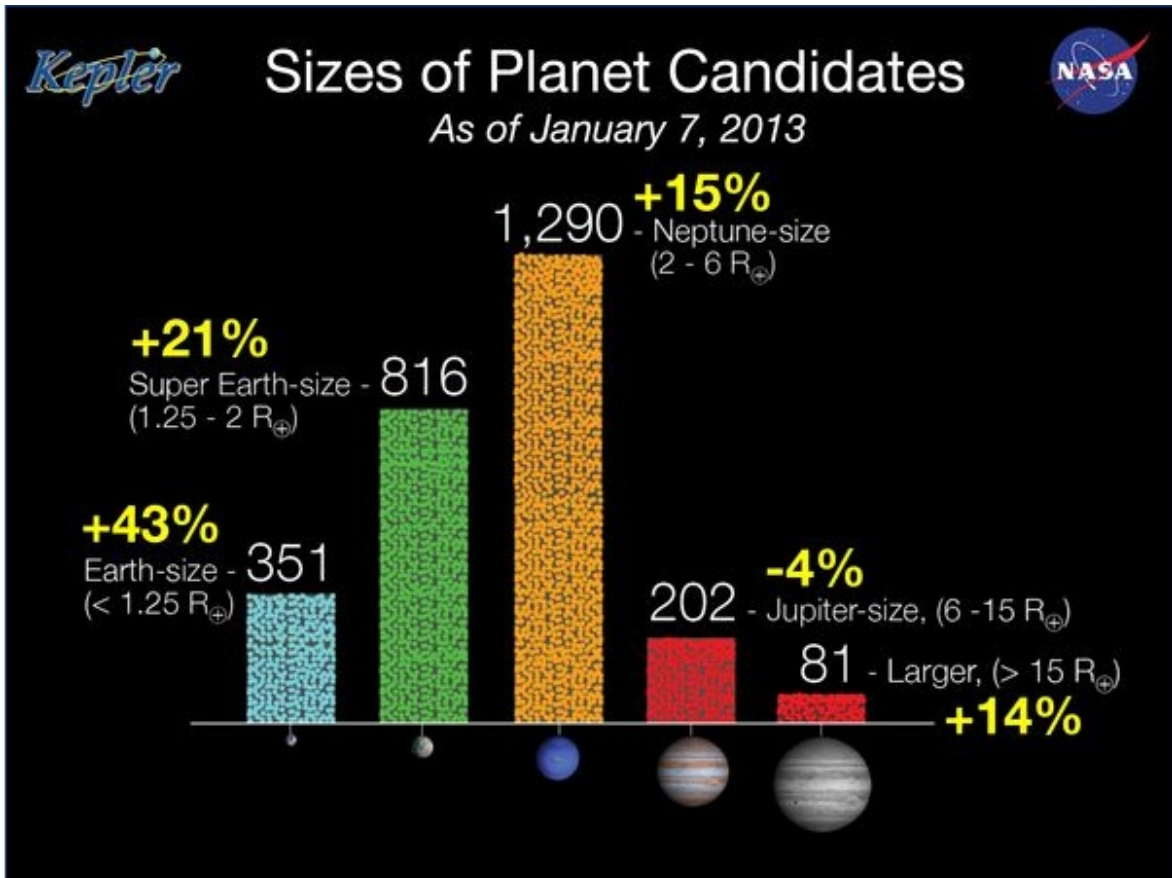
Figure 4.4: *A histogram showing the increase of Kepler's planets candidates from February 2012 to January 2013 where the most dramatic increases are seen in the number of Earth-size and super Earth-size candidates, growing by 43 and 21 percent respectively. Figure is taken from NASA Kepler News in the Kepler homepage* `http://kepler.nasa.gov/`

4.2 DR12 Sample

To be conservative, DR12, followed Schlaufman & Laughlin (2011)[95] and set the minimum planet candidate radius for her study at $R_p = 5R_\oplus$. Because for a $5R_\oplus$ candidate with a $+58\%$[6] measurement error on planet size, the true size would be $3.2R_\oplus$, still within the size range of giant planets (Rogers & Seager 2010 [86]).

Also, DR12 found that below $R_p = 20R_\oplus$, light curves that have no obvious problem[7] begin to dominate. Hence, she set an upper limit of $20R_\oplus$ to the giant planet candidates in her sample.

The sample selected in DR12 consists of 213 candidates (see table 1 in DR12) satisfying 2 criteria:

1. Candidate giant planets with $5R_\oplus < R_p < 20R_\oplus$

2. Their host stars have metallicities from the KIC

Using the same sample as that used in DR12 (table 1 in DR12), we plotted the variation of the eclipse depth of those 213 giant planet candidates as a function of their host star metallicity ((Fig. 4.5) which resembles fig 1 in DR12 (See fig 3.9). The best fit line relating the eclipse depth and the metallicity is[8]

$$R_p/R_* = (-0.017 \pm 0.009)[M/H] + (0.084 \pm 0.002) \qquad (4.3)$$

The negative slope indicates that there is a weak negative correlation giving a hint that eclipses may be deepest, on average, for low metallicity stars.

To first prove this negative correlation, we calculated the Kendall's τ correlation coefficient. It is used to measure the relation between two measured quantities. Its value ranges between -1 and +1. A negative value of τ indicates a negative correlation while a positive value means that we have a positive correlation. While a null value of τ refers to a null hypothesis (no correlation between the measured values). Once the τ correlation coefficient is computed, we calculated the standard deviation using the large-sample Gaussian approximation to the variance $\nu = \sigma^2$ of the τ sampling distribution (Abdi 2007[1])

$$\nu = \sigma^2 = \frac{2(2n+5)}{9n(n-1)} \qquad (4.4)$$

where n is the number of stars used in the sample.

Finally, the null hypothesis test is done to find the difference between the computed τ and the $\tau = 0$ expected in the case of no correlation, by calculating Z_τ:

---

[6]Brown et al. (2011)[25] quote a 0.4dex error bar on log(g), which translates into $+58\%/-37\%$ radius error for a planet transiting a Sunlike star

[7]Planet radius mismeasurement due to the V-shaped eclipses, odd/even eclipse depth differences that indicate eclipsing binaries or background eclipsing binaries...

[8]Graph and linear fit were done using a Python code. For more details about the code see the appendix B.1

$$Z_\tau = \frac{\tau}{\sigma} \tag{4.5}$$

Using a Python code (See the appendix B.2), we obtained $\tau = -0.108$. Then the standard deviation was found to be 0.046 (Eq. 4.4). Therefore, the computed value of $\tau = -0.108$ differs from the null hypothesis $\tau = 0$ by -2.3σ. This is the same result found by DR12, indicating that the decrease in the eclipse depth-metallicity trend is interesting but not conclusive.
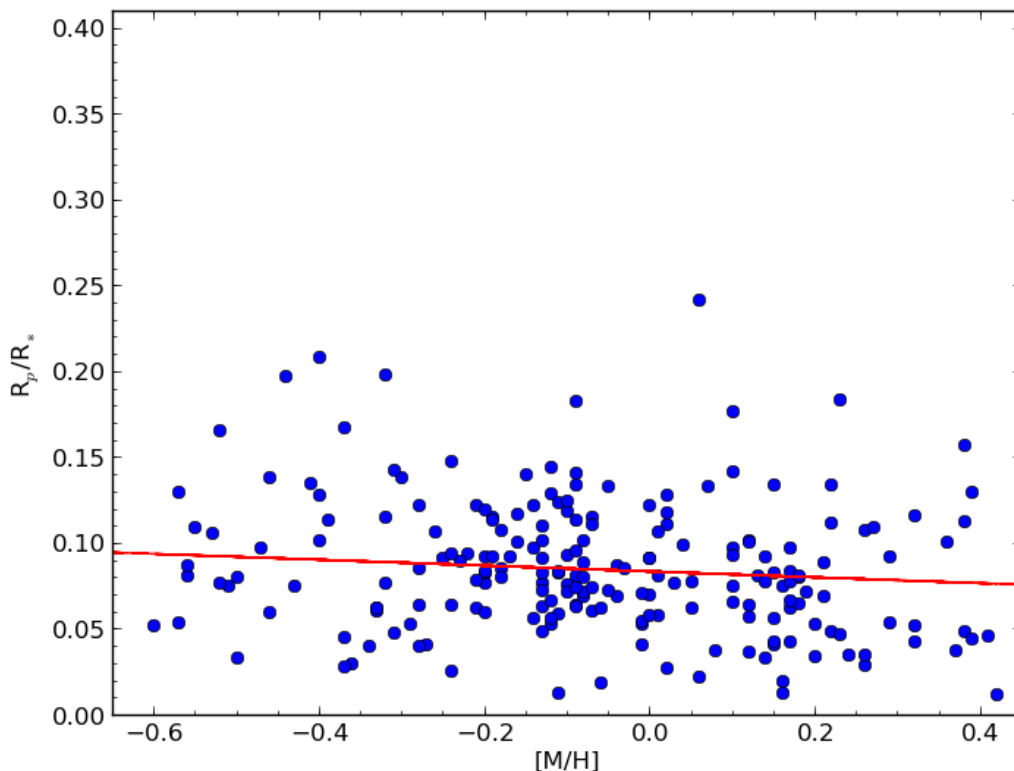
Figure 4.5: *Plot showing the variation of the eclipse depth of Kepler's giant candidates R_p/R_* as a function of the host star metallicty [M/H]. Candidate giant planets are taken from table 1 in DR12. The best-fit line (red line) is $R_p/R_* = (-0.017 \pm 0.009)[M/H] + (0.084 \pm 0.002)$ indicating a decrease in eclipse depth with [M/H].*

Another way to prove this negative correlation between the eclipse depth of Kepler's giant candidates and the metallicity of their host stars, is by dividing the data into four broad metallicity bins, as done in DR12 and plotting the fraction of giant planet candidates for which $R_p/R_* > 0.13$[9] in each bin (number of giant planet candidates

---

[9]DR12 choose $R_p/R_* = 0.13$ as the cutoff because it is a roughly typical eclipse depth of well studied inflated planets

having $R_p/R_* > 0.13$ in each bin divided by the total number of giant planet candidates in that bin). Then we calculated and over plotted a statistical error bar for each bin ($error = \dfrac{\sqrt{N'}}{N}$; where N' is the number of planet candidates with $R_p/R_* > 0.13$ and N is the total number of giant planets candidates in each bin)[10].
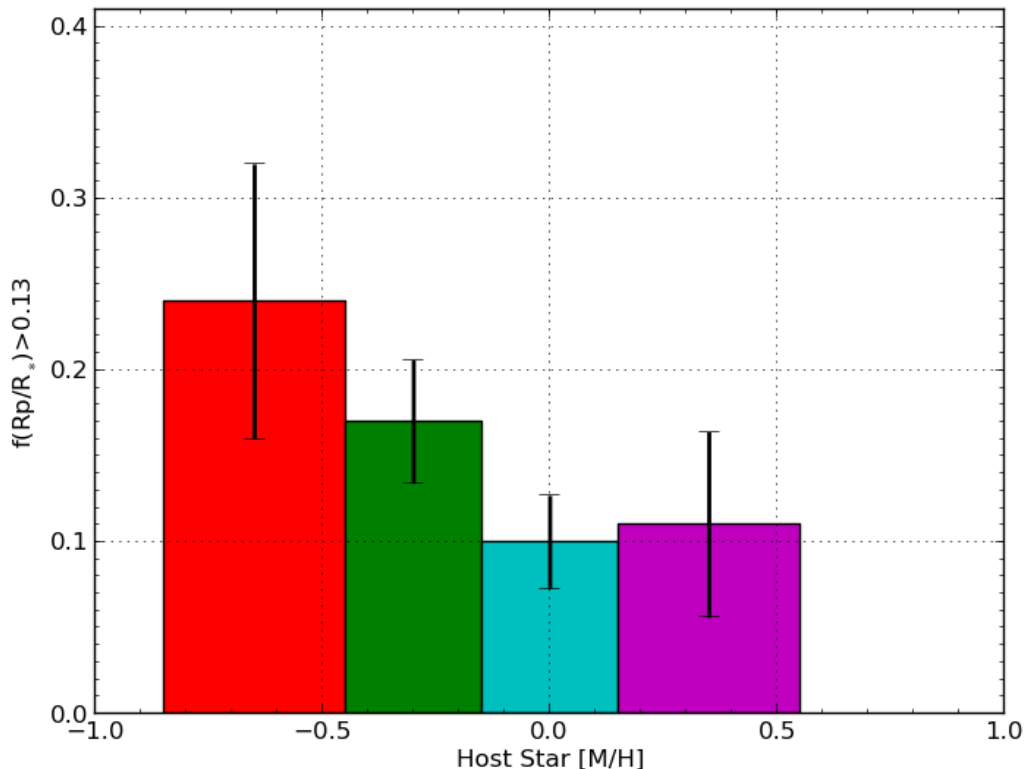
Figure 4.6: *Fraction of giant planet candidates having $R_p/R_* > 0.13$ in function of the metallicity of their parent's star. Planets orbiting lowest-metallicity host appear to have higher eclipse depth than planets orbiting higher-metallicity hosts. Candidate giant planets are taken from table 1 in DR12.*

Comparing our histogram (Fig. 4.6) and that done by DR12 (Fig. 3.10), we see that we were able to reproduce the same results obtained by DR12. This was expected, given that we used the same data with the same declared constraints as that in DR12. We plotted our graph following exactly the same way [11].

From figure 4.6, we can see clearly that the eclipse depth of giant planet candidates decreases, in average, with increasing metallicity. This was explained by the presence

---

[10]See the python script written to draw our histograms B.3

[11]This was verified by sending an email to DR12 asking about how the auther did calculate the fraction of giant planet candidates having $R_p/R_* > 0.13$ and its corresponding error bar in each bin

of two different planet formation theories; the core accretion at high metallicity and the disk instability model at small metallicities.

4.3   DR12 Sample: Cleaned

DR12 mentioned that her sample still has the possibility to be contaminated by as much as 40% eclipsing binaries, background eclipsing binaries and hierarchical triples. Follow-up observations and further analysis are done each day to confirm a candidate planet or to classify it as a false positive. After categorizing a KOI as a confirmed planet or a false positive, the science team updated the KOI-disposition in the Exoplanet Archive [12] where we can find also the data related to each KOI 4.1.

According to the data given by the Exoplanet Archive as on June 2013, we examined the data associated to each KOI in DR12's sample. Among the 213 giant planet candidates, we found that 23 giant planet candidates are now established as false positive, 25 are now confirmed planets and 36 are not in the range of radius chosen by DR12 ($5R_\oplus < R_p < 20R_\oplus$) (Table 4.1).

Table 4.1: Table showing the number of giant planets which do no longer satisfy the criteria of DR12's sample. 23 giant planet candidates are now false positives, 25 are now confirmed planets and 36 are not in the range of radius chosen.

	Number of planets not used in our sample
False positives	23
Confirmed planets	25
Out of range	36
Total number	84

We filtered DR12's sample from all planets that do not satisfy the sample selection criteria. A new sample consisting of 129 giant planet candidates is now obtained, hereafter called as the "cleaned sample".

We reproduced the eclipse depth as a function of [M/H] for the candidate giant planet hosts in the cleaned sample (See fig. 4.7). This figure shows that stars with different metallicities could harbor planets with different radii. We computed a linear fit:

$$R_p/R_* = (-0.02 \pm 0.012)[M/H] + (0.088 \pm 0.003) \tag{4.6}$$

We noticed that we have a negative slope giving hint of a negative eclipse depth-metallicity trend.

---

[12]http://exoplanetarchive.ipac.caltech.edu/

The Kendall's rank coefficient for mapping [M/H] onto R_p/R_* is $\tau = -0.039$. To test the null hypothesis we calculated the standard deviation of the τ sampling distribution: $\sigma = 0.059$. The computed value of $\tau = -0.039$ differs from $\tau = 0$ by -0.7σ. We cannot consider this result as significant so the null hypothesis could not be ruled out. This result lead us to ask about how significant is the negative eclipse depth-metallicity trend found by DR12.
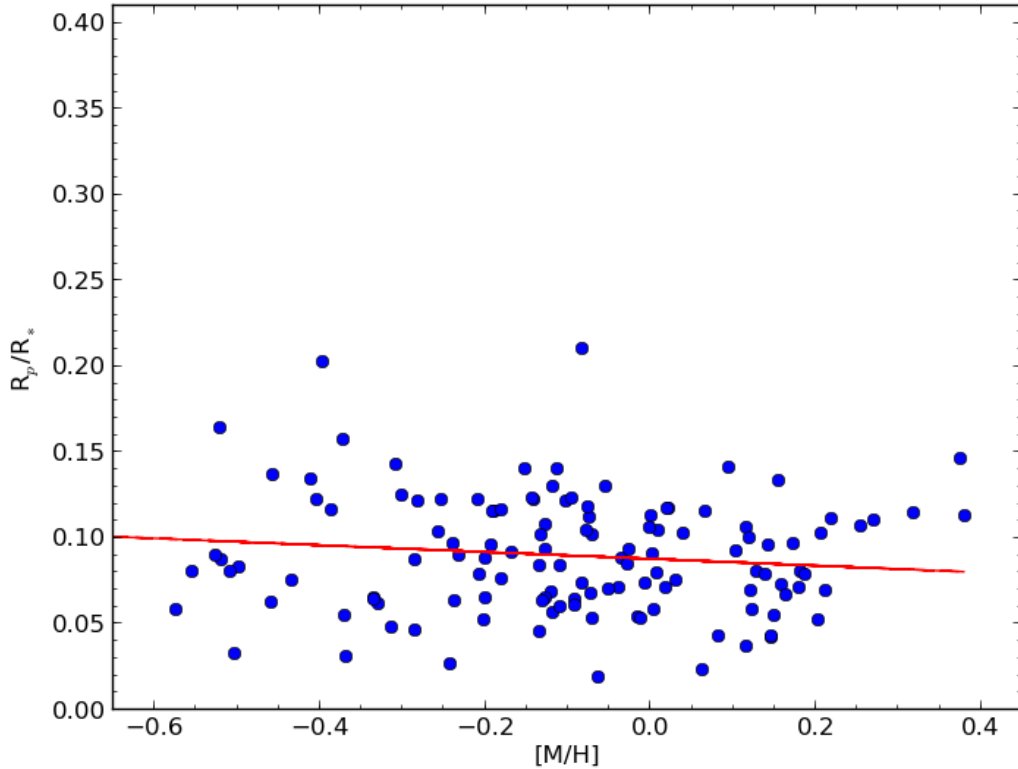
Figure 4.7: *Study of the eclipse depths of Kepler gas giant candidates in function of their parent stars metallicity. Candidate giant planets are taken from table 1 in DR12 and were filtered, as on June 2013, according to the sample selection criteria set by DR12. The red line is the best linear fit: $R_p/R_* = (-0.02 \pm 0.012)[M/H] + (0.088 \pm 0.003)$. With a near zero negative slope, it indicats the presecnce of weak negative negative eclipse depth correlation with metallicity.*

To better understand this trend, we divided the data into four broad bins, as done in DR12 and we plotted the fraction of planet candidates for which $R_p/R_* > 0.13$ in each bin (See fig. 4.8). This plot 4.8 shows that the fraction of candidate giant planets having $R_p/R_* > 0.13$ decreases for metallicities between $-0.85dex < [M/H] < 0.15dex$, but what is interesting is that this fraction increases again at high metallicities ($0.15dex < [M/H] < 0.55dex$). This result does not agree with that of DR12, who showed a negative eclipse depth correlation with metallicity. The question we are

asking: Is there really a negative correlation between the eclipse depths of Kepler gas planets and the metallicity of their parent stars? To answer this question we will update this work, in the following section, with an extended sample.
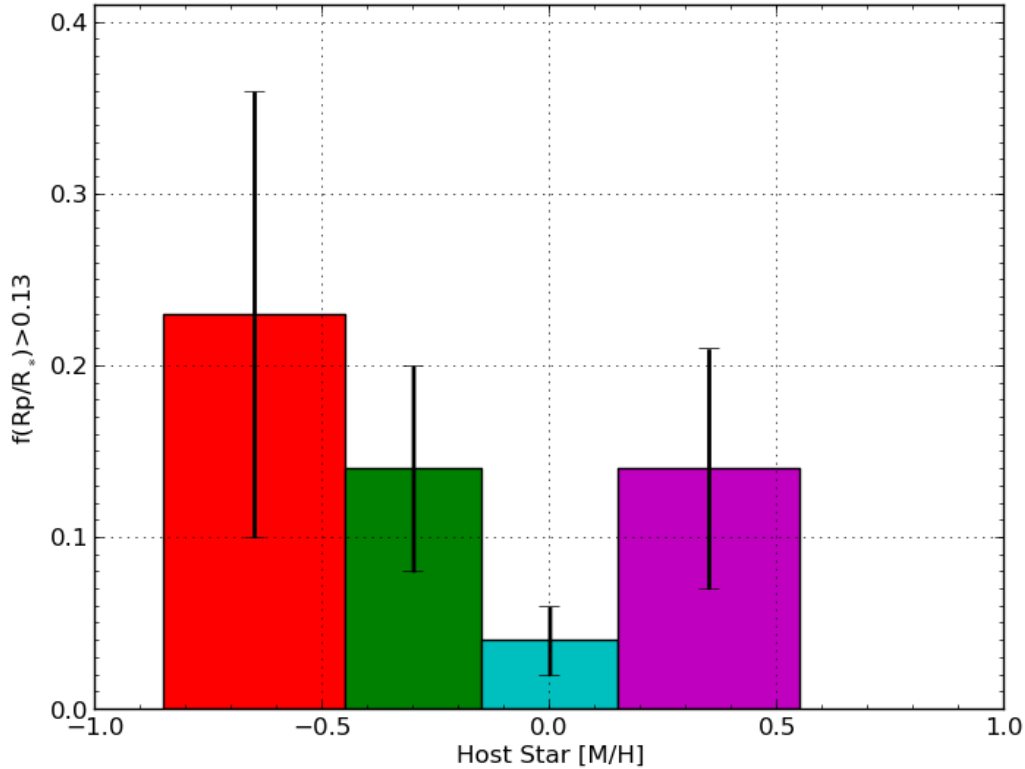
Figure 4.8: *Fraction of giant planet candidates having R_p/R_* > 0.13 in function of their host star metallicity. Planets orbiting lowest-metallicity host appear to have higher eclipse depth than planets orbiting higher-metallicity hosts. Candidate giant planets are taken from table 1 in DR12.*

4.4 To an Extended Sample

4.4.1 Q12 Sample: From Q0 till Q12

Data are taken from the NASA Exoplanet archive[13], having until June 2013, a table containing 5465 KOI (confirmed planets, eclipsing binaries, false positive) from quarters Q0 until Q12 along with there respective data[14]. 3095 of them are candidates having different radii. According to the criteria set by DR12, we choose all candidate planets having a radius between $5R_\oplus$ and $20R_\oplus$ to obtain a sample made up of 277

---

[13]See http://exoplanetarchive.ipac.caltech.edu/ for an updated data list
[14]See 4.1

giant planet candidates. Finally, we search for the metallicty of each giant planet candidate host star from the Kepler Data Archive[15], 10 candidate planets were removed since they do not present a metallicity measurment. We ended with a sample made up of 267 giant planet candidates.

In table A1 (See the appendix A), we can see all the 267 giant candidates used in our analysis. We present for each one the KOI number (KOInumber), the Kepler ID (KepID), the Planet-Star Radius Ratio (R_p/R_*) with the error on this ratio (R_p/R_* error) and the metallicity ([M/H]). All of those data are taken from the NASA Exoplanet archive except for the metallicty which is taken from Kepler Data archive.

Comparing our sample of giant planet candidates and the sample used in DR12 we can see that we have 267 giant planet candidates in our sample while there was 213 in the sample chosen by DR12. Among the 213 giant planet candidates of DR12's sample, 129 are in common with our sample while the other 84 were removed since they do not satisfy the sample selection criteria sets by DR12 (See table 4.1). The table below (Table 4.2), is to clarify the comparison between both samples.

Table 4.2: The number of giant candidates in DR12's sample, in our sample, and the number of planets which are not in common between both samples. We have 129 giant planet candidates in common between both samples therefore 138 giant planet candidates appear only in our sample.

	DR12 Sample	Q12 Sample
Total number of planets	213	267
Planets not in common	84	138

To decrease the contamination in the sample by a false positive, we added the confirmed planets found in table 4.1 to our sample (see table A2 in the appendix A).
The final sample consists of 291 giant confirmed/candidate planets with radius between $5R_\oplus < R_p < 20R_\oplus$ that also have metallicity measurement from the KIC. Hereafter, this sample will be referred as "Q12 sample". Among those 291 giant planets, 129 giant planet candidates are in common with the sample of DR12, 138 giant planet candidates appear only in our sample and 24[16] are confirmed planets (Table 4.3).

---

[15]Go to the following site `http://archive.stsci.edu/kepler/`, then click on Kepler Data Search, insert the Kepler ID for each candidate planet and find its metallicity

[16]Initially 25 confirmed planets, one was removed for not having $3.84R_\oplus$ thus out of the range of radius chosen by DR12.

Table 4.3: The 291 giant confirmed/candidate planets in the Q12 sample. 138 of them are in addition to DR12's sample and 24 are confirmed giant planets.

	Number
Giant planet candidates common with DR12	129
Giant planet candidates not in common with DR12	138
Confirmed giant planets	24
Total number of giant planets in our sample	291

With a bigger sample in hands we plotted the eclipse depth for the 291 giant planets hosts in our selected sample, as a function of the host star metallicity [M/H] (See the figure below 4.9).
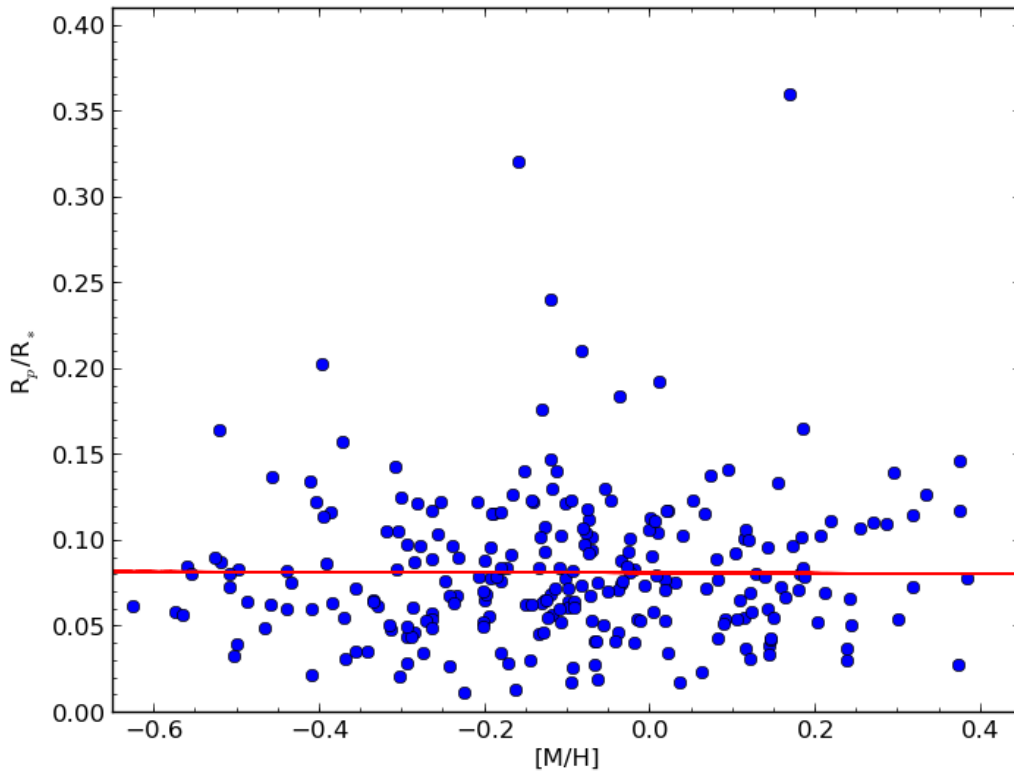
Figure 4.9: *Plot of the eclipse depths of Kepler giant confirmed/candidates planets in the Q12 sample, R_p/R_*, as a function of the host star metallicity [M/H]. The red line represents the best linear fit: $R_p/R_* = (-0.001 \pm 0.009)[M/H] + (0.082 \pm 0.002)$. With a near zero slope, the negative eclipse depth-metallicity trend could not be really significant.*

To interpret this plot, we divided the metallicity into four broad bins to see the number of planets with different radii in each metallicity bin. In the table below 4.1, we can see that planets of all radii can appear around stars of all metallicities. Therefore we cannot say that eclipse depth, in average, decreases or increases with metallicity.

Table 4.4: The total number of giant planets in each metallicity bin for the Q12 sample. Planets of all radii can appear around stars with all metallicities

[M/H]	[-0.85;-0.45[	[-0.45;-0.15[	[-0.15;0.15[	[0.15;0.55[
Total number of planets	24	83	134	47

To quantify the eclipse depth-metallicity trend, we computed a linear fit (the red line):

$$R_p/R_* = (-0.001 \pm 0.009)[M/H] + (0.082 \pm 0.002) \tag{4.7}$$

We can notice that even if the slope is negative its corresponding error bar relatively big. Thus we cannot have a definite conclusion about the eclipse depth-metallicity relation.

The computed Kendall's rank correlation coefficient for the Q12 sample is: $\tau = 0.017$. It is a positive correlation coefficient, giving a hint that we may have a positive eclipse depth-metallicity relation. To test this result, we calculated the standard deviation of the τ sampling: $\sigma = 0.039$. The computed value of $\tau = 0.017$ differs from the $\tau = 0$ expected in the case of the null hypothesis by 0.4σ. Considering the big value of the standard deviation per respect to that of τ, the positive eclipse depth-metallicity trend could not be considered as significant.

To visualize the eclipse depth-metallicity trend we plotted a histogram (see figure 4.10), showing the fraction of giant planets with $R_p/R_* > 0.13$ as a function of the metallicity of their host stars. As done in DR12, we divided the metallicity into four broad bins and we plotted the fraction of giant planets for which $R_p/R_* > 0.13$ and we over plotted a statistical error bar for each bin.

From histogram 4.10, we can see that planets orbiting the highest-metallicity hosts appear to be significantly bigger, relative to their parent stars, than the planets orbiting the lowest-metallicity hosts. The fraction of giant planet with $R_p/R_* > 0.13$ in the highest-metallicity bin is 0.152 ± 0.058, while the fraction of giant planet with $R_p/R_* > 0.13$ in the lowest-metallicity bin is 0.13 ± 0.072. Nevertheless, in the second and third bin, the fraction of giant planet with $R_p/R_* > 0.13$ is respectively 0.07 ± 0.03 and 0.067 ± 0.022 (approximately the same fraction, where the fraction in the second bin is slightly bigger than that in the third bin). Therefore we cannot say that we have a negative eclipse depth trend as found in DR12 (Fig. 3.10).
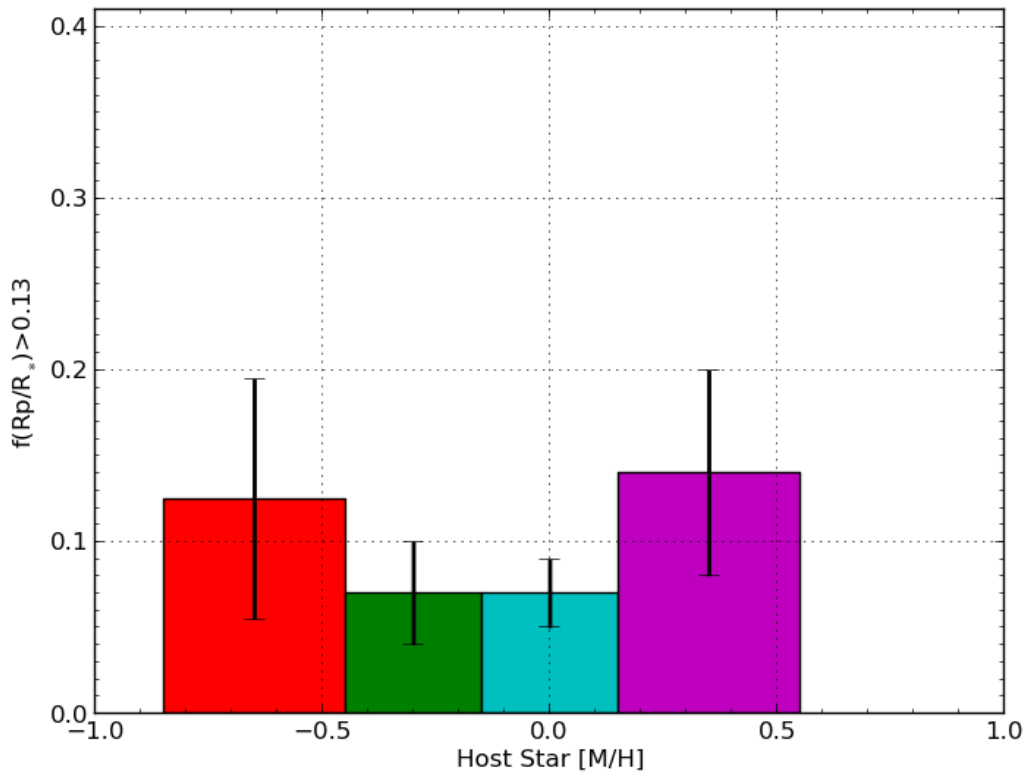
Figure 4.10: *Fraction of giant planets with $R_p/R_* > 0.13$ in function of the metallicity. The planets orbiting the highest-metallicity hosts appear to be significantly larger, relative to their parent stars, than the planets orbiting the lowest-metallicity hosts.*

4.4.2   Q16 Sample: From Q0 till Q16

In March 2014, the Kepler team released data from Q0 till Q16. Following the same criteria set by DR12 for her sample, we choose 324 giant candidate planets with radius between $5R_\oplus < R_p < 20R_\oplus$ and having the metallicity measurement from the KIC. Comparing this sample with that studied before (Q12 sample) we found that 34 giant candidate planets, that were in the Q12 sample, are now established as confirmed planets. We added those 34 confirmed giant planets and the 24 confirmed giant planets found before (Table 4.1) to our new extended sample, called "Q16 sample".

The final sample consists of 382 giant candidate/confirmed planets with radius between $5R_\oplus < R_p < 20R_\oplus$ that also have metallicity measurement from the KIC. 324 of them are giant candidates and 58 are confirmed planets (See table A3 in the appendix A).

With a clearly larger sample of giant candidate and confirmed planets in hand we plotted the eclipse depth in function of the metallicity in the aim of finding a more accurate trend for the eclipse depth-metallicity relation (Fig. 4.11). This figure shows a robust distribution; giant planets with different radii can appear around stars of all metallicities.

The linear fit was represented by:

$$R_p/R_* = (0.012 \pm 0.008)[M/H] + (0.082 \pm 0.002) \qquad (4.8)$$

It is a positive slope giving a hint of a positive eclipse depth-metallicity trend. To quantify this trend, we calculated the Kendall's correlation coefficient: $\tau = 0.03$. What this value also hints at, is that the fraction of giant planets tend to increase with the metallicity of their host stars. However, the calculation of the standard deviation $\sigma = 0.034$ shows that the $\tau = 0$ expected in the case of the null hypothesis differs from the computed $\tau = 0.03$ by only 0.9σ. This result still cannot be considered as conclusive.

We also divided the data into four broad metallicity bins and we plotted the fraction of giant planet with $R_p/R_* > 0.13$ in each bin. (Fig. 4.12)
What histogram 4.12 shows, is that the fraction of giant planets with $R_p/R_* > 0.13$ decreases for metallicities between $-0.85dex < [M/H] < 0.15dex$, increases then arbitrarily for metallicitues above $0.15dex$. As previously found by studying the Q12 sample, stars in higher-metallicity bin tend to host a higher fraction of planets that are large in comparison to their host stars than the stars in lower-metallicity bins. Therefore, we cannot say that the fraction of giant planets with big eclipse depths increases or decreases, in average, with metallicity. And the negative eclipse depth trend found by DR12 could not
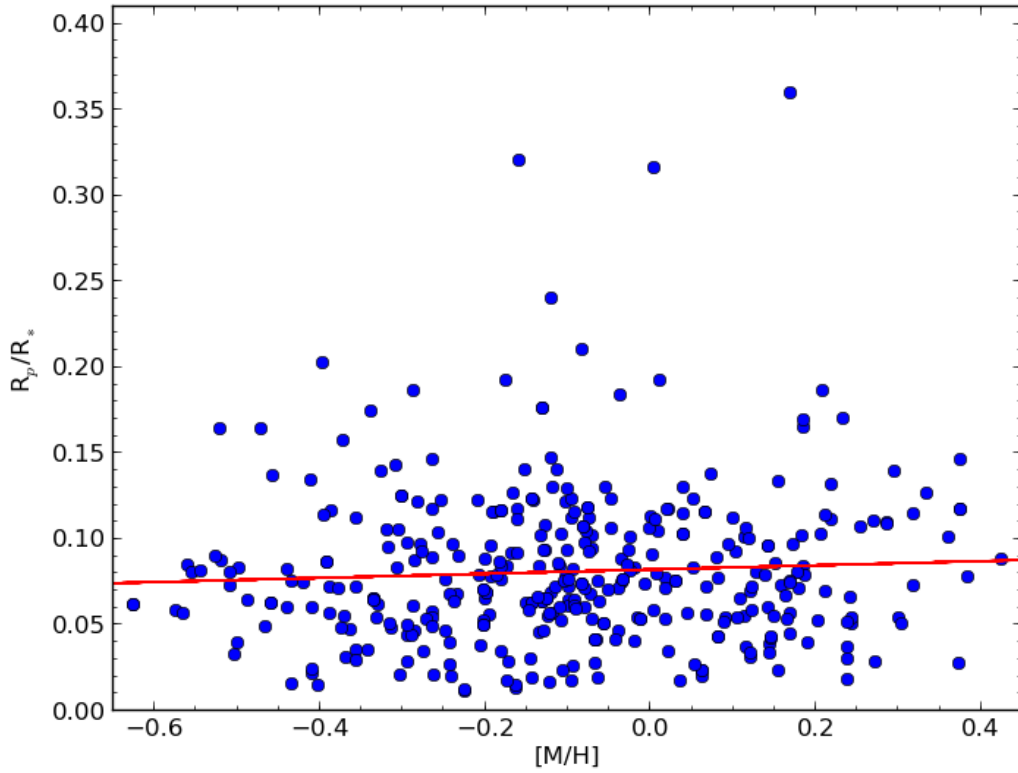
Figure 4.11: *Plot of the eclipse depths of Kepler giant candidate/confirmed planets in our extended Q16 sample, as a function of the host star metallicity [M/H]. The red line represents a linear fit: $R_p/R_* = (0.012 \pm 0.008)[M/H] + (0.082 \pm 0.002)$ indicating that there is a hint of having a positive eclipse depth-metallicity trend; the fraction of giant planets tend to increase with the metallicity of their host stars.*
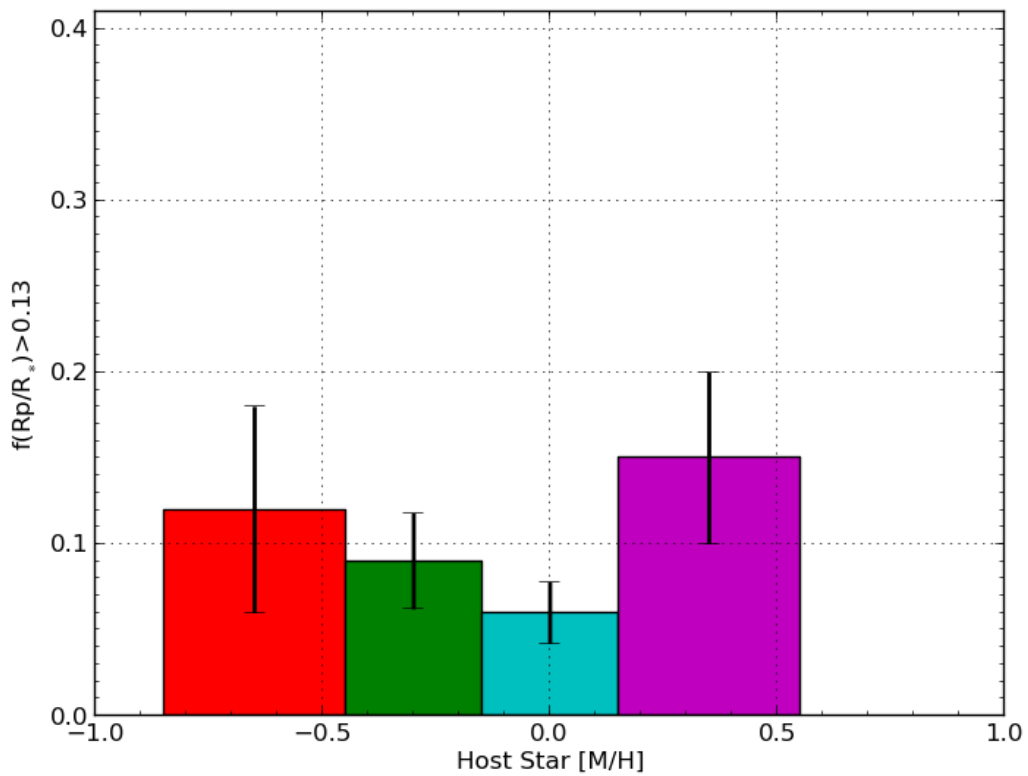
Figure 4.12: *Fraction of giant confirmed/candidate planets with eclipse depth above 0.13, from the extended Q16 sample, in function of their host stars metallicity. The planets orbiting the highest-metallicity hosts appear to be significantly larger, relative to their parent stars, than the planets orbiting the lowest-metallicity hosts.*

Comparing the 3 samples studies, we can notice that with time more candidate and confirmed giant planets are detected and added to our data. Therefore, by studying Q16 sample which contains 382 confirmed/giant planets we can have more accurate and significant result than by studying DR12 cleaned sample that contains only 129 candidate giant planets. Furthermore, the presence of 58 confirmed planets in the Q16 sample decreases the possibility of having a false positive.

In the table below, we can see the computed τ correlation coefficient for each sample studied in this work and that found by DR12. The calculated standard deviation of the τ sampling distribution and the result of the null hypothesis test are presented also for each sample.

Table 4.5: Table presenting the computed τ correlation coefficient for each sample studied in this work, with the calculated standard deviation of the τ sampling distribution and the result of the null hypothesis test Z_τ. One can notice 2 things: The increasing value of τ with the increasing size of the sample/confirmed added planets. The hint at the presence of a positive eclipse depth-metallicity trend.

	τ	σ	Z_τ
DR12 Sample	-0.108	0.046	-2.3σ
DR12 Cleaned	-0.039	0.059	-0.7σ
Q12 Sample	0.017	0.039	0.4σ
Q16 Sample	0.03	0.034	0.9σ

This table shows that by cleaning DR12's sample from all the data that do not satisfy the sample selection criteria, the computed τ correlation coefficient increases from -0.108 to -0.039. As the τ correlation coefficient approaches zero, the negative eclipse depth trend found by DR12 weakens. Although the positive values of the computed τ correlation coefficient found by studying the Q12 and the Q16 samples respectively give a hint that we may have a positive-eclipse depth-metallicity trend. However, the difference between the computed τ found in each sample and the $\tau = 0$ expected in the case of null hypothesis are 0.4σ and 0.9σ respectively for the Q12 and the Q16 sample, thus this statistical study cannot give us a conclusive answer about the eclipse depth-metallicity trend. Still, the fact that the computed τ correlation coefficient increases in each sample, with the use of a bigger and a more accurate sample, and since the statistical significance of the trend has been increased from 0.4σ as on June 2013 (Q12 sample) to 0.9σ as on March 2014 (Q16 sample), we may consider this positive eclipse depth-metallicity trend suggestive but not definitive. This suggestive correlation is consistent with planets orbiting high-metallicity stars being, on average, larger in comparison with their host stars than planets orbiting metal-poor stars. This result agrees with the core accretion model which states that planets form from a primordial nebular cloud; As the metallicity in this primordial cloud increases the metallicity of the host star increases, as well as the abundance of small condensed

particles which allows the formation of planetismals leading to the formation of bigger cores with higher mass thus they accrete more gas and form bigger giant planets with bigger eclipse depths.

4.4.3 Smaller Binning Test

To examine the eclipse depth-metallicity trend in more detail, we divided the data into smaller bins of $0.2dex$ (See fig. 4.13). This histogram shows also that planets orbiting high-metallicity hosts are larger in comparison to their counterparts orbiting low-metallicity stars. Thus, contradicting the negative eclipse depth trend found by DR12. At the same time not exhibiting a clear positive trend.
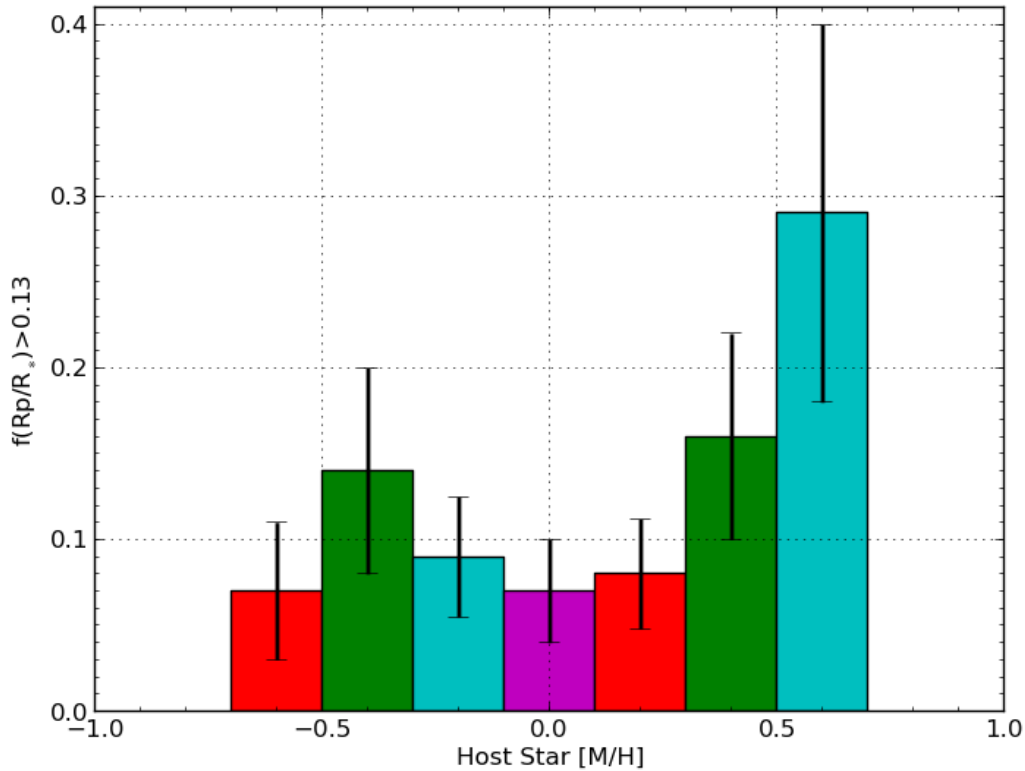
Figure 4.13: *Fraction of giant planets with $R_p/R_* > 0.13$ in function of the metallicity. Same result as in figure 4.12 but this time with smaller metallicity bins of $0.2dex$*

Chapter 5

Conclusion and Discussion

This thesis was done to examine the relation between the eclipse depths of Kepler giant planets and the metallicities of their parent stars. The purpose of this work is to find the best eclipse depth-metallicity trend for giant planets to better understand the conditions that lead to their formation. Therefore, it helps to speculate about the formation of our Solar system and the planetary system formation theories. This study may also be useful to narrow the number of stars selected when searching for giant planets.

DR12 introduced a decrease in median eclipse depth with metallicity, by studying the correlation between the eclipse depths of 213 Kepler giant planet candidates (from Q0 till Q5) and the metallicity of their host stars. The statistical significance of this negative eclipse depth-metallicity trend is -2.3σ, suggestive but not conclusive since so little is known about the distribution of giant planet eclipse depths and given that this trend may contradict the core accretion theory.

We filtered DR12 sample from all the data that no longer satisfy the sample selection criteria, as on June 2013, the significance of the negative eclipse depth-metallicity trend decreases from -2.3σ to -0.7σ. This result led us to ask whether or not we have a negative eclipse depth-metallicity trend.

With the announcement of new Kepler data a larger sample of gas giant candidates was available. Meanwhile, the Kepler team studied previous candidates and classified them as confirmed planets, eclipsing binaries or false positive. Providing the opportunity to statistically study an extended sample of candidate and confirmed gas giant planets.

On June 2013, we selected a sample made up of 291 confirmed and candidate Kepler gas giant planets (Q0 till Q12) to study the relation between their eclipse depths and the metallicity of their parent stars (Q12 sample).

We represented the eclipse depth in function of the metallicity of all the kepler giant confirmed and candidates planets found in the Q12 sample. We quantified a positive eclipse depth-metallicity trend with a small significance of 0.4σ (Fig. 4.9). The corresponding median eclipse depth variation histogram (Fig. 4.10) showed that planets orbiting the highest-metallicity host tend to have larger eclipse depth then the planets orbiting the smallest metallicity hosts. This result contradicts, therefore, the negative eclipse depth-metallicity trend found by DR12.Giving the small statistical significance

obtained (0.4σ), this result could not be considered as definitive.

The release of a more extended data provided by Kepler as on March 2014 (Q0 till Q16) allowed us to study the relation between the eclipse depths of an even more extended sample of 382 candidate and confirmed gas giant planets in function of their host stars metallicities (Q16 sample).

At the 0.9σ we found, again, a positive correlation between the eclipse depth of Kepler giant planet and the metallicity of their host stars. Despite the small statistical significance (0.9σ), the increase in its value from 0.4σ as on June 2013 to 0.9σ as on March 2014 hinted at the presence of a positive eclipse depth-metallicity trend.

Furthermore, the median eclipse depth variation histogram (Fig. 4.12) showed that the fraction of giant planets with eclipse depth bigger than 0.13 is relatively big at high metallicity. When performing a histogram with smaller metallicity bins ($0.2dex$), the positive eclipse depth-metallicty trend appeared to have an interesting shape (Fig. 4.13).

5.1   Possible Scenario

Assuming the suggested positive eclipse depth-metallicity trend in this thesis is real, how can we explain it physically? And what are the reasons behind it?

The most straightforward explanation for this positive trend is the formation of giant planets via the core accretion theory. Giant planets and their host stars formed from the same initial molecular cloud. As the metallicity increases in the primordial cloud, it increases in the parent star and the formation of planetesimals increases as well. This will lead to the formation of bigger cores that accrete more Hydrogen and Helium and form bigger giant planets with bigger eclipse depth.

However, the presence of high fraction of giant planets with big eclipse depth at small metallicities (Histogram: 4.10, 4.12) could not be explained by the core accretion theory. We may suggest the formation of those planets via the disk instability model. This model states that the probability to form a giant planet decreases with metallicity (Cai et al. (2006)[27] and Meru & Bate (2010)[78]); the metallicity increases the disk opacity which reduces the disk ability to cool and therefore the probability to fragments into giant planets decreases.

When looking at our median eclipse depth variation histogram (Fig.4.13), with smaller bins $0.2dex$, one can see possible negative correlation for low metallicities followed by a positive correlation for high metallicities. We propose the presence of two populations of planets formed by two different processes: the core accretion at high metallicity and the disk instability at low metallicity. This results coincides with that found by Santos et al. 2001 [88], Santos et al. 2004b [90], Fischer et al. 2005 [41] and Johnson et al. 2010 [65].

5.2 Future Work

Note, however that this positive eclipse depth-metallicity trend is statistically interesting and suggestive but not definitive and conclusive. To improve the eclipse depth-metallicity trend more investigations need to be done to better understand the secrets of planetary formation theories.

- We motivate follow-up spectroscopy measurements for the Kepler giant candidates, in the purpose of measuring more precise metallicities and star radii. Thus it could even be possible to study the planet eclipse depth-metallicity trend in function of R_p rather than R_p/R_* and with planet radii as low as $3.2R_\oplus$ rather than $5R_\oplus$.

- We motivate follow-up observations of the Kepler candidate and confirmed giant planets, to be able to reproduce the eclipse depth-metallicity trend with a better statistical footing using a data sample of confirmed giant planets rather than candidate giant planets.

- The next five years will witness the launch of a new family of exoplanet-hunting missions such as Gaia, CHaracterising ExOPlanets Satellite (CHEOPS), Transiting Exoplanet Survey Satellite (TESS) and James Webb Space Telescope (JWST) with much more powerful capabilities. This will help in gathering more data about the nature of these exoplanets and clarify all future statistical research.

- We propose to study the correlation between the eclipse depth of Earth-like confirmed planets and the metallicity of their parent stars, to be able to narrow the huge number of stars selected to search for Earth-like planets.

The eclipse depth metallicity trend is not yet under firm statistical footing as shown in this present work. We have to bear in mind that this is just the beginning of the exoplanet science. The statistical investigation of the properties of the exoplanets and their host stars will become invaluable because of the unprecedented upcoming sample of candidate and confirmed planets. All this will enhance accuracy of that kind of study and will have a significant impact on the planetary formation processes.

Bibliography

[1] Abdi H., *The Kendall Rank Correlation Coefficient*, Encyclopedia of Measurement and Statistics, ed. N. J. Salkind (Thousand Oaks, CA: Sage) Vol. 508, 2007

[2] Alonso R. et al., *TrES-1: The Transiting Planet of a Bright K0 V Star*, The Astrophysical Journal, Vol. 613, Issue 2, pp. L153-L156., 2004

[3] Alibert Y. et al., *Models of giant planet formation with migration and disc evolution*, Astronomy and Astrophysics, Vol. 434, Issue 1, pp.343-353, April IV 2005

[4] Bakos G. et al., *Wide-Field Millimagnitude Photometry with the HAT: A Tool for Extrasolar Planet Detection*, The Publications of the Astronomical Society of the Pacific, Vol. 116, Issue 817, pp. 266-277, 2004

[5] Baliunas S. L. et al., *Properties of Sun-like Stars with Planets: rho 1 Cancris, tau Bootis, and upsilon Andromedae*, The Astrophysical Journal Letters, Vol. 474, p.L119, 1997

[6] Barclay T. et al., *A sub-Mercury-sized exoplanet*, Nature, Vol. 494, Issue 7438, pp. 452-454, 2013

[7] Basri G. et al., *Photometric Variability in Kepler Target Stars: The Sun Among Starsa First Look*, The Astrophysical Journal Letters, Vol. 713, Issue 2, pp. L155-L159, 2010

[8] Batalha N. et al., *Characteristics of the Kepler target stars*, Highlights of Astronomy, Vol. 15, p. 712-713, 2009

[9] Batalha N. et al., *Selection, Prioritization, and Characteristics of Kepler Target Stars*, The Astrophysical Journal Letters, Vol. 713, Issue 2, pp. L109-L114, 2010

[10] Batalha et al., *Kepler's First Rocky Planet: Kepler-10b*, The Astrophysical Journal, Vol. 729, issue 1, article id. 27, 21 pp., 2011

[11] Batalha N. et al., *Planetary Candidates Observed by Kepler III: Analysis of the First 16 Months of Data*, arXiv:1202.5852v1, 2012

[12] Bodenheimer P. & Pollack J. B., *Calculations of the accretion and evolution of giant planets The effects of solid cores*, Icarus (ISSN 0019-1035), Vol. 67, Sept. 1986, p. 391-408. NASA-supported research, 1986

[13] Bonfils X. et al., *Gliese 581: A System with 3 Very Low-mass Planets*, Proceedings of the conference In the Spirit of Bernard Lyot: The Direct Detection of Planets and Circumstellar Disks in the 21st Century. June 04 - 08, 2007. University of California, Berkeley, CA, USA. Edited by Paul Kalas.

[14] Borucki W. J. et al., *Finding Earth-size planets in the habitable zone: the Kepler Mission*, Exoplanets: Detection, Formation and Dynamics, Proceedings of the International Astronomical Union, IAU Symposium, Vol. 249, p. 17-24, 2008

[15] Borucki W. J. et al., *Kepler Planet-Detection Mission: Introduction and First Results*, Science, Vol. 327, Issue 5968, pp. 977, 2010

[16] Borucki et al., *Characteristics of Kepler Planetary Candidates Based on the First Data Set*, The Astrophysical Journal, Vol. 728, Issue 2, article id. 117, 20 pp., 2011a

[17] Borucki et al., *Characteristics of Planetary Candidates Observed by Kepler. II. Analysis of the First Four Months of Data*, The Astrophysical Journal, Vol. 736, Issue 1, article id. 19, 22 pp., 2011b

[18] Borucki W. J. et al., *Kepler-22b: A 2.4 Earth-radius Planet in the Habitable Zone of a Sun-like Star*, The Astrophysical Journal, Vol. 745, Issue 2, article id. 120, 16 pp., 2012

[19] Borucki W. J. et al., *nKepler-62: A Five-Planet System with Planets of 1.4 and 1.6 Earth Radii in the Habitable Zone*, Science, Vol. 340, Issue 6132, pp. 587-590, 2013

[20] Boss A. P., *Evolution of the Solar Nebula. IV. Giant Gaseous Protoplanet Formation*, The Astrophysical Journal Vol. 503, p.923, 1998

[21] Boss A. P., *Stellar Metallicity and the Formation of Extrasolar Gas Giant Planets*, The Astrophysical Journal, Vol. 567, Issue 2, pp. L149-L153, 2002

[22] Boss A. P., *Formation of Giant Planets by Disk Instability on Wide Orbits Around Protostars with Varied Masses*, The Astrophysical Journal, Vol. 731, Issue 1, article id. 74, 13 pp., 2011

[23] Bouchy F. et al., *Radial velocity follow-up for confirmation and characterization of transiting exoplanets*, Transiting Planets, Proceedings of the International Astronomical Union, IAU Symposium, Vol. 253, p. 129-139, 2009

[24] Brown, M. E.; Trujillo, C. A.; Rabinowitz, D. L., *Discovery of a Planetary-sized Object in the Scattered Kuiper Belt*, The Astrophysical Journal, Vol. 635, Issue 1, pp. L97-L100, 2003

[25] Brown, T. M. et al. *Kepler Input Catalog: Photometric Calibration and Stellar Classification*, The Astronomical Journal, Vol. 142, Issue 4, article id. 112, pp. 18, 2011

[26] Burrows A., Hubbard W. B., Lunine J. I., Liebert J., *The theory of brown dwarfs and extrasolar giant planets*, Reviews of Modern Physics, Vol. 73, Issue 3, pp. 719-765, 2001

[27] Cai K. et al.,The Astrophysical Journal, Vol. 636, p. 149, 2006

[28] Cameron A. G. W., *The formation of the sun and planets*, Icarus, Vol. 1, Issues 16, pp. 1369, 19621963.

[29] Cameron A. G. W., *Physics of the primitive solar accretion disk*, Moon and the Planets, Vol. 18, Feb. 1978, p. 5-40, 1978

[30] Cassen P. & Moosman A., *On the formation of protostellar disks*, Icarus, Vol. 48, pp.353376, December 1981

[31] Chamberlin T. C., *The Planetesimal Hypothesis*, The Journal of the Royal Astronomical Society of Canada, Vol.10, 473C, November 1916

[32] Chaplin W. J. et al., *The Asteroseismic Potential of Kepler: First Results for Solar-Type Stars*, The Astrophysical Journal Letters, Vol. 713, Issue 2, pp. L169-L175, 2010

[33] Charbonneau D. et al., *A super-Earth transiting a nearby low-mass star*, Nature, Vol. 462, Issue 7275, pp. 891-894, 2009

[34] Christy J. W. & Harrington R. S., *The satellite of Pluto*, Astronomical Journal, Vol. 83, Aug. 1978, p. 1005, 1007, 1008.

[35] Deborah P. L. et al., *HUBBLE SPACE TELESCOPE/NICMOS Imaging of Disks and Envelopes around Very Young Stars*, Astronomical Journal, Vol. 117, Issue 3, pp. 1490-1504, 1999

[36] Demarcus W. C., *The constitution of Jupiter and Saturn*, Astronomical Journal, Vol. 63, p. 2, 1958

[37] Demory B. O. et al., *Detection of a transit of the super-Earth 55 Cancri e with warm Spitzer*, Astronomy & Astrophysics, Vol. 533, id.A114, 7 pp., 2011

[38] Doyle L. et al., *Kepler-16: A Transiting Circumbinary Planet*, Science, Vol. 333, Issue 6049, pp. 1602, 2011

[39] Durisen R. H. et al., *Gravitational Instabilities in Gaseous Protoplanetary Disks and Implications for Giant Planet Formation*, Protostars and Planets V, B. Reipurth, D. Jewitt, and K. Keil (eds.), University of Arizona Press, Tucson, 951 pp., 2007., p.607-622, 2007

[40] Dymock, R., *New definitions for solar system bodies*, Journal of the British Astronomical Association, Vol.116, no.6, p.293, 2006

[41] Fischer D. A. & Valenti J., *The Planet-Metallicity Correlation*, The Astrophysical Journal, Vol. 622, Issue 2, pp. 1102-1117, 2005

[42] Ford E. B. et al., *Structure and Evolution of Nearby Stars with Planets. I. Short-Period Systems*, The Astrophysical Journal, Vol. 514, Issue 1, pp. 411-429, 1999

[43] Fortney J. J. et al., *Planetary Radii across Five Orders of Magnitude in Mass and Stellar Insolation: Application to Transits*, The Astrophysical Journal, Vol. 659, Issue 2, pp. 1661-1672, 2007

[44] Fressin F. et al., *Two Earth-sized planets orbiting Kepler-20*, Nature, Vol. 482, Issue 7384, pp. 195-198, 2012

[45] Fuhrmann K. et al., *Solar-type stars with planetary companions: 51 Pegasi and 47 Ursae Majoris*, Astronomy and Astrophysics, Vol. 326, p.1081-1089, 1997

[46] Fuhrmann K., *Nearby stars of the Galactic disk and halo*, Astronomy and Astrophysics, Vol. 338, p.161-183, 1998

[47] Giménez. A., *Analysis of Extra-Solar Planetary Transits Using Tools from Eclipsing Binaries*, Astrophysics and Space Science, Vol. 304, Issue 1-4, pp. 21-24, 2006

[48] Gonzalez G.& Lambert D. L., *A Fine Abundance Analysis of Four Stars in the gamma Per Cluster- a Cautionary Tale*, Astronomical Journal, Vol. 111, p.424, 1996

[49] Gonzalez G., *Accurate determination of the projected rotational velocity of 51 Peg*, Astronomy and Astrophysics, Vol.310, p.L13-L15, 1996

[50] Gonzalez G., *The Stellar Metallicity-Giant Planet Connection*, Monthly Notices of the Royal Astronomical Society, Vol. 285, Issue 2, pp. 403-412, 1997

[51] Gonzalez G., *Spectroscopic analyses of the parent stars of extrasolar planetary system candidates*, Astronomy and Astrophysics, Vol. 334, p.221-238, 1998

[52] Gonzalez G. et al., *Parent Stars of Extrasolar Planets. VI. Abundance Analyses of 20 New Systems*, The Astronomical Journal, Vol. 121, Issue 1, pp. 432-452, 2001

[53] Grether D. & Lineweaver C. H., *The Metallicity of Stars with Close Companions*, The Astrophysical Journal, Vol. 669, Issue 2, pp. 1220-1234, 2007

[54] Guillot T. et al., *A correlation between the heavy element content of transiting extrasolar planets and the metallicity of their parent stars*, Astronomy and Astrophysics, Vol. 453, pp. L21-L24, 2006

[55] Haisch Karl E. Jr. et al., *Disk Frequencies and Lifetimes in Young Clusters*, The Astrophysical Journal, Vol. 553, Issue 2, pp. L153-L156, 2001

[56] Hass M. R. et al., *Kepler Science Operations*, The Astrophysical Journal Letters, Vol. 713, Issue 2, pp. L115-L119, 2010

[57] Hayashi C. et al., *Formation of the solar system*, Protostars and planets II (A86-12626 03-90). Tucson, AZ, University of Arizona Press, 1985, p. 1100-1153, 1985

[58] Haywood M., *On the Correlation between Metallicity and the Presence of Giant Planets*, The Astrophysical Journal, Vol. 698, pp. L1-L5, 2009

[59] Heger A. & Woosley S. E., *The Nucleosynthetic Signature of Population III*, The Astrophysical Journal, Vol. 567, Issue 1, pp. 532-543, 2002

[60] Henry G. W. et al., *Properties of Sun-like Stars with Planets: 51 Pegasi, 47 Ursae Majoris, 70 Virginis, and HD 114762*, The Astrophysical Journal, Vol. 474, p.503, 1997

[61] Hoyle F., *The Origin of the Solar Nebula*, Royal Astronomical Society, Vol. 1, 28H, 1960

[62] Howell S. B. et al., *The K2 Mission: Characterization and Early Results*, Publications of the Astronomical Society of the Pacific, Vol. 126, issue 938, pp.398-408, 2014

[63] Wright J. T. & Gaudi B. S., *Exoplanet Detection Methods*, Planets, Stars and Stellar Systems, by Oswalt, Terry D.; French, Linda M.; Kalas, Paul, ISBN 978-94-007-5605-2. Springer Science+Business Media Dordrecht, p. 489, 2013

[64] Johnson J. A. et al., *A Third Exoplanetary System with Misaligned Orbital and Stellar Spin Axes*, Publications of the Astronomical Society of the Pacific, Vol. 121, issue 884, pp.1104-1111, 2009

[65] Johnson J. A. et al., *Giant Planet Occurence in the Stellar Mass-Metallicity Plane*, Publications of the Astronomical Society of the Pacific, Vol. 122, issue 894, pp.905-915, 2010

[66] Johnson J. L. & Li H., *The First Planets: The Critical Metallicity for Planet Formation*, The Astrophysical Journal, Vol. 751, Issue 2, article id. 81, 11 pp., 2012

[67] Kasting et al.,*Habitable Zones around Main Sequence Stars*, Icarus, Vol. 101, Issue 1, p. 108-128, 1993

[68] Koch D. G. et al., *Kepler Mission Design, Realized Photometric Performance, and Early Science*, The Astrophysical Journal Letters, Vol. 713, Issue 2, article id. L79-L86, 2010

[69] Latham D. W. et al., *Kepler-7b: A Transiting Planet with Unusually Low Density*, The Astrophysical Journal Letters, Vol. 713, Issue 2, article id. L140-L144, 2010

[70] Laughlin G. & Adams F. C., *Possible Stellar Metallicity Enhancements from the Accretion of Planets*, The Astrophysical Journal, Letters Vol. 491, p.L51, 1997

[71] Laws C. et al., *Parent Stars of Extrasolar Planets. VII. New Abundance Analyses of 30 Systems*, The Astronomical Journal, Vol. 125, Issue 5, pp. 2664-2677, 2003

[72] Lin D. N. C. et al., *Orbital migration of the planetary companion of 51 Pegasi to its present location*, Nature, Vol. 380, Issue 6575, pp. 606-607, 1996

[73] Lineweaver C. H., Fenner Y., Gibson B. K.,*The Galactic Habitable Zone and the Age Distribution of Complex Life in the Milky Way*, Science, Vol. 303, Issue 5654, pp. 59-62, 2004

[74] Lissauer J. J., *Planet Formation*, Annual review of astronomy and astrophysics. Vol. 31 (A94-12726 02-90), p. 129-174, 1993

[75] Mandel K. & Agol E., *Analytic Light Curves for Planetary Transit Searches*, The Astrophysical Journal, Vol. 580, Issue 2, pp. L171-L175, 2002

[76] Matsuo T. et al., *Planetary Formation Scenarios Revisited: Core-Accretion versus Disk Instability*, The Astrophysical Journal, Vol. 662, Issue 2, pp. 1282-1292, 2007

[77] Mayor M., Queloz D., *A Jupiter-mass companion to a solar-type star*, Nature, Vol. 378, Issue 6555, pp. 355-359, 1995

[78] Meru F. & Bate M. R., *Exploring the conditions required to form giant planets via gravitational instability in massive protoplanetary discs*, Monthly Notices of the Royal Astronomical Society, Vol. 406, Issue 4, pp. 2279-2288, 2010

[79] Mizuno H., *Formation of the Giant Planets*, Progress of Theoretical Physics, Vol. 64, No. 2, pp. 544-557, 1980

[80] Perryman, M. A. C. et al., *HIPPARCOS distances and mass limits for the planetary candidates: 47 Ursae Majoris, 70 Virginis, and 51 Pegasi*, Astronomy and Astrophysics 310, L21, 1996

[81] Pollack J. B. et al., *Formation of the Giant Planets by Concurrent Accretion of Solids and Gas*, Icarus, Vol. 124, Issue 1, pp. 62-85, 1996

[82] Quintana E. V. et al., *An Earth-Sized Planet in the Habitable Zone of a Cool Star*, Science, Vol. 344, Issue 6181, pp. 277-280, 2014

[83] Rafikov R. R., *Can Giant Planets Form by Direct Gravitational Instability?*, The Astrophysical Journal, Vol. 621, Issue 1, pp. L69-L72, 2005

[84] Rasio F. A. & Ford E. B., *Dynamical instabilities and the formation of extrasolar planetary systems*, Science, Vol. 274, p. 954-956, 1996

[85] Reid I. N., *On the Nature of Stars with Planets*, The Publications of the Astronomical Society of the Pacific, Vol. 114, Issue 793, pp. 306-329, 2002

[86] Rogers L. A. & Seager S. *Three Possible Origins for the Gas Layer on GJ 1214b*, The Astrophysical Journal, Vol. 716, Issue 2, pp. 1208-1216, 2010

[87] Santos N. C. et al., *Chemical analysis of 8 recently discovered extra-solar planet host stars*, Astronomy and Astrophysics, Vol. 363, p.228-238, 2000

[88] Santos N. C. et al., *The metal-rich nature of stars with planets*, Astronomy and Astrophysics, Vol. 373, p.1019-1031, 2001

[89] Santos N. C. et al., *Statistical properties of exoplanets. II. Metallicity, orbital parameters, and space velocities*, Astronomy and Astrophysics, Vol. 398, p.363-376, 2003

[90] Santos N. C. et al., *Spectroscopic [Fe/H] for 98 extra-solar planet-host stars. Exploring the probability of planet formation*, Astronomy and Astrophysics, Vol. 415, p.1153-1166, 2004b

[91] Dodson-Robinson, S. E. *A Correlation between the Eclipse Depths of Kepler Gas Giant Candidates and the Metallicities of Their Parent Star*, The Astrophysical Journal, Vol. 752, Issue 1, article id. 72, 9 pp., 2012

[92] Schwamb M. E. et al., *Planet Hunters: A Transiting Circumbinary Planet in a Quadruple Star System*, The Astrophysical Journal, Vol. 768, Issue 2, article id. 127, 21 pp., 2013

[93] Seager S. et al., *Mass-Radius Relationships for Solid Exoplanets*, The Astrophysical Journal, Vol. 669, Issue 2, pp. 1279-1297, 2007

[94] Selis F.,*Habitability: the point of view of an astronomer*, In Gargaud M., Martin H., ; Claeys, P., Lectures in Astrobiology 2, Springer, pp. 210214, 2006

[95] Schlaufman K. C. & Laughlin G.*Kepler Exoplanet Candidates Host Stars are Prefeerentially Metal Rich*, The Astrophysical Journal, Vol. 738, Issue 2, article id 177, pp. 9, 2011

[96] Soderblom D. & King J.,*Solar-Type Stars:Basic Information on Their Classification and Characterization*, saco, conf:41, 1998

[97] Stello D. et al., *Radius Determination of Solar-type Stars Using Asteroseismology: What to Expect from the Kepler Mission*, The Astrophysical Journal, Vol. 700, Issue 2, pp. 1589-1602, 2009

[98] Taylor B. J., *Supermetallicity at the Quarter-Century Mark: A Conservative Statistician's Review of the Evidence*, The Astrophysical Journal Supplement, Vol. 102, p.105, 1996

[99] Terebey S. et al., *The collapse of the cores of slowly rotating isothermal clouds*, The Astrophysical Journal, Part 1 (ISSN 0004-637X), Vol. 286, p. 529-551, Nov. 15, 1984

[100] Terebey S. et al., *Solar System Formation and Early Evolution: the First 100 Million Years. Earth, Moon, and Planets*, Springer 98, 1-4, pp. 39-95, 2006

[101] Tuomi, M., *Evidence for nine planets in the HD 10180 system*, Astronomy & Astrophysics, Vol.543, id.A52, 12 pp, 2012

[102] Udry et al., *The CORALIE survey for southern extra-solar planets. II. The short-period planetary companions to HD 75289 and HD 130322*, Astronomy and Astrophysics, Vol. 356, p.590-598, 2000

[103] Udry S., Santos N. C., *Statistical Properties of Exoplanets*, Annual Review of Astronomy & Astrophysics, Vol. 45, Issue 1, pp.397-439, 2007

[104] Valencia D. et al., *Radius and Structure Models of the First Super-Earth Planet*, The Astrophysical Journal, Vol. 656, Issue 1, pp. 545-551, 2007

[105] Vorobyov & Basu, *The Burst Mode of Protostellar Accretion*, The Astrophysical Journal, Vol. 650, Issue 2, pp. 956-969, 2006

[106] Walter F. M. et al., *X-ray sources in regions of star formation. III - Naked T Tauri stars associated with the Taurus-Auriga complex*, Astronomical Journal (ISSN 0004-6256), Vol. 96, July 1988, p. 297-325, 1988

[107] Winn J. N., *Transits and Occultations*, eprint arXiv:1001.2010

[108] Wolszczan A., Frail D. A., *A planetary system around the millisecond pulsar PSR1257 + 12*, Nature (ISSN 0028-0836), Vol. 355, Jan. 9, p. 145-147, 1992

Appendix A

Kepler's Data

We tabulated all the Kepler's data used in our thesis in this appendix. We list the 267 Kepler giant planet candidates used in the Q12 sample (Ses table A1). The 24 confirmed Kepler gas giant planets found in DR12's sample, as on June 2013, and added to the Q12 sample are listed in table A2. The 382 candidate/confirmed Kepler giant planets used in the Q16 sample are listed in table A3.

Each table contain the the KOI number (KOInumber), the Kepler ID (KepID), the Planet-Star Radius Ratio (R_p/R_*) with the error on this ratio (R_p/R_* error) and the metallicity ([M/H]). All of those data are taken from the NASA Exoplanet archive except for the metallicty which is taken from Kepler Data archive.

Table A1: Kepler's giant planet candidates used in the Q12 sample's analysis

KOI number	KepID	Rp/Rs	Rp/Rs error	[M/H]
K00868.01	6867155	0.1515	1.00E-03	-0.708
K00871.01	7031517	0.20213	6.60E-04	-0.396
K00880.02	7366258	0.05404	2.80E-04	-0.014
K00882.01	7377033	0.203	1.20E-02	-1.244
K00883.01	7380537	0.15713	8.60E-04	-0.372
K00890.01	7585481	0.07533	8.70E-04	0.032
K00012.01	5812701	0.08805	1.10E-04	-0.035
K00895.01	7767559	0.10374	7.00E-04	-0.257
K00897.01	7849854	0.11035	9.40E-04	0.27
K00901.01	8013419	0.0828	2.90E-03	-0.305
K00753.01	10811496	0.0935	4.50E-03	-0.127
K00902.01	8018547	0.083	2.60E-03	-0.498V
K00908.01	8255887	0.0802	1.00E-03	0.128
K00913.01	8544996	0.12133	3.90E-04	-0.281
K00760.01	11138155	0.10388	4.90E-04	0.01
K00763.01	11242721	0.10721	4.90E-04	-0.126

Continued on next page...

Table A1 – Kepler's giant planet candidates used in the Q12 sample's analysis

KOI number	KepID	Rp/Rs	Rp/Rs error	[M/H]
K00918.01	8672910	0.11152	6.40E-04	-0.074
K00929.01	9141746	0.07831	7.20E-04	0.14
K00767.01	11414511	0.11722	5.80E-04	0.023
K00771.01	11465813	0.14	1.30E-03	-0.112
K00772.01	11493732	0.113	3.00E-02	0.001
K00774.01	11656840	0.14258	7.60E-04	-0.308
K00776.01	11812062	0.0642	2.20E-03	-0.098
K00777.01	11818800	0.0848	2.20E-03	-0.56
K00782.01	11960862	0.04813	7.90E-04	-0.313
K00791.01	12644822	0.07372	6.70E-04	-0.006
K00797.01	3115833	0.0872	2.60E-03	-0.518
K00801.01	3351888	0.08055	8.50E-04	0.182
K00802.01	3453214	0.1342	2.70E-03	-0.411
K00805.01	3734868	0.12165	1.40E-04	-0.101
K00809.01	3935914	0.11587	8.30E-04	-0.385
K00813.01	4275191	0.0868	2.20E-03	-0.285
K00822.01	5077629	0.12198	8.40E-04	-0.404
K00823.01	5115978	0.0754	9.10E-03	-0.433
K00824.01	5164255	0.1219	3.90E-03	-0.209
K00830.01	5358624	0.13283	6.10E-04	0.155
K00834.01	5436502	0.05955	2.00E-04	0.143
K00838.01	5534814	0.123	3.10E-02	-0.095
K00843.01	5881688	0.0523	1.20E-03	0.203
K00846.01	6061119	0.16396	5.40E-04	-0.521
K00847.01	6191521	0.05766	3.20E-04	-0.573
K00850.01	6291653	0.0954	1.40E-03	-0.193
K00851.01	6392727	0.0566	2.90E-03	-0.118
K00855.01	6522242	0.13662	6.80E-04	-0.456
K00856.01	6526710	0.1401	1.90E-03	-0.151
K00858.01	6599919	0.122	5.90E-02	-0.253
K01421.01	11342550	0.089	1.50E-03	0.081
K01423.01	11177707	0.0598	1.20E-03	-0.439
K01426.02	11122894	0.06839	9.20E-04	-0.12
K00186.01	12019440	0.11668	4.20E-04	0.021
K00187.01	7023960	0.14128	3.90E-04	0.095
K00139.01	8559644	0.0579	4.90E-04	0.005
K01426.03	11122894	0.147	5.10E-02	-0.12
K01431.01	11075279	0.0772	8.80E-04	0.083
K00188.01	5357901	0.10666	8.20E-04	0.255
K01054.01	6032981	0.01019	9.80E-04	-1.082
K01255.01	8494263	0.1005	1.60E-03	-0.024
K01257.01	8751933	0.0762	3.40E-03	-0.18

Continued on next page...

Table A1 – Kepler's giant planet candidates used in the Q12 sample's analysis

KOI number	KepID	Rp/Rs	Rp/Rs error	[M/H]
K01258.03	8630788	0.192	7.70E-02	0.012
K01261.01	8678594	0.06918	5.60E-04	0.121
K01439.01	11027624	0.04331	1.80E-04	-0.294
K00189.01	11391018	0.12945	5.60E-04	-0.053
K00190.01	5771719	0.11143	2.20E-04	0.22
K01066.01	8260218	0.0965	1.40E-03	-0.277
K00141.01	12105051	0.0533	1.60E-03	0.018
K01074.01	10272640	0.10271	7.80E-04	-0.107
K01268.01	8813698	0.1014	1.80E-03	-0.069
K01271.01	8631160	0.06759	3.40E-04	-0.233
K01456.01	7832356	0.07171	3.90E-04	-0.114
K01457.01	9643874	0.0838	2.50E-03	0.185
K01465.01	11702948	0.0834	1.60E-03	-0.173
K01466.01	9512981	0.1268	2.70E-03	0.335
K01472.01	7761545	0.0677	1.50E-03	-0.242
K01473.01	7499398	0.0729	2.10E-03	0.318
K01474.01	12365184	0.0614	3.50E-03	-0.329
K01761.01	4067336	0.077	3.70E-02	0.018
K00022.01	9631995	0.09282	2.60E-04	-0.025
K00195.01	11502867	0.11573	5.20E-04	-0.188
K01089.01	3247268	0.08364	5.60E-04	-0.133
K01089.02	3247268	0.04552	5.70E-04	-0.133
K01095.01	3329204	0.094	1.10E-02	-0.069
K01096.01	3230491	0.114	1.60E-02	-0.395
K01099.01	2853093	0.0624	1.10E-03	-0.15
K01288.01	10790387	0.0878	1.40E-03	-0.199
K01477.01	7811397	0.1061	2.70E-03	0
K01299.01	10864656	0.02683	3.00E-04	-0.242
K01478.01	12403119	0.04905	8.60E-04	-0.465
K01486.01	7898352	0.0962	1.40E-03	-0.238
K00191.01	5972334	0.1152	5.10E-04	-0.191
K01675.01	5360920	0.097	4.80E-02	-0.293
K01684.01	6048024	0.061	1.70E-02	-0.098
K01103.01	2860866	0.05405	6.20E-04	0.092
K01496.01	4828341	0.105	4.60E-02	-0.304
K00192.01	7950644	0.09007	4.00E-04	-0.231
K01727.01	6185331	0.06073	4.90E-04	-0.287
K00193.01	10799735	0.12958	5.10E-04	-0.118
K00931.01	9166862	0.11408	5.70E-04	0.319
K00127.01	8359498	0.09633	3.60E-04	0.174
K01320.01	4164994	0.1004	2.80E-03	0.114
K01323.01	4076098	0.0777	1.70E-03	-0.101

Table A1 – Kepler's giant planet candidates used in the Q12 sample's analysis

KOI number	KepID	Rp/Rs	Rp/Rs error	[M/H]
K01328.01	4074736	0.064	2.00E-02	-0.486
K01335.01	4155328	0.04576	4.40E-04	-0.285
K00149.01	3835670	0.02812	1.40E-04	-0.294
K01353.01	7303287	0.1039	4.30E-04	-0.077
K01355.01	7211141	0.0559	5.20E-03	-0.194
K01356.01	7363829	0.0831	1.40E-03	-0.018
K00131.01	7778437	0.07292	1.60E-04	0.159
K01359.02	6946199	0.0728	6.60E-03	-0.508
K01546.01	5475431	0.10624	8.40E-04	0.116
K01547.01	5283458	0.1232	2.40E-03	-0.046
K00179.02	9663113	0.0436	3.50E-04	-0.288
K01552.01	7984047	0.11097	6.70E-04	0.006
K01553.01	7951018	0.0693	1.40E-03	0.213
K00972.01	11013201	0.01916	7.10E-04	-0.062
K01176.01	3749365	0.1461	1.60E-03	0.376
K00151.01	2307199	0.0505	6.60E-03	-0.315
K00152.01	8394721	0.05699	1.90E-04	-0.263
K01564.01	5184584	0.0538	4.60E-03	0.301
K01193.01	3942446	0.09	2.20E-02	-0.525
K01573.01	5031857	0.0542	2.90E-03	-0.263
K01574.01	10028792	0.06719	2.60E-04	-0.072
K00183.01	9651668	0.12237	2.30E-04	-0.141
K01206.01	3756801	0.0398	1.60E-03	-0.018
K01208.01	3962440	0.0525	3.70E-03	-0.202
K01209.01	3534076	0.085	8.40E-03	-0.735
K00152.04	8394721	0.089	3.40E-02	-0.263
K01391.01	8958035	0.0784	1.20E-03	-0.206
K01582.01	4918309	0.078	1.00E-02	-0.193
K01587.01	9932970	0.21	1.00E-01	-0.082
K01010.01	1027438	0.06298	7.50E-04	-0.384
K02528.01	9205907	0.053	2.50E-02	-0.27
K00209.02	10723750	0.0463	1.30E-04	-0.038
K01932.01	5202905	0.01692	7.70E-04	-0.094
K01935.01	5396122	0.139	6.80E-02	0.296
K00211.01	10656508	0.0798	5.50E-03	0.009
K01944.01	2438513	0.028	2.00E-03	-0.171
K00212.01	6300348	0.0635	1.20E-03	-0.236
K02573.01	8256453	0.0622	2.30E-03	-0.798
K00214.01	11046458	0.0706	3.20E-03	0.018
K01986.01	8257205	0.041	6.10E-03	-0.041
K00216.01	6152974	0.0706	1.10E-03	0.18
K02299.01	9963265	0.102	2.90E-02	0.184

Table A1 – Kepler's giant planet candidates used in the Q12 sample's analysis

KOI number	KepID	Rp/Rs	Rp/Rs error	[M/H]
K00219.01	6305192	0.05638	1.00E-04	-0.564
K02037.01	9634821	0.044	1.90E-02	0.469
K02640.01	9088780	0.02086	7.20E-04	-0.303
K02042.01	9111849	0.0339	2.40E-03	-0.274
K02370.01	5385304	0.034	8.80E-03	0.023
K02672.01	11253827	0.0464	1.50E-03	-0.129
K00242.01	3642741	0.05427	1.80E-04	0.15
K02674.01	8022489	0.0544	1.40E-03	-0.123
K02677.01	9958387	0.0491	1.20E-03	-0.263
K01779.01	9909735	0.03832	9.50E-04	0.145
K01779.02	9909735	0.0329	8.50E-04	0.145
K01783.01	10005758	0.0759	1.90E-03	-0.247
K01784.01	10158418	0.0543	7.10E-03	0.115
K01786.01	3128793	0.09027	2.50E-04	-1.574
K01787.01	5864975	0.0821	2.10E-03	-0.438
K01788.01	2975770	0.066	5.00E-03	0.243
K01790.01	6504954	0.0646	4.10E-03	0.109
K01798.01	6867766	0.082	1.90E-02	-0.093
K01800.01	11017901	0.06	9.70E-03	-0.409
K01805.01	4644952	0.03447	9.00E-04	0.487
K02681.01	6878240	0.0741	2.50E-03	-0.035
K00197.01	2987027	0.09071	9.90E-04	0.003
K01816.01	8624520	0.0631	8.60E-03	-0.962
K02696.01	11071200	0.0303	3.10E-03	-0.145
K00199.01	10019708	0.09217	3.10E-04	0.104
K02128.01	7019489	0.24	1.00E-01	-0.119
K00201.01	6849046	0.07825	5.90E-04	0.187
K02133.01	8219268	0.01798	2.60E-04	0.509
K02715.01	9837661	0.0779	9.00E-03	0.385
K00202.01	7877496	0.09995	2.30E-04	0.12
K01872.01	9883311	0.079	3.30E-02	-0.186
K01873.01	4939346	0.0512	1.10E-03	0.09
K01879.01	8367644	0.054	1.30E-02	0.106
K01884.01	4851530	0.0498	2.80E-03	-0.293
K00205.01	7046804	0.0915	1.00E-03	-0.168
K01894.01	11673802	0.01733	1.90E-04	0.037
K00206.01	5728139	0.06459	7.00E-05	-0.127
K01902.01	5809954	0.36	1.80E-01	0.17
K01906.01	11773328	0.184	9.00E-02	-0.036
K00208.01	3762468	0.10252	4.50E-04	0.207
K02513.01	9653622	0.105	4.90E-02	-0.319
K02519.01	4047631	0.079	3.10E-02	-0.748

Table A1 – Kepler's giant planet candidates used in the Q12 sample's analysis

KOI number	KepID	Rp/Rs	Rp/Rs error	[M/H]
K01914.01	8426567	0.027	4.90E-03	0.373
K00209.01	10723750	0.07058	1.10E-04	-0.038
K00094.01	6462863	0.06856	1.20E-04	-0.761
K00458.01	7504328	0.0649	2.10E-03	-0.199
K00601.02	10973664	0.084	3.20E-02	-0.18
K00279.01	12314973	0.0352	1.20E-03	-0.342
K00075.01	7199397	0.03931	8.00E-05	-0.499
K00464.01	8890783	0.0662	1.80E-03	0.165
K00466.01	9008220	0.075	9.80E-03	-0.063
K00467.01	9583881	0.05178	9.90E-04	-0.107
K00469.01	9703198	0.0528	2.70E-03	-0.069
K00094.03	6462863	0.04058	1.30E-04	-0.761
K00607.01	5441980	0.0803	4.60E-03	-0.508
K00611.01	6309763	0.102	2.40E-02	-0.132
K00302.01	3662838	0.02774	1.40E-04	-0.067
K00304.01	6029239	0.02533	5.40E-04	-0.093
K00614.01	7368664	0.0809	9.10E-03	-0.023
K00620.02	11773022	0.09717	2.40E-04	-0.079
K00622.01	12417486	0.07	1.30E-03	-0.051
K00100.01	4055765	0.05478	6.40E-04	-0.369
K02992.01	8509442	0.32	1.60E-01	-0.159
K00318.01	8156120	0.03451	1.40E-04	-0.179
K00005.01	8554498	0.03651	2.60E-04	0.116
K00490.02	3239945	0.12306	8.10E-04	0.052
K00338.02	10552611	0.00838	7.70E-04	0.538
K00505.01	5689351	0.0302	3.30E-03	0.238
K00633.01	4841374	0.03095	4.80E-04	-0.368
K00340.01	10616571	0.13743	6.00E-05	0.074
K00505.05	5689351	0.037	1.10E-02	0.238
K00351.01	11442793	0.084	1.10E-03	-0.108
K00351.02	11442793	0.0597	3.90E-03	-0.108
K00353.01	11566064	0.06404	6.10E-04	-0.091
K00356.01	11624249	0.03273	8.50E-04	-0.503
K00368.01	6603043	0.08453	3.00E-05	-0.028
K00063.01	11554435	0.0582	1.60E-03	0.124
K00372.01	6471021	0.08045	4.40E-04	-0.555
K00523.01	8806123	0.06091	8.10E-04	-0.091
K00525.01	9119458	0.0406	2.00E-03	-0.066
K00375.01	12356617	0.06302	4.30E-04	-0.131
K00398.01	9946525	0.096	1.30E-03	0.143
K00401.01	3217264	0.042	2.80E-03	0.147
K00401.02	3217264	0.0425	9.10E-03	0.147

Table A1 – Kepler's giant planet candidates used in the Q12 sample's analysis

KOI number	KepID	Rp/Rs	Rp/Rs error	[M/H]
K00554.01	5443837	0.07355	7.50E-04	-0.082
K00412.01	5683743	0.05262	9.00E-04	-0.011
K00415.01	6289650	0.0651	1.80E-03	-0.334
K00564.02	6786037	0.06791	3.30E-04	-0.197
K00417.01	6879865	0.123	2.80E-02	-0.143
K00421.01	9115800	0.11786	9.60E-04	-0.075
K00422.01	9214713	0.1248	1.40E-03	-0.3
K00425.01	9967884	0.11559	8.60E-04	0.066
K00089.02	8056665	0.02286	3.50E-04	0.063
K00433.02	10937029	0.1173	1.00E-03	0.375
K00435.02	11709124	0.086	1.30E-03	-0.391
K00734.02	10272442	0.176	4.30E-02	-0.13
K00735.01	10287242	0.0618	1.20E-03	-0.626
K00674.01	7277317	0.04259	2.20E-04	0.083
K00680.01	7529266	0.06242	4.00E-05	-0.458
K00682.01	7619236	0.07626	9.00E-04	-0.033
K00683.01	7630229	0.0493	3.80E-03	-0.201
K00686.01	7906882	0.11658	4.80E-04	-0.18
K00716.01	9846348	0.064	1.50E-02	-0.334
K00728.01	10221013	0.1024	3.30E-03	0.04
K04390.01	8330207	0.035	1.10E-02	-0.356
K04446.01	10329196	0.011	2.40E-02	-0.224
K04670.01	9837828	0.05	2.20E-01	0.245
K03627.02	10091110	0.1267	2.10E-03	-0.166
K03663.01	12735740	0.09218	3.00E-04	-0.073
K03680.01	9025971	0.1069	1.00E-03	-0.081
K03721.01	7763269	0.117	1.80E-02	-0.263
K03683.01	10795103	0.06225	2.40E-04	-0.143
K03263.01	11853130	0.1646	8.30E-03	0.185
K04886.01	7692248	0.05	4.00E-01	-0.056
K03309.01	5563300	0.065	1.40E-02	-0.125
K03433.01	7093401	0.072	1.90E-02	0.069
K03835.01	2581554	0.031	1.60E-02	0.121
K03728.01	7515679	0.04138	9.90E-04	-0.064
K03762.01	11518142	0.06993	9.30E-04	-0.201
K03780.01	6775985	0.072	2.00E-02	-0.355
K03891.01	8765560	0.021	2.30E-02	-0.408
K03787.01	7813039	0.072	4.60E-02	-0.098
K03908.01	10363115	0.0128	7.10E-03	-0.162
K03801.01	8827930	0.1092	2.50E-03	0.287
K03811.01	4638237	0.065	1.40E-02	-0.726

Table A2: The 24 giant confirmed planets found in DR12's sample and added to the Q12 sample

KOI number	KepID	Rp/Rs	Rp/Rs error	[M/H]
K00010.01	6922244	0.09328	0.00018	-0.128
K00020.01	11804465	0.11716	0.00008	-0.161
K00097.01	5780885	0.08284	0.00003	0.052
K00098.01	10264660	0.05608	0.00005	-0.122
K00128.01	11359879	0.1006	0.00028	0.362
K00135.01	9818381	0.08054	0.00039	0.178
K00137.01	8644288	0.04452	0.0006	0.169
K00137.02	8644288	0.05629	0.00077	0.169
K00196.01	9410930	0.09635	0.00039	0.096
K00200.01	6046540	0.08575	0.00068	0.152
K00203.01	10619192	0.12953	0.00033	0.041
K00204.01	9305831	0.0749	0.00095	-0.104
K00217.01	9595827	0.13166	0.00048	0.22
K00254.01	5794240	0.17	0.0013	0.234
K00377.01	3323887	0.07502	0.00077	0.17
K00377.02	3323887	0.0744	0.00077	0.17
K00423.01	9478990	0.08641	0.00074	-0.181
K00428.01	10418224	0.05954	0.00009	-0.079
K00620.01	11773022	0.07074	0.0002	-0.079
K00806.01	3832474	0.09288	0.00078	-0.1
K00806.02	3832474	0.12915	0.00099	-0.1
K00872.01	7109675	0.0858	0.0012	-0.11
K00889.01	757450	0.1118	0.0029	-0.094
K01241.01	6448890	0.02292	0.00033	0.156

Table A3: Kepler's Giant confirmed/candidate planets
used in Q16 sample's analysis

KOI number	KepID	Rp/Rs	Rp/Rs error	[M/H]
K00868.01	6867155	0.1515	0.001	-0.708
K00871.01	7031517	0.20213	0.00066	-0.396
K00880.02	7366258	0.05404	0.00028	-0.014
K00883.01	7380537	0.15713	0.00086	-0.372
K00890.01	7585481	0.07533	0.00087	0.032
K00012.01	5812701	0.08805	0.00011	-0.035
K00895.01	7767559	0.10374	0.0007	-0.257
K00897.01	7849854	0.11035	0.00094	0.27
K00901.01	8013419	0.0828	0.0029	-0.305
K00753.01	10811496	0.0935	0.0045	-0.127
K00902.01	8018547	0.083	0.0026	-0.498
K00908.01	8255887	0.0802	0.001	0.128
K00913.01	8544996	0.12133	0.00039	-0.281
K00760.01	11138155	0.10388	0.00049	0.01
K00763.01	11242721	0.10721	0.00049	-0.126
K00918.01	8672910	0.11152	0.00064	-0.074
K00929.01	9141746	0.07831	0.00072	0.14
K00767.01	11414511	0.11722	0.00058	0.023
K00771.01	11465813	0.14	0.0013	-0.112
K00772.01	11493732	0.113	0.03	0.001
K00774.01	11656840	0.14258	0.00076	-0.308
K00776.01	11812062	0.0642	0.0022	-0.098
K00777.01	11818800	0.0848	0.0022	-0.56
K00782.01	11960862	0.04813	0.00079	-0.313
K00791.01	12644822	0.07372	0.00067	-0.006
K00797.01	3115833	0.0872	0.0026	-0.518
K00801.01	3351888	0.08055	0.00085	0.182
K00802.01	3453214	0.1342	0.0027	-0.411
K00805.01	3734868	0.12165	0.00014	-0.101
K00809.01	3935914	0.11587	0.00083	-0.385
K00813.01	4275191	0.0868	0.0022	-0.285
K00823.01	5115978	0.0754	0.0091	-0.433
K00824.01	5164255	0.1219	0.0039	-0.209
K00830.01	5358624	0.13283	0.00061	0.155
K00834.01	5436502	0.05955	0.0002	0.143
K00838.01	5534814	0.123	0.031	-0.095
K00843.01	5881688	0.0523	0.0012	0.203
K00846.01	6061119	0.16396	0.00054	-0.521
K00847.01	6191521	0.05766	0.00032	-0.573
K00850.01	6291653	0.0954	0.0014	-0.193

Table A3 – Kepler's Giant confirmed/candidate planets used in Q16 sample's analysis

KOI number	KepID	Rp/Rs	Rp/Rs error	[M/H]
K00851.01	6392727	0.0566	0.0029	-0.118
K00855.01	6522242	0.13662	0.00068	-0.456
K00856.01	6526710	0.1401	0.0019	-0.151
K00858.01	6599919	0.122	0.059	-0.253
K01421.01	11342550	0.089	0.0015	0.081
K01423.01	11177707	0.0598	0.0012	-0.439
K01426.02	11122894	0.06839	0.00092	-0.12
K00186.01	12019440	0.11668	0.00042	0.021
K00139.01	8559644	0.0579	0.00049	0.005
K01426.03	11122894	0.147	0.051	-0.12
K01431.01	11075279	0.0772	0.00088	0.083
K00188.01	5357901	0.10666	0.00082	0.255
K01255.01	8494263	0.1005	0.0016	-0.024
K01257.01	8751933	0.0762	0.0034	-0.18
K01258.03	8630788	0.192	0.077	0.012
K01261.01	8678594	0.06918	0.00056	0.121
K01439.01	11027624	0.04331	0.00018	-0.294
K00189.01	11391018	0.12945	0.00056	-0.053
K00190.01	5771719	0.11143	0.00022	0.22
K01066.01	8260218	0.0965	0.0014	-0.277
K00141.01	12105051	0.0533	0.0016	0.018
K01074.01	10272640	0.10271	0.00078	-0.107
K01268.01	8813698	0.1014	0.0018	-0.069
K01271.01	8631160	0.06759	0.00034	-0.233
K01456.01	7832356	0.07171	0.00039	-0.114
K01457.01	9643874	0.0838	0.0025	0.185
K01465.01	11702948	0.0834	0.0016	-0.173
K01466.01	9512981	0.1268	0.0027	0.335
K01472.01	7761545	0.0677	0.0015	-0.242
K01473.01	7499398	0.0729	0.0021	0.318
K01474.01	12365184	0.0614	0.0035	-0.329
K01761.01	4067336	0.077	0.037	0.018
K00022.01	9631995	0.09282	0.00026	-0.025
K00195.01	11502867	0.11573	0.00052	-0.188
K01089.01	3247268	0.08364	0.00056	-0.133
K01089.02	3247268	0.04552	0.00057	-0.133
K01095.01	3329204	0.094	0.011	-0.069
K01096.01	3230491	0.114	0.016	-0.395
K01099.01	2853093	0.0624	0.0011	-0.15
K01288.01	10790387	0.0878	0.0014	-0.199
K01477.01	7811397	0.1061	0.0027	0
K01299.01	10864656	0.02683	0.0003	-0.242

Table A3 – Kepler's Giant confirmed/candidate planets used in Q16 sample's analysis

KOI number	KepID	Rp/Rs	Rp/Rs error	[M/H]
K01478.01	12403119	0.04905	0.00086	-0.465
K01486.01	7898352	0.0962	0.0014	-0.238
K00191.01	5972334	0.1152	0.00051	-0.191
K01675.01	5360920	0.097	0.048	-0.293
K01684.01	6048024	0.061	0.017	-0.098
K01103.01	2860866	0.05405	0.00062	0.092
K01496.01	4828341	0.105	0.046	-0.304
K00192.01	7950644	0.09007	0.0004	-0.231
K01727.01	6185331	0.06073	0.00049	-0.287
K00193.01	10799735	0.12958	0.00051	-0.118
K00931.01	9166862	0.11408	0.00057	0.319
K00127.01	8359498	0.09633	0.00036	0.174
K01320.01	4164994	0.1004	0.0028	0.114
K01323.01	4076098	0.0777	0.0017	-0.101
K01328.01	4074736	0.064	0.02	-0.486
K01335.01	4155328	0.04576	0.00044	-0.285
K00149.01	3835670	0.02812	0.00014	-0.294
K01353.01	7303287	0.1039	0.00043	-0.077
K01355.01	7211141	0.0559	0.0052	-0.194
K01356.01	7363829	0.0831	0.0014	-0.018
K00131.01	7778437	0.07292	0.00016	0.159
K01359.02	6946199	0.0728	0.0066	-0.508
K01546.01	5475431	0.10624	0.00084	0.116
K01547.01	5283458	0.1232	0.0024	-0.046
K00179.02	9663113	0.0436	0.00035	-0.288
K01552.01	7984047	0.11097	0.00067	0.006
K01553.01	7951018	0.0693	0.0014	0.213
K00972.01	11013201	0.01916	0.00071	-0.062
K01176.01	3749365	0.1461	0.0016	0.376
K00151.01	2307199	0.0505	0.0066	-0.315
K00152.01	8394721	0.05699	0.00019	-0.263
K01564.01	5184584	0.0538	0.0046	0.301
K01193.01	3942446	0.09	0.022	-0.525
K01573.01	5031857	0.0542	0.0029	-0.263
K01574.01	10028792	0.06719	0.00026	-0.072
K00183.01	9651668	0.12237	0.00023	-0.141
K01206.01	3756801	0.0398	0.0016	-0.018
K01208.01	3962440	0.0525	0.0037	-0.202
K01209.01	3534076	0.085	0.0084	-0.735
K00152.04	8394721	0.089	0.034	-0.263
K01391.01	8958035	0.0784	0.0012	-0.206
K01582.01	4918309	0.078	0.01	-0.193

Continued on next page...

Table A3 – Kepler's Giant confirmed/candidate planets used in Q16 sample's analysis

KOI number	KepID	Rp/Rs	Rp/Rs error	[M/H]
K01587.01	9932970	0.21	0.1	-0.082
K02528.01	9205907	0.053	0.025	-0.27
K00209.02	10723750	0.0463	0.00013	-0.038
K01932.01	5202905	0.01692	0.00077	-0.094
K01935.01	5396122	0.139	0.068	0.296
K00211.01	10656508	0.0798	0.0055	0.009
K01944.01	2438513	0.028	0.002	-0.171
K00212.01	6300348	0.0635	0.0012	-0.236
K02573.01	8256453	0.0622	0.0023	-0.798
K00214.01	11046458	0.0706	0.0032	0.018
K01986.01	8257205	0.041	0.0061	-0.041
K00216.01	6152974	0.0706	0.0011	0.18
K02299.01	9963265	0.102	0.029	0.184
K00219.01	6305192	0.05638	0.0001	-0.564
K02037.01	9634821	0.044	0.019	0.469
K02640.01	9088780	0.02086	0.00072	-0.303
K02042.01	9111849	0.0339	0.0024	-0.274
K02370.01	5385304	0.034	0.0088	0.023
K02672.01	11253827	0.0464	0.0015	-0.129
K00242.01	3642741	0.05427	0.00018	0.15
K02674.01	8022489	0.0544	0.0014	-0.123
K02677.01	9958387	0.0491	0.0012	-0.263
K01779.01	9909735	0.03832	0.00095	0.145
K01779.02	9909735	0.0329	0.00085	0.145
K01783.01	10005758	0.0759	0.0019	-0.247
K01784.01	10158418	0.0543	0.0071	0.115
K01786.01	3128793	0.09027	0.00025	-1.574
K01787.01	5864975	0.0821	0.0021	-0.438
K01788.01	2975770	0.066	0.005	0.243
K01790.01	6504954	0.0646	0.0041	0.109
K01798.01	6867766	0.082	0.019	-0.093
K01800.01	11017901	0.06	0.0097	-0.409
K01805.01	4644952	0.03447	0.0009	0.487
K02681.01	6878240	0.0741	0.0025	-0.035
K00197.01	2987027	0.09071	0.00099	0.003
K01816.01	8624520	0.0631	0.0086	-0.962
K02696.01	11071200	0.0303	0.0031	-0.145
K00199.01	10019708	0.09217	0.00031	0.104
K02128.01	7019489	0.24	0.1	-0.119
K00201.01	6849046	0.07825	0.00059	0.187
K02133.01	8219268	0.01798	0.00026	0.509
K02715.01	9837661	0.0779	0.009	0.385

Continued on next page...

Table A3 – Kepler's Giant confirmed/candidate planets used in Q16 sample's analysis

KOI number	KepID	Rp/Rs	Rp/Rs error	[M/H]
K00202.01	7877496	0.09995	0.00023	0.12
K01872.01	9883311	0.079	0.033	-0.186
K01873.01	4939346	0.0512	0.0011	0.09
K01879.01	8367644	0.054	0.013	0.106
K01884.01	4851530	0.0498	0.0028	-0.293
K00205.01	7046804	0.0915	0.001	-0.168
K01894.01	11673802	0.01733	0.00019	0.037
K00206.01	5728139	0.06459	0.00007	-0.127
K01902.01	5809954	0.36	0.18	0.17
K01906.01	11773328	0.184	0.09	-0.036
K00208.01	3762468	0.10252	0.00045	0.207
K02513.01	9653622	0.105	0.049	-0.319
K02519.01	4047631	0.079	0.031	-0.748
K01914.01	8426567	0.027	0.0049	0.373
K00209.01	10723750	0.07058	0.00011	-0.038
K00094.01	6462863	0.06856	0.00012	-0.761
K00458.01	7504328	0.0649	0.0021	-0.199
K00601.02	10973664	0.084	0.032	-0.18
K00279.01	12314973	0.0352	0.0012	-0.342
K00075.01	7199397	0.03931	0.00008	-0.499
K00464.01	8890783	0.0662	0.0018	0.165
K00466.01	9008220	0.075	0.0098	-0.063
K00467.01	9583881	0.05178	0.00099	-0.107
K00469.01	9703198	0.0528	0.0027	-0.069
K00094.03	6462863	0.04058	0.00013	-0.761
K00607.01	5441980	0.0803	0.0046	-0.508
K00611.01	6309763	0.102	0.024	-0.132
K00302.01	3662838	0.02774	0.00014	-0.067
K00304.01	6029239	0.02533	0.00054	-0.093
K00614.01	7368664	0.0809	0.0091	-0.023
K00620.02	11773022	0.09717	0.00024	-0.079
K00622.01	12417486	0.07	0.0013	-0.051
K00100.01	4055765	0.05478	0.00064	-0.369
K02992.01	8509442	0.32	0.16	-0.159
K00318.01	8156120	0.03451	0.00014	-0.179
K00005.01	8554498	0.03651	0.00026	0.116
K00490.02	3239945	0.12306	0.00081	0.052
K00338.02	10552611	0.00838	0.00077	0.538
K00505.01	5689351	0.0302	0.0033	0.238
K00633.01	4841374	0.03095	0.00048	-0.368
K00340.01	10616571	0.13743	0.00006	0.074
K00505.05	5689351	0.037	0.011	0.238

Continued on next page...

Table A3 – Kepler's Giant confirmed/candidate planets used in Q16 sample's analysis

KOI number	KepID	Rp/Rs	Rp/Rs error	[M/H]
K00351.01	11442793	0.084	0.0011	-0.108
K00351.02	11442793	0.0597	0.0039	-0.108
K00353.01	11566064	0.06404	0.00061	-0.091
K00356.01	11624249	0.03273	0.00085	-0.503
K00368.01	6603043	0.08453	0.00003	-0.028
K00063.01	11554435	0.0582	0.0016	0.124
K00372.01	6471021	0.08045	0.00044	-0.555
K00523.01	8806123	0.06091	0.00081	-0.091
K00523.02	9119458	0.0406	0.002	-0.066
K00375.01	12356617	0.06302	0.00043	-0.131
K00398.01	9946525	0.096	0.0013	0.143
K00401.01	3217264	0.042	0.0028	0.147
K00401.02	3217264	0.0425	0.0091	0.147
K00554.01	5443837	0.07355	0.00075	-0.082
K00412.01	5683743	0.05262	0.0009	-0.011
K00415.01	6289650	0.0651	0.0018	-0.334
K00564.02	6786037	0.06791	0.00033	-0.197
K00417.01	6879865	0.123	0.028	-0.143
K00421.01	9115800	0.11786	0.00096	-0.075
K00422.01	9214713	0.1248	0.0014	-0.3
K00425.01	9967884	0.11559	0.00086	0.066
K00089.02	8056665	0.02286	0.00035	0.063
K00433.02	10937029	0.1173	0.001	0.375
K00435.02	11709124	0.086	0.0013	-0.391
K00734.02	10272442	0.176	0.043	-0.13
K00735.01	10287242	0.0618	0.0012	-0.626
K00674.01	7277317	0.04259	0.00022	0.083
K00680.01	7529266	0.06242	0.00004	-0.458
K00682.01	7619236	0.07626	0.0009	-0.033
K00683.01	7630229	0.0493	0.0038	-0.201
K00686.01	7906882	0.11658	0.00048	-0.18
K00716.01	9846348	0.064	0.015	-0.334
K00728.01	10221013	0.1024	0.0033	0.04
K04390.01	8330207	0.035	0.011	-0.356
K04446.01	10329196	0.011	0.024	-0.224
K04670.01	9837828	0.05	0.22	0.245
K03627.02	10091110	0.1267	0.0021	-0.166
K03663.01	12735740	0.09218	0.0003	-0.073
K03680.01	9025971	0.1069	0.001	-0.081
K03721.01	7763269	0.117	0.018	-0.263
K03683.01	10795103	0.06225	0.00024	-0.143
K03263.01	11853130	0.1646	0.0083	0.185

Continued on next page...

Table A3 – Kepler's Giant confirmed/candidate planets used in Q16 sample's analysis

KOI number	KepID	Rp/Rs	Rp/Rs error	[M/H]
K04886.01	7692248	0.05	0.4	-0.056
K03309.01	5563300	0.065	0.014	-0.125
K03433.01	7093401	0.072	0.019	0.069
K03835.01	2581554	0.031	0.016	0.121
K03728.01	7515679	0.04138	0.00099	-0.064
K03762.01	11518142	0.06993	0.00093	-0.201
K03780.01	6775985	0.072	0.02	-0.355
K03891.01	8765560	0.021	0.023	-0.408
K03787.01	7813039	0.072	0.046	-0.098
K03908.01	10363115	0.0128	0.0071	-0.162
K03801.01	8827930	0.1092	0.0025	0.287
K03811.01	4638237	0.065	0.014	-0.726
K00523.48	6922244	0.09328	0.00018	-0.128
K00523.49	11804465	0.11716	0.00008	-0.161
K00523.50	5780885	0.08284	0.00003	0.052
K00523.51	10264660	0.05608	0.00005	-0.122
K00523.52	11359879	0.1006	0.00028	0.362
K00523.53	9818381	0.08054	0.00039	0.178
K00523.54	8644288	0.04452	0.0006	0.169
K00523.55	8644288	0.05629	0.00077	0.169
K00523.56	9410930	0.09635	0.00039	0.096
K00523.57	6046540	0.08575	0.00068	0.152
K00523.58	10619192	0.12953	0.00033	0.041
K00523.59	9305831	0.0749	0.00095	-0.104
K00523.60	9595827	0.13166	0.00048	0.22
K00523.61	5794240	0.17	0.0013	0.234
K00523.62	3323887	0.07502	0.00077	0.17
K00523.63	3323887	0.0744	0.00077	0.17
K00523.64	9478990	0.08641	0.00074	-0.181
K00523.65	10418224	0.05954	0.00009	-0.079
K00523.66	11773022	0.07074	0.0002	-0.079
K00523.67	3832474	0.09288	0.00078	-0.1
K00523.68	3832474	0.12915	0.00099	-0.1
K00523.69	7109675	0.0858	0.0012	-0.11
K00523.70	757450	0.1118	0.0029	-0.094
K00523.71	6448890	0.02292	0.00033	0.156
K00890.01	7585481	0.07533	8.70E-04	0.032
K01463.01	6346809	0.054	2.50E-02	-0.33
K01375.01	8803882	0.0197	1.40E-03	0.064
K02775.01	6716021	0.111	1.60E-02	-0.16
K02679.01	8326342	0.0718	8.80E-03	-0.388
K02680.01	9119458	0.0406	2.00E-03	-0.066

Table A3 – Kepler's Giant confirmed/candidate planets used in Q16 sample's analysis

KOI number	KepID	Rp/Rs	Rp/Rs error	[M/H]
K00366.01	12356617	0.06302	4.30E-04	-0.131
K00525.01	9946525	0.096	1.30E-03	0.143
K00375.01	5443837	0.07355	7.50E-04	-0.082
K00398.01	5683743	0.05262	9.00E-04	-0.011
K00554.01	6289650	0.0651	1.80E-03	-0.334
K00412.01	6786037	0.06791	3.30E-04	-0.197
K00415.01	6879865	0.123	2.80E-02	-0.143
K00564.02	9115800	0.11786	9.60E-04	-0.075
K00417.01	9214713	0.1248	1.40E-03	-0.3
K00421.01	9967884	0.11559	8.60E-04	0.066
K00422.01	8056665	0.02286	3.50E-04	0.063
K00425.01	10937029	0.1173	1.00E-03	0.375
K00089.02	11709124	0.086	1.30E-03	-0.391
K00433.02	10272442	0.176	4.30E-02	-0.13
K00435.02	10287242	0.0618	1.20E-03	-0.626
K00734.02	7277317	0.04259	2.20E-04	0.083
K00735.01	7529266	0.06242	4.00E-05	-0.458
K00674.01	7619236	0.07626	9.00E-04	-0.033
K00682.01	7630229	0.0493	3.80E-03	-0.201
K00683.01	7906882	0.11658	4.80E-04	-0.18
K00686.01	9846348	0.064	1.50E-02	-0.334
K00698.01	10221013	0.1024	3.30E-03	0.04
K00728.01	8752940	0.0286	1.82E-02	0.272
K04730.01	8330207	0.0292	2.69E-02	-0.356
K04390.01	12069414	0.0567853672	0.00E+00	-0.388
K04512.01	5436161	0.0593839426	0.00E+00	-1.05
K04351.01	10329196	0.01216	6.33E-03	-0.224
K04446.01	9837828	0.054	1.88E-01	0.245
K04670.01	9776794	0.05	1.80E-01	0.304
K04363.01	5103998	0.185985556	0.00E+00	-0.286
K03660.01	9025971	0.10712	2.04E-03	-0.081
K03678.01	7017372	0.092597	5.39E-04	-0.276
K03680.01	11241814	0.1741	3.14E-02	-0.337
K03689.01	7763269	0.1462	6.00E-02	-0.263
K03721.01	10795103	0.062211	2.37E-04	-0.143
K03683.01	5903301	0.09497	1.78E-03	-0.316
K03692.01	11853130	0.1688	9.87E-03	0.185
K03263.01	8905246	0.0262	1.08E-02	0.054
K03473.01	7692248	0.05	4.00E-01	-0.056
K04886.01	5563300	0.0647	1.06E-02	-0.125
K03309.01	6025124	0.1142	1.00E-02	0.041
K03411.01	6023859	0.3157	1.14E-02	0.004

Continued on next page...

Table A3 – Kepler's Giant confirmed/candidate planets used in Q16 sample's analysis

KOI number	KepID	Rp/Rs	Rp/Rs error	[M/H]
K03414.01	5876805	0.0914	4.73E-04	-0.161
K03331.01	7093401	0.0559	2.12E-02	0.069
K03433.01	5384713	0.0879	4.94E-02	0.426
K03444.02	10676927	0.164	1.23E-01	-0.471
K03830.01	2581554	0.03345	5.02E-03	0.121
K03835.01	9593528	0.04672	5.68E-03	-0.363
K03939.01	9761573	0.0705	4.87E-02	-0.377
K03837.01	6973796	0.18628	3.25E-03	0.209
K03726.01	11547869	0.333	2.33E-01	0.573
K03855.01	9752982	0.01827	2.59E-03	-1.029
K03871.01	11518142	0.069842	7.59E-04	-0.201
K03762.01	8323764	0.1922	1.51E-03	-0.175
K03767.01	5008245	0.05321	3.54E-03	0.167
K03770.01	9517393	0.05647	2.50E-03	0.045
K02076.02	10555365	0.13912	1.09E-03	-0.325
K03771.01	6775985	0.1123	2.70E-02	-0.355
K03780.01	8765560	0.02351	7.41E-03	-0.408
K03891.01	5688997	0.1152	3.17E-02	-0.092
K03783.01	7813039	0.07642	8.97E-03	-0.098
K03787.01	5437945	0.047424	7.01E-04	-0.374
K03791.01	10363115	0.01439	2.06E-03	-0.162
K03908.01	8827930	0.10833	2.11E-03	0.287
K03801.01	4638237	0.0838	1.19E-02	-0.726
K03811.01	6507433	0.07171	8.13E-03	0.124
K03815.01	10788461	0.03893	3.33E-03	0.191
K03823.01	4820550	0.058387	8.11E-04	-0.146
K01783.02	10005758	0.04634	6.60E-04	-0.247
K01411.01	9425139	0.0589	5.10E-03	-0.09
K01804.01	11187436	0.074	2.00E-02	-0.419
K01995.01	5942093	0.081	3.70E-02	-0.544
K05230.01	6043490	0.019	3.47E-02	-0.142
K05379.01	7282470	0.0157	1.69E-02	-0.434
K05018.01	3854101	0.1122	4.85E-02	0.1
K05039.01	4077767	0.066	1.55E-01	-0.135
K05057.01	4346339	0.0196	4.49E-02	-0.24
K04939.01	2437209	0.10588	2.15E-03	-0.047
K04946.01	2570432	0.051	1.34E-01	0.239
K04975.01	3355104	0.063	1.16E-01	-0.061
K05632.01	9166700	0.02293	1.05E-03	-0.105
K05517.01	8432249	0.0172	2.10E-02	-0.172
K05782.01	10272858	0.0164	2.55E-02	-0.122
K05660.01	9363944	0.0205	6.72E-02	-0.262

Table A3 – Kepler's Giant confirmed/candidate planets used in Q16 sample's analysis

KOI number	KepID	Rp/Rs	Rp/Rs error	[M/H]	
K05416.01	7731281	0.11363	8.72E-03	0.212	
K05816.01	10656842	0.0182	2.74E-02	0.239	
K05461.01	8016650	0.01764	7.04E-03	0.486	
K05472.01	8076215	0.0149	2.53E-02	-0.401	
K05480.01	8129333	0.0375	5.63E-02	-0.204	
K05485.01	8197176	0.039	1.26E-01	-0.242	

Appendix B

Python Scripts

We present in this appendix all the Python scripts used to analyse our data in this thesis.

B.1 Pyhton code to draw the variation of R_p/R_* in function of the metallicity in each sample studied and to compute the best linear fit.

```
import csv
import matplotlib.pyplot as plt
import numpy as np
from matplotlib.ticker import MultipleLocator
from scipy import stats

def plotGraph(X,Y,title):

    fig, ax = plt.subplots()
    fit = np.polyfit(X,Y,1)
    fit_fn = np.poly1d(fit)
    ax.plot(X,Y, 'bo', X, fit_fn(X), '--r')
    start, end = ax.get_xlim()
    slope, intercept, r_value, p_value, std_err = stats.linregress(X,Y)
    print 'slope', slope
    print 'intercept', intercept
    print 'std_err', std_err
    majorLocator   = MultipleLocator(0.2)
    minorLocator   = MultipleLocator(0.05)
    ax.xaxis.set_major_locator(majorLocator)
    ax.xaxis.set_minor_locator(minorLocator)
    plt.yticks(np.arange(0, 0.41, 0.05))
    ml = MultipleLocator(0.01)
    plt.axes().yaxis.set_minor_locator(ml)
```

```python
        plt.axis([-0.65, 0.45, 0, 0.41])
        plt.xlabel('[M/H]')
        plt.ylabel('R$_p$/R$_*$')
        plt.title(title)
        plt.show()
        plt.savefig('sample.png')

def DR12():
    X=[]
    Y=[];
    with open('sara.dat', 'rb') as csvfile:
        spamreader = csv.reader(csvfile, delimiter=' ', quotechar='|')
        for row in spamreader:
            X.append(float(row[0]))
            Y.append(float(row[1]))
    plotGraph(X,Y,'DR12')




def CV():
    X=[]
    Y=[];
    with open('cv.dat', 'rb') as csvfile:
        spamreader = csv.reader(csvfile, delimiter=' ', quotechar='|')
        for row in spamreader:
            X.append(float(row[0]))
            Y.append(float(row[1]))
    plotGraph(X,Y,'CV')




def Q12():
    X=[]
    Y=[];
    with open('Q12.dat', 'rb') as csvfile:
        spamreader = csv.reader(csvfile, delimiter=' ', quotechar='|')
        for row in spamreader:
            X.append(float(row[1]))
            Y.append(float(row[0]))
    plotGraph(X,Y,'Q12')
```

```
def Q16():
    X=[]
    Y=[];
    with open('Q16.dat', 'rb') as csvfile:
        spamreader = csv.reader(csvfile, delimiter=' ', quotechar='|')
        for row in spamreader:
            X.append(float(row[0]))
            Y.append(float(row[1]))
    plotGraph(X,Y,'Q16')


if __name__ == "__main__":
    DR12()
    CV()
    Q12()
    Q16()
```

B.2 Python code to calculate the Kendall's τ correlation coefficient

```python
from math import sqrt
import csv


def countties(Xranks, issorted = True, ztol = 1.0e-5):
    """
    Returns an array of pairs (n, x) where n is the tied count
    and x is the tied value.
    """
    tiescount = []
    if not issorted:
        X = sorted(Xranks)
    else:
        X = Xranks
    x       = X[0]
    ncount = 1
    n       = len(X)
    for j in range(1, n):
        if abs(X[j] - x)< ztol:
            ncount += 1
        else:
            if ncount > 1:
                tiescount.append((ncount, x))
            ncount = 1
            x = X[j]
    # last pair value
    if ncount > 1:
        tiescount.append((ncount, x))

    return tiescount

def kendall(X,Y, ztol = 1.0e-5):
    """
    Computes the Kendall tau correlation coefficient for
    input ordinal data X and Y.
    """
    n = len(X)
```

[1]We took the code from Dr. Ernesto P. Adorio http://adorio-research.org/wordpress/?p=10787 and we update it to find the Kendall's Tau correlation coefficient for each sample in our study

```python
        xi = [(x,i) for i, x in enumerate(X)]
        xi.sort()
        yi = [Y[i] for (x,i) in xi]

        L, G = 0, 0

        # count ties.
        tx = countties(X, issorted=True)

        ty = countties(yi)
        Tx = sum([i*(i-1) for (i, x) in tx])*0.5
        Ty = sum([i*(i-1) for (i, x) in ty])*0.5
        for i in range(n):
            '''

            Count number of < and > ranked data for the
            corresponding y elements.
            '''

            l, g = 0, 0
            ycmp = yi[i]
            for j in range(i+1, n):
                if   yi[j] > ycmp:
                    g += 1
                elif yi[j] < ycmp:
                    l += 1
            L+= l
            G+= g
        f =   0.5 * n * (n-1)
        den = sqrt((f - Tx)* (f - Ty))
        tau = (G - L)/ den
        return tau

def DR12():
    X=[]
    Y=[];
    with open('sara.dat', 'rb') as csvfile:
        spamreader = csv.reader(csvfile, delimiter=' ', quotechar='|')
        for row in spamreader:
            X.append(float(row[0]))
            Y.append(float(row[1]))
    return kendall(X,Y)

def Q16():
    X=[]
    Y=[];
    with open('Q16.dat', 'rb') as csvfile:
```

```python
        spamreader = csv.reader(csvfile, delimiter=' ', quotechar='|')
        for row in spamreader:
            X.append(float(row[0]))
            Y.append(float(row[1]))
    return kendall(X,Y)

def CV():
    X=[]
    Y=[];
    with open('cv.dat', 'rb') as csvfile:
        spamreader = csv.reader(csvfile, delimiter=' ', quotechar='|')
        for row in spamreader:
            X.append(float(row[0]))
            Y.append(float(row[1]))
    return kendall(X,Y)


def Q12():
    X=[]
    Y=[];
    with open('Q12.dat', 'rb') as csvfile:
        spamreader = csv.reader(csvfile, delimiter=' ', quotechar='|')
        for row in spamreader:
            X.append(float(row[0]))
            Y.append(float(row[1]))
    return kendall(X,Y)

if __name__ == "__main__":
    print "DR12: %.9f" % DR12()
    print "DR12 cleaned: %.9f" % CV()
    print "Q12: %.9f" % Q12()
    print "Q16: %.9f" % Q16()
```

B.3 Python code to draw the histogram of the fraction of giant planets with $R_p/R_* > 0.13$ in function of the metallicity of their parent stars for each sample studied.

```python
import csv
import pylab
import matplotlib.pyplot as plt
import numpy as np
from matplotlib.ticker import MultipleLocator

def plotHistogram(X1,X2,Y,E,title):
    pos=[(X1[j]+X2[j])/2 for j in range(len(X1))]
    fig, ax = plt.subplots()
    barlist=ax.bar(pos,Y,width=[(X1[j]-X2[j]) for j in range(len(X1))],al
    color = ['r','g','c','m'],yerr=E,error_kw=dict(ecolor='black', lw=2,
    start, end = ax.get_xlim()
    pos.insert(0,-1)
    pos.append(1)
    ax.set_xticks(pos)
    majorLocator   = MultipleLocator(0.5)
    minorLocator   = MultipleLocator(0.1)
    ax.xaxis.set_major_locator(majorLocator)
    ax.xaxis.set_minor_locator(minorLocator)
    plt.yticks(np.arange(0, 0.41, 0.1))
    ml = MultipleLocator(0.01)
    plt.axes().yaxis.set_minor_locator(ml)
    plt.axis([-1, 1, 0, 0.41])
    plt.xlabel('Host Star [M/H]')
    plt.ylabel('f(Rp/R$_*$)>0.13')
    plt.title(title)
    plt.grid()
    plt.show()


def DR():
    X1=[]
    X2=[]
    Y=[];
    E=[];
    with open('HistData/HistDR.dat', 'rb') as csvfile:
        spamreader = csv.reader(csvfile, delimiter=' ', quotechar='|')
        for row in spamreader:
            X1.append(float(row[0]))
```

```python
            X2.append(float(row[1]))
            Y.append(float(row[2]))
            E.append(float(row[3]))
    plotHistogram(X1,X2,Y,E,'DR')


def CV():
    X1=[]
    X2=[]
    Y=[];
    E=[];
    with open('HistData/HistCV.dat', 'rb') as csvfile:
        spamreader = csv.reader(csvfile, delimiter=' ', quotechar='|')
        for row in spamreader:
            X1.append(float(row[0]))
            X2.append(float(row[1]))
            Y.append(float(row[2]))
            E.append(float(row[3]))
    plotHistogram(X1,X2,Y,E,'CV')


def Q12():
    X1=[]
    X2=[]
    Y=[];
    E=[];
    with open('HistData/HistQ12.dat', 'rb') as csvfile:
        spamreader = csv.reader(csvfile, delimiter=' ', quotechar='|')
        for row in spamreader:
            X1.append(float(row[0]))
            X2.append(float(row[1]))
            Y.append(float(row[2]))
            E.append(float(row[3]))
    plotHistogram(X1,X2,Y,E,'Q12')


def Q16():
    X1=[]
    X2=[]
    Y=[];
    E=[];
    with open('HistData/HistQ16.dat', 'rb') as csvfile:
        spamreader = csv.reader(csvfile, delimiter=' ', quotechar='|')
        for row in spamreader:
            X1.append(float(row[0]))
```

```python
            X2.append(float(row[1]))
            Y.append(float(row[2]))
            E.append(float(row[3]))
    plotHistogram(X1,X2,Y,E,'Q16')


def Q16b():
    X1=[]
    X2=[]
    Y=[];
    E=[];
    with open('HistData/HistQ16b.dat', 'rb') as csvfile:
        spamreader = csv.reader(csvfile, delimiter=' ', quotechar='|')
        for row in spamreader:
            X1.append(float(row[0]))
            X2.append(float(row[1]))
            Y.append(float(row[2]))
            E.append(float(row[3]))
    plotHistogram(X1,X2,Y,E,'Q16b')


if __name__ == "__main__":
    DR()
    CV()
    Q12()
    Q16()
    Q16b()
```